Model Specification and Time-Varying Risk Premia: Evidence from Spot and Option Markets

Chang-Shu Chung* Ting-Fu Chen† Shih-Kuei Lin‡

January 15, 2019

Abstract

In this paper, we attempt to answer four questions: (i) On average, what do the proportion of the stochastic volatility and return jumps account for the total return variations in S&P500 index? In particular, which one has more influence than the other does on the total return variations? (ii) Is the fitting performance of infinite-activity jump models better than that of finite-activity jump models both in the spot and option markets? (iii) When will investors require significantly higher risk premiums? Specifically, were there significant changes in volatility and jump risk premiums during the time period of the extreme events? (iv) Whether the variance risk premium has predictive power on S&P500 returns, especially can a portfolio based on the diffusive variance risk premium (DVRP) gain excess returns? For the first question, we find that most of return variations are explained by the stochastic volatility, and the return jump accounts for the higher percentage than the stochastic volatility at the beginning of financial crises. For the second question, we adopt the dynamic joint estimation to obtain the stochastic volatility model with double-exponential jumps and correlated jumps in volatility (SV-DEJ-JV) and the stochastic volatility model with normal inverse Gaussian jumps (SV-NIG) fit S&P500 returns and options well in different criteria. For the third question, the time-varying risk premiums show that both the volatility and jump risk premiums increase after the financial crisis, which represents the panic in the post-crisis period causes more expected returns. For the fourth question, we find that DVRP has predictive power on S&P500 returns both in-sample and out-of-sample, with R^2 statistics of 5.40% and 3.46%, respectively. Finally, we further investigate the economic significance of the out-of-sample predictability on the basis of asset allocations with DVRP, and the mean-variance portfolio generates substantial economic gains of over 166 basis points per annum.

JEL classification: C51; G01; G12.

Keywords: Jump Risk Premium, Variance Risk Premium, Particle Filter, Dynamic Joint Estimation, Return Predictability.

*Department of Money and Banking, National Chengchi University. Email: rorysrose@gmail.com.

†Department of Applied Mathematics, Feng Chia University. Email: tfchen@fcu.edu.tw.

‡Department of Money and Banking, National Chengchi University. Email: square@nccu.edu.tw.

1. Introduction

In this paper, we focus on how the volatility and jump risks affect the financial market and we adopt various types of risk models with the proposed estimation method for the empirical study. We attempt to answer the following questions: (i). On average, what do the proportions of the stochastic volatility and return jumps account for the total return variations in S&P 500 index, respectively? Which one has more influence than the other does on the total return variations? (ii). Is the fitting performance of infinite-activity jump models better than that of finite-activity jump models both in the spot and option markets? (iii) When will investors require significantly higher risk premiums than before, during, or after the financial crisis? Specifically, were there significant changes in volatility risk premiums or in jump risk premiums, or both? (iv) Does the model-based variance risk premium (VRP) have predictive power on S&P500 index returns?

For the first question, we attempt to understand the composition of return variations so that we can find the suitable model for pricing and hedging in the financial market (Aït-Sahalia (2004); Andersen, Bollerslev, and Diebold (2007); Huang and Tauchen (2005)). In this paper, we utilize the affine jump-diffusion models and Lévy-type jump models with stochastic volatility to fit the dynamic of index returns, and thus the return variations consist of two components: stochastic volatility risk and jump risk.[1] Thus, in order to fit our models well, there is an important issue that how to set up the proportion of these two components in total return variations. Moreover, we also want to investigate which type of jump models has better fitting performance in the spot market. Further, an appropriate model of return dynamics is essential for option pricing and risk management, because different model specifications lead to different option pricing results for equity options. Thus, if one model fits index returns well, will this model has superior forecasting ability in the option market?

For the second question, Kou, Yu, and Zhong (2016) documents the stochastic volatility model with double-exponential jump outperforms that with other jump-size specifications. We further extend their works to compare different jump-types model between infinite-activity[2] jump models and finite-activity jump models in capturing the joint dynamics of index returns and option prices, simultaneously. We attempt to involve broader jump models with more market information for a comprehensive comparison to know how the jump risk

[1]For empirical studies that implement the Heston (1993) model by itself or in combination with different types of Lévy jumps in returns (see Andersen, Benzoni, and Lund (2002), Bates (1996, 2000, 2006, 2012), Bakshi, Cao, and Chen (1997), Broadie, Chernov, and Johannes (2007), Carr, Geman, Madan, and Yor (2003), Chernov and Ghysels (2000), Christoffersen, Jacobs, and Mimouni (2010), Eraker, Johannes, and Polson (2003), Eraker (2004), Huang and Wu (2004), Kou, Yu, and Zhong (2016), Li, Wells, and Yu (2008, 2011), and Pan (2002))

[2]The asset pricing studies adds an infinite-activity jumps to a Brownian increment in order to model small or large crashes (see, e.g., Carr, Geman, Madan, and Yor (2003); Carr and Wu (2004); Kou, Yu, and Zhong (2016); Li, Wells, and Yu (2008, 2011)).

presents in the financial market with respect to the specific models and periods.

To compare the fitness of models and calibrate the models' parameters, we need the appropriate estimation method corresponding to the models. The maximum likelihood estimation (MLE) is an important method for estimating the model's parameters. However, MLE is applicable to computes the log-likelihood function from the observable data having closed-form density functions. For the model including the latent variables or unobservable data, many researchers introduced the Bayesian Markov chain Monte Carlo (MCMC) or particle filter (PF)[3] algorithms which can estimate model's parameters with latent variables numerically.

In this study, we adopt particle filter for the unobserved latent variables including return jump risk, stochastic volatility risk, and volatility jump risk to fit Bayesian posterior distribution corresponding to the model. Extending the existing joint estimation method[4], we apply the expectation-maximization (EM) algorithm based on the particle filtering to estimate models' parameters with rolling window approach in the spot and option markets. The main advantages of our new approach, dynamic joint estimation, is that it captures time-varying risk premiums for volatility and jump risks against time for further analysis of risk premiums before, during or after the financial crisis.

The third question is about the risk premiums in different financial environments. Daily option surface has two characteristics which are the term structure and implied volatility smile. The term structure of implied volatility primarily identifies diffusive volatility risk premium (Broadie, Chernov, and Johannes (2007)) and the implied volatility smile of cross-sectional option prices which are primarily due to investors' fear of large adverse price jumps identifies jump risk premium (Bakshi, Cao, and Chen (1997); Bates (2000); Pan (2002)). That is, the jump risk premium is the reward required by a risk-averse investor for being exposed to risk stemming from jumps in its price (Bollerslev and Todorov (2011); Todorov (2010)).

We use the time series returns and the index option surfaces to analyze the economic implications of the volatility and jump risk premiums. In the basis of the dynamic joint estimation, we investigate the pattern of both jump and volatility risk premiums and observe the changing structure of the option market in different period time. Then, we can answer the interesting question: when would the time series of the jump risk premium change to a

[3]Earlier studies that apply MCMC methods to continuous-time models include Eraker, Johannes, and Polson (2003), Li, Wells, and Yu (2008, 2011), Johannes,, Polson, and Stroud (2009), and Kou, Yu, and Zhong (2016), among others. Some studies apply particle filter to track the latent variables and estimate the models' parameters including Johannes,, Polson, and Stroud (2009), Christoffersen, Jacobs, and Mimouni (2010), and Ornthanalai (2014).

[4]Existing joint estimation studies use data that cover short time periods of equity index or small subset of the cross section of options (see, e.g., Chernov and Ghysels (2000); Pan (2002); Eraker (2004); Bakshi, Carr, and Wu (2008); Bakshi and Wu (2010); Santa-Clara and Yan (2010); Li, Wells, and Yu (2011)). Empirical studies use data that cover long time periods of equity index and large subset of the cross section of options (see, e.g., Christoffersen, Jacobs, and Ornthanalai (2012); Ornthanalai (2014)).

different level, which reflects expectation of the risk of the investors in the option market?

The empirical analysis focus on data sets of the S&P 500 daily returns and weekly call option contracts from January 1, 2007 to August 31, 2017 for a total of 3827 business days which covers the 2008-2009 financial crisis and the European sovereign debt crisis. We compare the empirical results of nested models as follows. The fundamental model is a stochastic volatility model in Heston (1993), which can clearly capture volatility clustering during the financial crisis. Next, we adopt the finite-activity compound Poisson processes with normal and double-exponential jump sizes, and the time-changed Lévy jump processes to the stochastic volatility model in order to capture the dramatic changes of index returns.

In summary, our answer to the first question is that most of the return variations are dominated by the stochastic volatility. In fact, the return jump accounts for the higher percentage than the stochastic volatility only at the beginning of financial crisis events. Take the the stochastic volatility with correlated double-exponential jumps model (SV-DEJ-JV) as an example, the percentage of return jump accounts for the return variation up to 92.35% on September 29, 2008 and 78.73% on October 28, 2008 during the early stages of a financial crisis. The average percentage of return jump accounts for the total return variation only 0.76 percent. Based on the stochastic volatility model, we observe that the variations of index returns caused by significant jump are rare and the stochastic volatility can interpret not only small variations but also a part of jumps of return variations.

On the other hand, we observe that most of the small jumps of index returns can be explained by the stochastic volatility. Our empirical study emphasizes the low-frequency character of jumps in index return. At the beginning of the financial crisis, the dramatic index shocks are caused by both jump risk and volatility risk, and the jumps lead to more variations of return than volatility does. However, the return spillovers bring the increase of stochastic volatility so that it enhances the explanatory power of volatility to the variation of returns in the financial crisis.

Our empirical finding for the second question indicate that the stochastic volatility with correlated double-exponential jumps model and the stochastic volatility with normal inverse Gaussian process jumps model (SV-NIG) perform well in the S&P 500 index return and option markets. When we choose the log-likelihood function to be the criterion, the finite-activity jumps model, the SV-DEJ-JV model, has the best fitting performance in both spot and option markets. If we use the Bayesian information criterion (BIC), which considers a penalty term for both the number of parameters and sample sizes in the model as the criterion for model selection, the infinite-activity jumps model, the SV-NIG model, will represent the best performance. For the further examination, the out-of-sample test reports that the SV-DEJ-JV model has the best forecasting ability since it has less absolute pricing

error in weekly option prices on average. Our findings indicate the benefit of specifications with the double-exponential jump components and the correlated jumps in volatility, with the more richly parameterized model performing relative better both for the in-sample fitness and for the out-of-sample prediction test.

From the empirical result for the third question, different risk factors such as return diffusion, return jump, and volatility jump risks drive the return variations and the variations of return variations. It not only may risk factors command the separate premiums such as volatility risk and jump risk premiums, but also each premium could be time-vary with the different time periods (Carr and Wu (2009); Todorov (2010)). In this paper, we characterize the time-varying risk premia, implied by the large panel of S&P500 index and options, and the risk premium dynamics directly reflect the hedging behavior of investors in stock market. Andersen, Fusari, and Todorov (2015b).

We observe an interesting phenomenon to the jump risk premiums that significantly increase after the large shock period in the financial crisis[5]. Take the SV-DEJ-JV model as an example, we find the average annualized jump risk premiums are 0.003% during the large shock period in the financial crisis. However, after the financial crisis, the average annualized jump risk premiums significantly rise to 0.019%. These special patterns also appear during and after the large shock time period in the European debt crisis. These patterns illustrate that investors reflect the panic of bearing jump risk in the post-crisis period more significant and request more expected returns.

For the fourth question, we investigate the statistical and economic significance of the variance risk premium which represents the premium that the investor pay to insure themselves against variance risk (Carr and Wu (2009); Bakshi and Kapadia (2003)). We conduct additional analysis on both in- and out-of-sample return predictability afforded by the SV-DEJ-JV model's[6] diffusive variance risk premium (DVRP) and examine the economic significance of the DVRP via an asset allocation experiment. We use the fundamental way of forming an out-of-sample forecast by running the predictive ordinary least-squares (OLS) regression on a rolling basis for one year sample. In-sample tests show that DVRP produces predictive regression with positive the statistically significant adjusted R^2 (3.55%-5.40%).

[5]Note that we define two time intervals September 15, 2008 to March 23, 2009 and August 4, 2011 to November 30, 2011 as the large shock periods in the 2008-2009 financial crisis (From August 1, 2007 to June 30, 2009) and the European debt crisis (From October 1, 2010 to December 30, 2012) according to the ± 0.03 returns to split these time intervals. We conduct the empirical analysis in five time intervals: (1) Before the large shock time period in the financial crisis (From August 1, 2007 to September 15, 2008), (2) During the large shock time period in the financial crisis (From September 15, 2008 to March 23, 2009), (3) After the large shock time period in the financial crisis and before the large shock time period in the European debt crisis (From March 23, 2009 to October 1, 2010), (4) During the large shock time period in the European debt crisis (From October 1, 2010 to December 30, 2012), (5) After the large shock time period in the European debt crisis (From December 30, 2012 to August 31, 2017).

[6]We adopt the SV-DEJ-JV model to examine the return predictability based on the variance risk premiums because it has the best fitting performance in both the spot and option markets

The maximum adjusted R^2 statistics of 5.40% is at the four-month horizon while the weighting least-squares (WLS) regression is used for the robustness check and is still statistically significant at the 5% level with adjusted R^2 of 1.12% for the quarterly horizon. We further find that the maximum adjusted R^2 can achieve 34.96% at four-month horizon for 2008:09-2009:03 sample period (During large shock period in the 2008-2009 financial crisis). Moreover, the return predictability of DVRP can even be extended to one year (twelve-month) with adjusted R^2 of 8.40% that is statistically significant at 5% level in the large shock period.

Goyal and Welch (2008) indicate that, despite significant evidence of in-sample predictive ability, popular predictor variables fail to predict the excess returns based on the out-of-sample tests. In this paper, we also examine the out-of-sample return predictability of the SV-DEJ-JV's model DVRP. The out-of-smaple R^2 (OOS R^2) is calculated by comparing the mean-squared errors for predicting excess returns using the predictive model versus the average historic estimate of the equity premium. We obtain the positive OOS R^2 statistics 1.49%, 0.39%, 3.46%, 3.28%, and 1.58% at horizons of two, three, four, five, and six months, respectively, but those results are not statistically significant even at 10% level. However, the positive OOS R^2 means that the empirical model outperforms the historical average out-of-sample in the S&P500 index excess returns. On the period after the large shock (March, 1, 2009 to December 31, 2009), there are statistically significant and positive at one- to seven-month horizons, and DVRP can produce the maximum predictive regression OOS R^2 statistics of 35.00% at the two-month horizon.

In addition, we examine the economic significance of DVRP's predictive ability via an asset allocation analysis and find that DVRP generates large utility gains for a mean-variance investor who allocates between equities and risk-free bills[7]. When a relative risk aversion coefficient is three and without short selling constraint and predictive excess returns is at three-month horizon, a mean-variance investor would be willing to pay 166 basis points in annualized portfolio management fees at various rebalancing frequencies to have access to excess return forecasts based on DVRP and this trading strategy generates a Sharpe ratio of 0.44 per annum at three-month horizon.

This study provides several contributions to the existing literature. Our first contribution is to find that the return jumps account for a large proportion of the total return variations in S&P 500 index returns during the early stages of a financial crisis. After these days, the stochastic volatility becomes the major impact factor to the total return variations. In fact, we also find that most of the small jumps in index returns which are explained by the stochastic volatility. Therefore, we only need to focus on capturing the large jumps of index

[7]We use the S&P500 index futures to be the risky assets and three-month U.S. Treasury bills (T-bills) to be risk-free assets.

returns when we consider the model with the stochastic volatility.

The second contribution is to find that the SV-DEJ-JV model has the better fitting performance in both the spot and option markets owing to the double-exponential distribution has the monotonicity and heavy-tail feature properties to capture small and large jumps well (Kou (2002); Kou, Yu, and Zhong (2016)). Moreover, the correlated jumps in volatility make latent stochastic volatility rapidly track the return variations, that is, it has the better performance than the models without volatility jumps. With respect to the computational efficiency, the SV-NIG model has fewer parameters than the SV-DEJ-JV model though they have similar fitting performances. Therefore, the SV-NIG model has superior performance based on the Bayesian information criterion.

Our third contribution is to extend the estimation methodology. We use the sequential importance resampling and the particle filtering to track the latent variables of the models, such as jump sizes, jump times and stochastic volatility, and these filtered latent variables are beneficial for our analysis to obtain more implied market information. Then we further use the rolling windows approach to calibrate the time series of model parameters and risk premiums of stochastic volatility and return jump risks. In basis of the time varying risk premiums.

The fourth contribution in this study is to observe that the jump risk premium is increasing after the crisis by dynamic joint estimation, which shows the panic in the post-crisis period causes more expected returns. Moreover, we find the DVRP has predictive power on S&P500 index excess returns both in-sample and out-of-sample test. The out-of-sample validation shows the DVRP has economic significance of stock return predictability after a large financial shocks and the mean-variance portfolio on the basis of asset allocation with DVRP can generate certainty equivalent gains over 166 basis point per annum for the last 10 years.

The rest of the paper is organized as follows. Section 2 introduces the models for different distributions on jump size. Section 3 introduces the particle filtering, smoothing algorithm and the EM algorithm utilized in our study and discuss model diagnostics to evaluate model performance. Section 4 presents the in-sample and out-of-sample predictive regression and the asset allocation analysis for DVRP. Finally, Section 5 concludes this paper.

2. Theoretical framework

2.1. Model specification

Let asset returns, $(y_t)_{t=0}^{T}$, denote the logarithm of the equity index returns, S_t, i.e., $y_t = \ln(S_t)$, following the nested versions of a general model with mean-reverting stochastic volatility. We add the Lévy-type jumps in returns and/or volatility in order to model the sudden changes induced by rare events. Under the physical probability measure ($\mathbb{P}$), the general dynamic process of the return and variance are described by the following stochastic differential equations (SDE):

$$\begin{aligned} dy_t &= \left(\mu - \frac{1}{2}v_t - \psi_J^{\mathbb{P}}(-i)\right)dt + \sqrt{v_t}dW_{y,t}^{\mathbb{P}} + dJ_{y,t}^{\mathbb{P}}, \\ dv_t &= \kappa^{\mathbb{P}}\left(\theta^{\mathbb{P}} - v_t\right)dt + \sigma_v\sqrt{v_t}dW_{v,t}^{\mathbb{P}} + dJ_{v,t}^{\mathbb{P}}, \end{aligned} \tag{1}$$

where μ_t is the physical time-varying drift term of index returns, measuring the expected rate of return, v_t is the instantaneous variance process of return. Moreover, $dW_{y,t}^{\mathbb{P}}$ and $dW_{v,t}^{\mathbb{P}}$ are a pair of correlated Brownian motions with correlation coefficient ρdt. The ρ controls the correlation between the index returns and variance and captures the leverage effect which is typically found to be negative (Black (1976)). $dJ_{y,t}^{\mathbb{P}}$ represents the Lévy-type jump of finite or infinite activity in return process and $dJ_{v,t}^{\mathbb{P}}$ represent jumps in volatility. $\psi_J^{\mathbb{P}}(u)$ calculated from $E^{\mathbb{P}}\left[e^{iuJ_{y,t}^{\mathbb{P}}}\right] = e^{-t\psi_J^{\mathbb{P}}(u)}$, is a characteristic exponent of the jump component. We can use the various specifications of distribution of jump components in the above general model, and it can generate different fitting performance for distinct situations. The basic stochastic volatility (hereafter SV) model which we restrict the general model's jump component to zero, i.e., $dJ_{y,t}^{\mathbb{P}} = dJ_{v,t}^{\mathbb{P}} = 0$, is shown in Heston (1993) who assumed that the variation of index return follows the square-root process (Cox, Ingersoll, and Ross (1985)).

The SV model has several characteristics for capturing the dynamic process of index returns: (i) It can avoid the negative variations which is the drawback of the SV model of Hull and White (1987). (ii) The variation of equity index return have the mean-reverting property with the physical long-term level mean of variance and the physical rate of mean reversion coefficient of variance . (iii) The correlated coefficient between variance and returns servers to control the long-term skewness and captures the leverage effect. (iv) The volatility variation coefficient serves to control the long-term kurtosis. Thus, this model can capture several important features of the S&P500 return dynamics and also provide an analytically tractable method of pricing options in Heston (1993).

Since the SV model belongs to the continuous-time model, it cannot capture the large

return jumps in short-term, "smile" and "smirkiness" exhibited in cross-sectional option data (Bakshi, Cao, and Chen (1997); Bates (2000)). Intuitively, the diffusive stochastic volatility only increases gradually with a sequence of small normally distributed increments, that is, it cannot measure the rapid shock of returns. In order to modify those problems of the SV model, we introduce the SV model with a pure jump Lévy process to measure the jump risk. Because their flexibility in generating desired distributions and jumps and their path does not have to be continuous, they may help to resolve some known empirical biases of the Black-Scholes model (Black and Scholes (1973)), such as the realized skewness and excess kurtosis in the distribution of the index returns.

2.1.1. Finite-activity lévy jumps

The first jump-diffusion model is the increment of compound Poisson jump process[8] of Merton's jump (hereafter MJ) (Merton (1976)) which assumes that jump size is independently drawn from the normal distribution, $f_{MJ}(x)$. Furthermore, Bates (1996, 2000), Bakshi, Cao, and Chen (1997), and Pan (2002) developed an affine jump-diffusion model with the stochastic volatility and Gaussian jumps (hereafter SV-MJ). That is, we set $dJ^{\mathbb{P}}_{v,t} = 0$, and assume the total return shocks, $dJ^{\mathbb{P}}_{y,t}$, following a compound Poisson process with a constant jump intensity, $dJ^{\mathbb{P}}_{y,t} = \xi^{\mathbb{P}}_{y,t} dN^{\mathbb{P}}_{y,t} = d\left(\sum_{n=0}^{N^{\mathbb{P}}_{y,t}} \xi^{\mathbb{P}}_{y,n}\right)$, where we assume return jump sizes are normally distributed, $\xi^{\mathbb{P}}_{y,n} \sim \mathcal{N}\left(\gamma^{\mathbb{P}}, \left(\delta^{\mathbb{P}}\right)^2\right)$, $N^{\mathbb{P}}_{y,t} \sim \text{Poisson}\left(\lambda^{\mathbb{P}}_y dt\right)$, so that the compensator of the return jump is

$$\psi^{\mathbb{P}}_{\text{MJ}}(-i) = \lambda^{\mathbb{P}}_y \cdot \left(\exp\left(\gamma^{\mathbb{P}} + \frac{1}{2}\left(\delta^{\mathbb{P}}\right)^2\right) - 1\right).$$

For this dynamics process, we have observations $\{y_t\}_{t=0}^T$, latent volatility variables $\{v_t\}_{t=0}^T$, jump times $\{N^{\mathbb{P}}_{y,t}\}_{t=0}^T$, jump sizes $\{\xi^{\mathbb{P}}_{y,n}\}_{n=0}^{N^{\mathbb{P}}_{y,t}}$ and model parameters space $\Theta = \{\mu, \kappa^{\mathbb{P}}, \theta^{\mathbb{P}}, \sigma_v, \rho, \gamma^{\mathbb{P}}, \delta^{\mathbb{P}}, \lambda^{\mathbb{P}}_y\}$. Thus, the SV-MJ model can capture two important features of equity index return dynamics, namely stochastic volatility and return jumps, and also provide analytical tractability for option pricing (see, e.g., Bates (1996); Bakshi, Cao, and Chen (1997); Pan (2002)).

Duffie, Pan, and Singleton (2000) proposes the stochastic volatility model with correlated Merton's price jumps and jumps in volatility (hereafter SV-MJ-JV) model. Correlated jump in return and volatility help to model rapid increase in volatility that cannot be easily

[8]The asset pricing studies adds a compound Poisson jump (finite-activity jumps) to a Brownian increment in order to model large crashes (see, e.g., Andersen, Benzoni, and Lund (2002); Bates (1996, 2000, 2006); Bakshi, Cao, and Chen (1997); Broadie, Chernov, and Johannes (2007); Chernov and Ghysels (2000); Christoffersen, Jacobs, and Mimouni (2010); Duffie, Pan, and Singleton (2000); Eraker, Johannes, and Polson (2003); Eraker (2004); Huang and Wu (2004); Kou (2002); Kou, Yu, and Zhong (2016); Li, Wells, and Yu (2008); Pan (2002); Santa-Clara and Yan (2010); Li, Wells, and Yu (2011))

captured by the square-root process. The SV-MJ-JV model has contemporaneous arrivals, i.e., $N_{y,t}^{\mathbb{P}} = N_{v,t}^{\mathbb{P}} = N_t^{\mathbb{P}}$, which follows a Poisson process with intensity, $\lambda_y^{\mathbb{P}} = \lambda_v^{\mathbb{P}} = \lambda^{\mathbb{P}}$. The compound Poisson process of volatility jump which jump sizes follow the exponential distribution and we assume the variance jump sizes, $\xi_v^{\mathbb{P}}$, is exponentially distributed with mean $\mu_v^{\mathbb{P}}$, i.e., $\xi_v^{\mathbb{P}} \sim \exp\left(\mu_v^{\mathbb{P}}\right)$. On the other hand, the return jump size are conditional normal distributed, i.e., $\xi_y^{\mathbb{P}} \,|\, \xi_v^{\mathbb{P}} \sim \mathcal{N}\left(\gamma^{\mathbb{P}} + \rho_J \, \xi_v^{\mathbb{P}}, \left(\delta^{\mathbb{P}}\right)^2\right)$, $f_{\text{MJ-JV}}\left(x\right)$, where ρ_J is a correlation coefficient between return jumps and jumps in volatility. The compensator of the return jump and the average jump amplitude is

$$\psi_{\text{MJ-JV}}^{\mathbb{P}}\left(-i\right) = \lambda_y^{\mathbb{P}} \cdot \left(\frac{\exp\left(\gamma^{\mathbb{P}} + \frac{1}{2}\left(\delta^{\mathbb{P}}\right)^2\right)}{1 - \rho_J \mu_v^{\mathbb{P}}} - 1 \right).$$

For this dynamics process, we have observations $\{y_t\}_{t=0}^T$, latent volatility variables $\{v_t\}_{t=0}^T$, return and volatility jump times $\{N_t^{\mathbb{P}}\}_{t=0}^T$, jump sizes $\{\xi_{y,n}^{\mathbb{P}}\}_{n=0}^{N_t^{\mathbb{P}}}$, volatility jump sizes $\{\xi_{v,n}^{\mathbb{P}}\}_{n=0}^{N_t^{\mathbb{P}}}$ and model parameters space $\Theta = \{\mu, \kappa^{\mathbb{P}}, \theta^{\mathbb{P}}, \sigma_v, \rho, \gamma^{\mathbb{P}}, \delta^{\mathbb{P}}, \lambda^{\mathbb{P}}, \mu_v^{\mathbb{P}}, \rho_J\}$.

We further consider the model with the increment of compound Poisson jump process of double-exponential (see Kou (2002)) jumps (hereafter DEJ) which assumes that jump size is independently drawn from the double-exponential distribution with parameters $p^{\mathbb{P}}$, $\eta^{+,\mathbb{P}}$, and $\eta^{-,\mathbb{P}}$, $f_{\text{DEJ}}\left(x\right)$. This distribution has an important property: the asymmetric leptokurtic feature. With this feature, the return distribution is skewed to the left, and has a higher peak and two heavier tails than those of the normal distribution (see Kou (2002)). This resulting in a potentially better fit for small jumps, and the heavy-tail features also helps fit both large positive and negative jumps during the crisis period. Furthermore, Kou, Yu, and Zhong (2016) developed an affine jump-diffusion model with the stochastic volatility and double-exponential jumps (hereafter SV-DEJ). That is,

$$dJ_{y,t}^{\mathbb{P}} = d\left(\sum_{n=0}^{N_{y,t}^{\mathbb{P}}} \left(1_{(N_n=1)} \xi_{y,n}^{+,\mathbb{P}} + 1_{(N_n=-1)} \left(-\xi_{y,n}^{-,\mathbb{P}} \right) \right) \right),$$

$$N_n = \begin{cases} 1, & \text{with probability } p^{\mathbb{P}}, \\ -1, & \text{with probability } q^{\mathbb{P}}, \end{cases}$$

where $N_{y,t}^{\mathbb{P}}$ is used to depict the number of the return jump which follows a Poisson process with the intensity $\lambda_y^{\mathbb{P}}$. N_n is the jump direction, i.e., $N_n = 1$ means upward jump, $N_n = -1$

means downward jump, the jump size

$$\xi_y^{\mathbb{P}} \overset{d}{=} {}^{9} \begin{cases} \xi_y^{+,\mathbb{P}}, & \text{with probability } p^{\mathbb{P}}, \\ -\xi_y^{-,\mathbb{P}}, & \text{with probability } q^{\mathbb{P}}, \end{cases}$$

and the compensator of the return jump and average jump amplitude is

$$\psi_{\text{DEJ}}^{\mathbb{P}}(-i) = \lambda_y^{\mathbb{P}} \cdot \left(\frac{p^{\mathbb{P}}}{1-\eta^{+,\mathbb{P}}} + \frac{q^{\mathbb{P}}}{1+\eta^{-,\mathbb{P}}} - 1 \right),$$

where $p^{\mathbb{P}}$ is the return upward probability with $0 \leq p^{\mathbb{P}}, q^{\mathbb{P}} \leq 1$ and $p^{\mathbb{P}} + q^{\mathbb{P}} = 1$, and $\xi_{y,t}^{+,\mathbb{P}}$ and $\xi_{y,t}^{-,\mathbb{P}}$ are exponential random variables with means $\eta^{+,\mathbb{P}}$ and $\eta^{-,\mathbb{P}}$, respectively. For this dynamics process, we have observations $\{y_t\}_{t=0}^T$, latent volatility variables $\{v_t\}_{t=0}^T$, return jump times $\{N_{y,t}^{\mathbb{P}}\}_{t=0}^T$, upward jump sizes $\{\xi_{y,n}^{+,\mathbb{P}}\}_{n=0}^{N_{y,t}^{\mathbb{P}}}$, downward jump sizes $\{\xi_{y,n}^{-,\mathbb{P}}\}_{n=0}^{N_{y,t}^{\mathbb{P}}}$, and model parameters space $\Theta = \{\mu, \kappa^{\mathbb{P}}, \theta^{\mathbb{P}}, \sigma_v, \rho, \eta^{+,\mathbb{P}}, \eta^{-,\mathbb{P}}, p^{\mathbb{P}}, \lambda_y^{\mathbb{P}}\}$.

Kou, Yu, and Zhong (2016) considered the stochastic volatility with correlated double-exponential jumps (hereafter SV-DEJ-JV) model. The SV-DEJ-JV model also has contemporaneous arrival. The compound Poisson process of the correlated double-exponential jump is:

$$dJ_{y,t}^{\mathbb{P}} = d\left(\sum_{n=0}^{N_{y,t}^{\mathbb{P}}} \left(1_{(N_n=1)} \left(\xi_{y,n}^{+,\mathbb{P}} + \rho_J \xi_{v,n}^{\mathbb{P}} \right) + 1_{(N_n=-1)} \left(-\xi_{y,n}^{-,\mathbb{P}} + \rho_J \xi_{v,n}^{\mathbb{P}} \right) \right) \right),$$

$$N_n = \begin{cases} 1, & \text{with probability } p^{\mathbb{P}}, \\ -1, & \text{with probability } q^{\mathbb{P}}, \end{cases}$$

where the jump size

$$\xi_{y,n}^{\mathbb{P}} = \begin{cases} \xi_{y,n}^{+,\mathbb{P}} + \rho_J \xi_{v,n}^{\mathbb{P}}, & \text{with probability } p^{\mathbb{P}}, \\ -\xi_{y,n}^{-,\mathbb{P}} + \rho_J \xi_{v,n}^{\mathbb{P}}, & \text{with probability } q^{\mathbb{P}}, \end{cases}$$

and the compensator of the return jump and average jump amplitude is

$$\psi_{\text{DEJ-JV}}^{\mathbb{P}}(-i) = \lambda_y^{\mathbb{P}} \cdot \left(\left(\frac{1}{1-\rho_J \mu_v^{\mathbb{P}}} \right) \cdot \left(\frac{p^{\mathbb{P}}}{1-\eta^{+,\mathbb{P}}} + \frac{q^{\mathbb{P}}}{1+\eta^{-,\mathbb{P}}} \right) - 1 \right).$$

For this dynamics process, we have observations $\{y_t\}_{t=0}^T$, latent volatility variables $\{v_t\}_{t=0}^T$, return jump times (volatility jump times) $\{N_{y,t}^{\mathbb{P}}\}_{t=0}^T$, upward jump sizes $\{\xi_{y,n}^{+,\mathbb{P}}\}_{n=0}^{N^{\mathbb{P}}}$, downward jump sizes $\{\xi_{y,n}^{-,\mathbb{P}}\}_{n=0}^{N^{\mathbb{P}}}$, volatility jump sizes $\{\xi_{v,n}^{\mathbb{P}}\}_{n=0}^{N^{\mathbb{P}}}$ and model parameters space $\Theta = \{\mu^{\mathbb{P}}, \kappa^{\mathbb{P}}, \theta^{\mathbb{P}}, \sigma_v, \rho, \eta^{+,\mathbb{P}}, \eta^{-,\mathbb{P}}, p^{\mathbb{P}}, \lambda_y^{\mathbb{P}}, \mu_v^{\mathbb{P}}, \rho_J\}$.

[9] The notation $\overset{d}{=}$ mean equal in distribution.

2.1.2. *Infinite-activity lévy jumps*

In this paper, we consider two types of infinite-activity Lévy jumps[10], namely, the Variance-Gamma (hereafter VG) process and Normal Inverse Gaussian (hereafter NIG) process. First, we introduce the increment of the VG process introduced by Madan and Seneta (1990) and Madan, Carr, and Chang (1998). Carr and Wu (2004) proposed the theoretical framework and had established Lévy processes as an attractive alternative to Compound Poisson processes for modelling the asset prices dynamics.

The VG process is obtained by evaluating an arithmetic Brownian process at a stochastic time interval T_t (time-changed) with drift γ and variance σ_J by an independent gamma process. That is, $dJ^{\mathbb{P}}_{y,t} = \gamma^{\mathbb{P}} T_t + \sigma^{\mathbb{P}}_J \sqrt{T_t}\varepsilon_{J,t}$, where $\varepsilon_{J,t}$ is a standard Brownian motion, independent of T_t, and T_t follows the gamma distribution, i.e., $dJ^{\mathbb{P}}_{y,t} \sim \mathcal{N}\left(\gamma^{\mathbb{P}} T_t, \left(\sigma^{\mathbb{P}}_J T_t\right)^2\right)$ and $T_t \sim Gamma\left(\alpha^{\mathbb{P}} dt, 1/\beta^{\mathbb{P}}\right)$. The compensator of the return jumps which is log characteristic function by setting $u = -i$ is

$$\psi^{\mathbb{P}}_{\mathrm{VG}}(-i) = -\alpha^{\mathbb{P}} t \cdot \ln\left(1 - \frac{\gamma^{\mathbb{P}} + \frac{1}{2}\left(\sigma^{\mathbb{P}}_J\right)^2}{\beta^{\mathbb{P}}}\right).$$

Furthermore, Li, Wells, and Yu (2008, 2011) consider the stochastic volatility with the VG jumps to model the dynamic of index returns and option pricing.

We consider another example of an infinite-activity jump model is the NIG process introduced by Barndorff-Nielsen (1997, 1998). The NIG process is obtained by evaluating an arithmetic Brownian process at a stochastic time interval (time-changed) T_t with drift $\beta\delta^2$ and variance δ by an independent inverse Gaussian process with parameter δ, α and β. That is, $dJ^{\mathbb{P}}_{y,t} = \beta^{\mathbb{P}}\left(\delta^{\mathbb{P}}\right)^2 T_t + \delta^{\mathbb{P}}\sqrt{T_t}\varepsilon_{J,t}$ where T_t follows the inverse Gaussian distribution, $dJ^{\mathbb{P}}_{y,t} \sim \mathcal{N}\left(\beta^{\mathbb{P}}\left(\delta^{\mathbb{P}}\right)^2 T_t, \left(\delta^{\mathbb{P}} T_t\right)^2\right)$, $T_t \sim \mathcal{IG}\left(1, \delta^{\mathbb{P}} dt\sqrt{\left(\alpha^{\mathbb{P}}\right)^2 - \left(\beta^{\mathbb{P}}\right)^2}\right)$, and the compensator of the return jump is

$$\psi^{\mathbb{P}}_{\mathrm{NIG}}(-i) = t\delta^{\mathbb{P}}\left(\sqrt{\left(\alpha^{\mathbb{P}}\right)^2 - \left(\beta^{\mathbb{P}}\right)^2} - \sqrt{\left(\alpha^{\mathbb{P}}\right)^2 - \left(\beta^{\mathbb{P}} + 1\right)^2}\right).$$

Table 1 summarizes the Lévy measures and characteristic functions for selected pure jump Lévy processes.

[10] The asset pricing studies add infinite-activity jumps to a Brownian increment in order to model large crashes (see, e.g., Carr, Geman, Madan, and Yor (2003); Carr and Wu (2004); Huang and Wu (2004); Kou, Yu, and Zhong (2016); Li, Wells, and Yu (2008, 2011), Ornthanalai (2014)).

2.2. *The risk-neutral dynamics and risk premium specification*

For the purpose of option pricing, we need to change the return dynamics under the physical measure to the risk-neutral measure ($\mathbb{Q}$). Thus, we need to consider the change of probability measure between $\mathbb{P}$ and $\mathbb{Q}$ for each model. We follow Gerber and Shiu (1994) to use the Esscher transform (Esscher (1932)) to define the change of the probability measure and find the equivalent probability measure for continuous and discrete processes in order to price derivatives. Table 2 summarizes the resulting risk-neutral measure distributions from the change of the probability measure through the Esscher transform for selected pure Lévy jump that we present in Table 1.

Under the $\mathbb{Q}$ measure, the general dynamic process of the return and variance follow:

$$\begin{aligned} dy_t &= \left(\mu - \frac{1}{2}v_t - \psi_J^{\mathbb{Q}}(-i)\right)dt + \sqrt{v_t}dW_{y,t}^{\mathbb{Q}} + dJ_{y,t}^{\mathbb{Q}}, \\ dv_t &= \kappa^{\mathbb{Q}}\left(\theta^{\mathbb{Q}} - v_t\right)dt + \sigma_v\sqrt{v_t}dW_{v,t}^{\mathbb{Q}} + dJ_{v,t}^{\mathbb{Q}}, \end{aligned} \tag{2}$$

Since we assume the coefficient of the risk premium of the Brownian motion of the return process, η_S, we can rewrite μ as follows:

$$\mu = r_t - \eta_S v_t - \psi_J^{\mathbb{Q}}(-i) + \psi_J^{\mathbb{P}}(-i). \tag{3}$$

The difference between μ and r_t is the total equity risk premium, composed of the risk premium of Brownian motion of the return process and the risk premium of the return jump process. The price jump risk premium (hereafter PJRP) in index returns is given by $\eta_J = \psi_J^{\mathbb{P}}(-i) - \psi_J^{\mathbb{Q}}(-i)$, where η_J governs the compensation demanded by investors for bearing to the discontinuous component of the return process. On the other hand, since we assume the risk premium of the Brownian motion of the variation process, η_v, we can rewrite the variance dynamics (Heston (1993)) under $\mathbb{Q}$ as follows:

$$\kappa^{\mathbb{Q}}\theta^{\mathbb{Q}} = \kappa^{\mathbb{P}}\theta^{\mathbb{P}},\ \kappa^{\mathbb{Q}} = \kappa^{\mathbb{P}} + \eta_v,\ \text{and}\ \theta^{\mathbb{Q}} = \frac{\kappa^{\mathbb{P}}\theta^{\mathbb{P}}}{\kappa^{\mathbb{P}} + \eta_v}. \tag{4}$$

The instantaneous variance risk premium (hereafter VRP) is obtained as follows:

$$E_t^{\mathbb{Q}}(dV_t) - E_t^{\mathbb{P}}(dV_t) = \left(\kappa^{\mathbb{Q}} - \kappa^{\mathbb{P}}\right)v_t\,dt + \left(\mu_v^{\mathbb{Q}}\lambda_v^{\mathbb{Q}} - \mu_v^{\mathbb{P}}\lambda_v^{\mathbb{P}}\right)dt. \tag{5}$$

The equation 5 shows that the VRP can be decomposed into two components[11] when we

[11] The decompensition of the VRP are also discussed in Bollerslev and Todorov (2011), Li and Zinna (2018), Bardgett, Gourier, and Leippold (2018), Aït-Sahalia, Karaman, and Mancini (2018), Kilic and Shaliastovich (2018), and Fan, Xiao, and Zhou (2018)

consider the correlated jumps in volatility model, i.e., SV-MJ-JV and SV-DEJ-JV. The first component is the diffusive variance risk premium (hereafter DVRP $= \left(\kappa^{\mathbb{Q}} - \kappa^{\mathbb{P}}\right) v_t = \eta_v \times v_t$), and the second component is variance jump risk premium (hereafter VJRP=$\mu_v^{\mathbb{Q}}\lambda_v^{\mathbb{Q}} - \mu_v^{\mathbb{P}}\lambda_v^{\mathbb{P}}$). Note that under our model specification, all the risk premiums have analysis formulas. We can further decompose the VJRP of the SV-DEJ-JV model into two parts: the variance upside jump risk premium (hereafter VUJRP $= p^{\mathbb{Q}}\lambda_v^{\mathbb{Q}}\mu_v^{\mathbb{Q}} - p^{\mathbb{P}}\lambda_v^{\mathbb{P}}\mu_v^{\mathbb{P}}$) and variance downside jump risk premium (hereafter VDJRP $= q^{\mathbb{Q}}\lambda_v^{\mathbb{Q}}\mu_v^{\mathbb{Q}} - q^{\mathbb{P}}\lambda_v^{\mathbb{P}}\mu_v^{\mathbb{P}}$).

2.3. Characteristic functions and option pricing formula

In this paper, we use the options price with the European framework and derive the characteristic function of each model under $\mathbb{Q}$ by the partial integro-differential equation (PIDE). The probability density function can be computed by the Fourier inversion approach for option pricing (see Heston (1993); Bates (1996); Bakshi, Cao, and Chen (1997); Bakshi and Madan (2000); Duffie, Pan, and Singleton (2000)). We define the characteristic function of the state variable y_t (the log-price at the time T) as

$$\Phi\left(y_t, v_t, t, T : \phi\right) = E^{\mathbb{Q}}\left(e^{i\phi y_T} | y_t, v_t\right) \tag{6}$$

where i denotes the imaginary unit and ϕ is the Fourier transform variable. The Feynman-Kac theorem provides the link between SDEs and partial differential equations (PDEs). It also assures that the solving the expectation is equivalent to solving the corresponding PDE.

Given the risk-neutral dynamic of the log-price in SV series models discussed in the section 2.2, the Feynman-Kac formula yields the following partial integro-differential equation (PIDE) which can be solved by the characteristic function Φ in the equation 6:

$$\begin{aligned}
&\frac{\partial \Phi}{\partial t} + \left(r - \frac{1}{2}v_t - \psi_{\mathrm{RJ}}^{\mathbb{Q}}(-i) - \psi_{\mathrm{CRJ}}^{\mathbb{Q}}(-i)\right)\frac{\partial \Phi}{\partial y_t} + \kappa^{\mathbb{Q}}\left(\theta^{\mathbb{Q}} - v_t\right)\frac{\partial \Phi}{\partial v_t} \\
&\quad + \frac{v_t}{2}\frac{\partial^2 \phi}{\partial y_t^2} + \frac{\sigma_v^2 v_t}{2}\frac{\partial^2 \phi}{\partial v_t^2} + \rho\sigma_v v_t \frac{\partial^2 \phi}{\partial y_t \partial v_t} \\
&\quad + \int_{-\infty}^{\infty}\left[\Phi\left(y_t + J_y, v_t, t, T; u\right) - \Phi\left(y_t, v_t, t, T; u\right)\right] \cdot \pi_{\mathrm{RJ}}^{\mathbb{Q}}\left(J_y\right) dJ_y \\
&\quad + \int_{-\infty}^{\infty}\left[\Phi\left(y_t, v_t + J_v, t, T; u\right) - \Phi\left(y_t, v_t, t, T; u\right)\right] \cdot \pi_{\mathrm{CRJ}}^{\mathbb{Q}}\left(J_y, J_v\right) dJ_y dJ_v = 0,
\end{aligned} \tag{7}$$

where $\psi_{\mathrm{RJ}}^{\mathbb{Q}}(-i)$ and $\psi_{\mathrm{CRJ}}^{\mathbb{Q}}(-i)$ are compensators of return jumps and correlated return jumps, respectively. $\pi_{\mathrm{RJ}}^{\mathbb{Q}}$ and $\pi_{\mathrm{CRJ}}^{\mathbb{Q}}$ are the Lévy measures for return jump (RJ) and correlated return jump (CRJ) under $\mathbb{Q}$, respectively.

In order to compute theoretical options prices using the proposed stock price dynamics in equations 2, we invert characteristic functions of the transition probability for the stock price. The solution to characteristic function is founded by exploiting the affine structure of the modelling framework:

$$\Phi\left(y_t, v_t, t, T : \phi\right) = \exp\left(i\phi y_t + A(\tau;\phi) + B(\tau;\phi)v_t + C(\tau;\phi)y_t\right)$$

where $\tau = T - t$ and the terminal conditions are $A(0;\phi) = B(0;\phi) = C(0;\phi) =$. The solutions of the PIDE in equation 7 can be solved as follows:

$$\begin{aligned}
A\left(\tau;u\right) &= \kappa^{\mathbb{Q}}\theta^{\mathbb{Q}} \cdot \left(D\tau - \frac{2}{\sigma_v^2} \cdot \ln\left(\frac{1-de^{h\tau}}{1-d}\right)\right) + \tau\left(\left(r - \psi^{\mathbb{Q}}_{\mathrm{RJ}}(-i) - \psi^{\mathbb{Q}}_{\mathrm{CRJ}}(-i)\right)i\phi\right), \\
&\quad + \tau g_{\mathrm{RJ}} + \int_0^{\tau} g_{\mathrm{CRJ}}(s)ds, \\
B\left(\tau;u\right) &= D \cdot \frac{1-e^{h\tau}}{1-dr^{h\tau}}, \\
C\left(\tau;u\right) &= 0
\end{aligned}$$

with

$$\begin{aligned}
g_{\mathrm{RJ}} &= \int_{-\infty}^{\infty} \left(\exp\left(i\phi J_y\right) - 1\right) \cdot \pi^{\mathbb{Q}}_{\mathrm{RJ}}\left(J_y\right) dJ_y, \\
g_{\mathrm{CRJ}} &= \int_{-\infty}^{\infty}\int_{-\infty}^{\infty} \left(\exp\left(i\phi J_y + B\left(\tau;\phi\right)J_y\right) - 1\right) \cdot \pi^{\mathbb{Q}}_{\mathrm{CRJ}}\left(J_y, J_v\right) dJ_y dJ_v, \\
h &= \sqrt{(\kappa^{\mathbb{Q}} - \rho\sigma_v i\phi)^2 + \sigma_v^2(i\phi + \phi^2)}, \\
D &= \frac{\kappa^{\mathbb{Q}} - \rho\sigma_v i\phi + h}{\sigma_v^2}, \quad d = \frac{\kappa^{\mathbb{Q}} - \rho\sigma_v i\phi + h}{\kappa^{\mathbb{Q}} - \rho\sigma_v i\phi - h},
\end{aligned}$$

The specifications of g_{RJ} and $g_{\mathrm{CRJ}}\left(\tau\right)$ considered in this papers are listed in Table 3. Given that the risk-neutral characteristic function of asset price Φ, European-style derivatives can be valued using the Fourier inversion method as in Heston (1993), Bates (1996), Bakshi, Cao, and Chen (1997), Bakshi and Madan (2000), and Duffie, Pan, and Singleton (2000). Then we can develop an analytical expression in terms of Φ and obtain call prices by using the Fourier inversion approach (the fast Fourier transform) with factor $e^{-i\phi k}$ (see Carr and Madan (1999)):

$$C\left(S_t, K, t, T\right) = \frac{e^{-\alpha k}}{\pi} \cdot \mathrm{Real}\left(\int_0^{\infty} \frac{e^{-i\phi k}\Phi\left(y_t, v_t, t, T; \phi - i\left(\alpha+1\right)\right)}{\alpha^2 + \alpha - \phi^2 + i\phi(2\alpha+1)} d\phi\right)$$

3. Estimation method

The maximum likelihood estimation (hereafter MLE) is an important method for estimating the model's parameters. However, if the sample data includes the latent or unobservable data, we cannot directly use MLE method to estimate parameters because MLE only computes the log-likelihood function from the observable data which have closed-form density functions. In order to improve this drawback, many researchers introduced the Bayesian Markov chain Monte Carlo or combined the MLE with Kalman filter or Particle filter methods (see, e.g., Pitt and Shephard (1999); Pitt (2002); Johannes,, Polson, and Stroud (2009); Christoffersen, Jacobs, and Mimouni (2010); Li, Wells, and Yu (2008, 2011); Ornthanalai (2014)) which are numerically based and does not rely on closed-form density function, and thus we can estimate parameters with latent variables.

In this paper, our models have the unobserved latent variables such as return jump risk, stochastic volatility risk, and volatility jump risk. Since the stochastic volatility and jump are unobserved variables, the particle filtering algorithm provides the common and convenient tool for the analysis of latent factor models though sampling the particles to fit this model and obtain the Bayesian posterior distribution. However, the particles may lose some information if a time series of the sample is a longer period of time after resampling the particles. That is, the resampling will cause the particles to be more monotonous and the particles cannot track the series of the state variables accurately. In order to modify those drawbacks, Pitt (2002) and Godsill, Doucet, and West (2004) provide the backward simulation method to resample the particles in the reverse-time direction conditioning on future states. Moreover, we combine further the EM algorithm which is an iterative method to fit complete likelihood function with Bayesian posterior distribution with particle filters and smoothers (Kimand and Stoffer (2008)) in order to estimate parameters of our models.

3.1. Parameter estimation with PF and EM algorithms

To simplify our empirical analysis, we consider the first-order Euler discretized version of the continuous-time model at daily frequency. We transform the equation 1 into the discrete-time version, and it becomes:

$$\begin{aligned} R_{t+1} &= \left(\mu - \frac{1}{2}v_t - \psi_J^{\mathbb{P}}(-i)\right)\Delta + \sqrt{v_t\Delta}\epsilon_{y,t+1}^{\mathbb{P}} + J_{y,t+1}^{\mathbb{P}}, \\ v_{t+1} &= v_t + \kappa^{\mathbb{P}}\left(\theta^{\mathbb{P}} - v_t\right)\Delta + \sigma_v\sqrt{v_t\Delta}\left(\rho\epsilon_{y,t+1}^{\mathbb{P}} + \sqrt{1-\rho^2}\epsilon_{v,t+1}^{\mathbb{P}}\right) + J_{v,t+1}^{\mathbb{P}}, \end{aligned} \tag{8}$$

where Δ is the time length. The return, $R_t = y_{t+1} - y_t$, follows the normal distribution with mean, $\left(\mu - \frac{1}{2}v_t - \phi^{\mathbb{P}_J(-i)}\right)\Delta + J^{\mathbb{P}}_{y,t+1}$, and variance, v_t. In order to use the particle filtering method to track the dynamics of the latent variables, we substitute the measure equation (the second equation of 8) into the state equation (the first equation of 8)) and set $\Delta = 1$(1 day). Then we get the state equation of associating with the return, R_t, as follows:

$$\begin{aligned} v_{t+1} = v_t + \kappa^{\mathbb{P}}\left(\theta^{\mathbb{P}} - v_t\right) + \rho\sigma_v\left(R_{t+1} - \left(\mu - \frac{1}{2}v_t - \psi^{\mathbb{P}}_J(-i)\right) - J^{\mathbb{P}}_{y,t+1}\right) \\ + \sigma_v\sqrt{v_t}\sqrt{1-\rho^2}\epsilon^{\mathbb{P}}_{v,t+1} + J^{\mathbb{P}}_{v,t+1}. \end{aligned} \tag{9}$$

According to the state equation and measure equation, we can construct the state-space of stochastic volatility model. Then we can use the particle filtering algorithm to track the latent variables and estimate the parameters with the EM algorithm. We divided the estimation process into three steps:

3.1.1. Step 1: Particle filtering algorithm

Given observable return, R_t, we sample each random variables with M[12] particles for each time t from their corresponding distributions. Then we can evaluate the weight $\widehat{\omega}_t$ corresponding to v_t and latent random variables through the equation 8. The weight is given by:

$$\widetilde{\omega}_{t+1} \propto p\left(R_{t+1}|v_t\right) = \left(2\pi v_t\right)^{-\frac{1}{2}}\exp\left(-\frac{1}{2v_t}\left(R_{t+1} - \left(\mu - \frac{1}{2}v_t - \psi^{\mathbb{P}}_J\left(-i\right)\right) - J^{\mathbb{P}}_{y,t+1}\right)^2\right).$$

Given the sampling latent random variables and the weight $\widetilde{\omega}_t$ at time t, the posterior distribution of stochastic volatility is given by normalizing the weight ω_t:

$$p\left(v^i_{t+1}|R_{t+1}\right) = \omega^i_{t+1} = \frac{\widetilde{\omega}^i_{t+1}}{\sum_{j=1}^{M}\widetilde{\omega}^i_{t+1}}, \quad \text{for } i = 1, ..., M.$$

Thus, we can also use the resampling algorithm to resample the state variables with corresponding weight, ω_{t+1}.

3.1.2. Step 2: Smoothing algorithm

After repeating the iteration for particle filtering from time 0 to $T-1$, we obtain the particle series of the state variables. However, the particles may loss some information if a

[12] We apply a particle filtering algorithm with 300 particles to track the latent variables in this paper.

time series of the sample is a longer period of time after resampling the particles. That is, the resampling will cause the particles to be more monotonous and the particles cannot track the series of the state variables accurately. In order to modify those drawbacks, Pitt (2002) and Godsill, Doucet, and West (2004) provide the backward simulation method to resample the particles in the reverse-time direction conditioning on future states. The weight for the smoothing process is associated with the equation 9 as follows:

$$\widetilde{\omega}_{t|t+1} \propto p\left(v_t|v_{t+1}, R_{t+1}\right) = \left(2\pi\Lambda_1\right)^{-\frac{1}{2}} \exp\left(-\frac{1}{2\Lambda_1}\left(v_{t+1} - \Lambda_2\right)^2\right), \tag{10}$$

$$\Lambda_1 = \sigma_v^2 v_t\left(1-\rho^2\right),$$
$$\Lambda_2 = v_{t+1} - \kappa^{\mathbb{P}}\left(\theta^{\mathbb{P}} - v_t\right) - \rho\sigma_v\left(R_{t+1} - \left(\mu - \frac{1}{2}v_t - \psi_J^{\mathbb{P}}\left(-i\right)\right) - J_{y,t+1}^{\mathbb{P}}\right) - J_{v,t+1}^{\mathbb{P}}.$$

Given the sampling latent random variables and the weight $\widetilde{\omega}_{t|t+1}$ at time t, the posterior distribution of stochastic volatility is given by normalizing the weight $\omega_{t|t+1}^i$:

$$p\left(v_t^i|v_{t+1}^i, R_{t+1}\right) = \omega_{t|t+1}^i = \frac{\widetilde{\omega}_{t|t+1}^i}{\sum_{j=1}^M \widetilde{\omega}_{t|t+1}^i}, \quad \text{for } i = 1, ..., M.$$

Thus, we can use the smoothing algorithm to resample the state variables with corresponding weight $\omega_{t|t+1}^i$ from time $T-1$ to 0.

3.1.3. Step 3: Expectation-maximization algorithm

After particle filtering step and smoothing step, we obtain the state variables for each model. Now, we combine the EM algorithm with particle filters and smoothers (Kimand and Stoffer (2008)) to estimate parameters of model. Let Ψ be the set of the parameters of model, the general complete likelihood function is

$$\begin{aligned}\mathcal{L}\left(\Psi|R_{1:T}, v_{0:T}, J_{y,1:T}^{\mathbb{P}}, J_{v,1:T}^{\mathbb{P}}\right) = f(v_0)\cdot\prod_{t=1}^{T} f(J_{v,t}^{\mathbb{P}})\cdot\prod_{t=1}^{T} f(J_{y,t}^{\mathbb{P}}|J_{v,t}^{\mathbb{P}})\cdot\prod_{t=1}^{T} f(R_t|v_{t-1}, J_{y,t}^{\mathbb{P}}, J_{v,t}^{\mathbb{P}}) \\ \cdot\prod_{t=1}^{T} f(v_t|v_{t-1}, R_t, J_{y,t}^{\mathbb{P}}, J_{v,t}^{\mathbb{P}}).\end{aligned} \tag{11}$$

There are two steps for the EM algorithm. (i) *E*-step: Computing the expectation of the complete log-likelihood function given the observable data (log-return data), latent variables

and the k-th estimated parameters, denoted by $\mathcal{Q}\left(\Psi|\Psi^{(k)}\right)$.

$$\begin{aligned}\mathcal{Q}\left(\Psi|\Psi^{(k)}\right) &= E\left[\left(\ln\mathcal{L}\left(\Psi|R_{1:T}, v_{0:T}, J^{\mathbb{P}}_{y,t}, J^{\mathbb{P}}_{v,t}\right)|y_{1:T}, \Psi^{(k)}\right)\right] \\ &= \frac{1}{M}\sum_{j=1}^{M}\ln\mathcal{L}\left(\Psi|R_{1:T}, v^{j}_{0:T}, J^{j,\mathbb{P}}_{y,1:T}, J^{j,\mathbb{P}}_{v,1:T}\right),\end{aligned} \tag{12}$$

where M is the number of the particles. (ii) M-step: we find the specific parameters by maximize the equation 12 and obtain the estimated parameters, Ψ^{k+1}. That is,

$$\Psi^{k+1} = \arg\max_{\Psi}\mathcal{Q}\left(\Psi|\Psi^{k}\right).$$

Repeating above two steps of the EM algorithm until the log-likelihood function converge and obtain the estimated parameters.

3.2. Dynamic joint estimation

The joint estimation establishes the connections between the spot market and option market, and we further extend the implied information based on the model parameters to dynamic joint estimation. For each date t, we use the rolling time-window for four years historical S&P500 index returns to evaluate the log-likelihood value under $\mathbb{P}$, and jointly adopt the option prices on the date t to calibrate model parameters and risk premiums. For example, on August 31, 2017, we do the particle filtering and smoothing to obtain the latent variables during the period from August 31, 2013, to August 30, 2017, and then estimate the parameter with the cross-sectional of call options data on August 31, 2017.

Following Hu and Zidek (2002) and Ornthanalai (2014), the weighted joint log-likelihood for each day:

$$L^{\text{Joint}}_{t} = \frac{T+N_t}{2}\frac{L^{\mathbb{P}}_{\text{returns,t}}}{T} + \frac{T+N_t}{2}\frac{L^{\mathbb{Q}}_{\text{options,t}}}{N_t}, \quad \text{for} \quad t = 1, ..., T^{*}, \tag{13}$$

where T[13] is the number of days in the rolling windows on each trading date, and N_t is the total number of call options data on each trading date time t. $0.5\cdot(T+N)$ serves as a scaling constant and does not impact the parameter estimates.

The log-likelihood for daily S&P500 index returns, $L^{\mathbb{P}}_{\text{returns,t}}$, is related to particle filtering, smoothing and EM algorithm at time t. However, there is an issue about the log likelihood function, $L^{\mathbb{P}}_{\text{returns,t}}$, when we compare the model performance of the dynamic fitting, the log likelihood function of each model has different numbers of parameters. That is, we cannot

[13] In this paper, we set the rolling time interval, T, to four years.

directly compare the models with log likelihood function, because they have different a dimension of the model parameters. Therefore, we change the log likelihood function which is corresponding to returns. That is,

$$L^{\mathbb{P}}_{\text{returns,t}} = \sum_{t=1}^{T} -\frac{1}{2}\ln\left(2\pi v_{t-1}\right) - \frac{\left(R_t - \left(\mu - \frac{1}{2}v_{t-1} - \psi^{\mathbb{P}}_J(-i)\right) - J^{\mathbb{P}}_{y,t}\right)^2}{2v_{t-1}}. \tag{14}$$

Note that this log-likelihood function under $\mathbb{P}$ in the equation 14 is only used to examine the performance of the model. When we optimize the joint likelihood function, we still use the log-likelihood function in the equation 13. Moreover, in order to compute the log-likelihood for fitting call options, $L^{\mathbb{Q}}_{\text{options,t}}$, we assume that the option pricing errors related to the implied volatility following a normal distribution,

$$\varepsilon_{t,j} = IV_t\left(O^{\text{BS}}_{t,j}\right) - IV_t\left(O^{\text{Model}}_{t,j}\right), \quad \text{for} \quad j = 1, ..., N_t. \tag{15}$$

Assume that the implied volatility error , $\varepsilon_{t,j} \sim \mathcal{N}\left(0, \sigma^2_{\varepsilon,t}\right)$, where $\sigma^2_{\varepsilon,t}$ is the variance of the Black-Scholes implied volatility of the market option price for each day. Thus, the complete log-likelihood of option price is:

$$L^{\mathbb{Q}}_{\text{options,t}} = -\frac{1}{2}\ln\left(2\pi\sigma^2_{\varepsilon,t}\right) + \sum_{j=1}^{N_t}\left(\frac{IV_t\left(O^{\text{BS}}_{t,j}\right) - IV_t\left(O^{\text{Model}}_{t,j}\right)}{\sigma_{\varepsilon,t}}\right)^2, \tag{16}$$

where $IV_t\left(O^{\text{BS}}_{t,j}\right)$ is the Black-Scholes implied volatility of the j-th market-observed call option price , $O^{\text{BS}}_{t,j} = C\left(S_t, K_{t,j}, \tau_{t,j}, r_{t,j}\right)$. $IV_t\left(O^{\text{Model}}_{t,j}\right)$ is the Black-Scholes implied volatility of the j-th call options price, $O^{\text{Model}}_{t,j} = C\left(\Psi_t | S_{t,j}, K_{t,j}, \tau_{t,j}, r_{t,j}\right)$ computed using the model, where the parameters $S_{t,j}$, $K_{t,j}$, $\tau_{t,j}$, and $r_{t,j}$ are the underlying S&P500 index, strike, days-to-expiration, and riskless rate and Ψ_t is the parameter vector containing the model risk-neutral parameter and risk premiums $h_{1,t}$ and $h_{2,t}$.

4. Empirical analysis

Section 4.1 summarize the S&P500 index returns and options data. Section 4.2 reports model estimation results under the physical measure ($\mathbb{P}$) and discusses the decompositions of return variances and jump risks. Section 4.3 reports model fitting results using dynamic joint estimation method under the risk-neutral measure ($\mathbb{Q}$) and explores performances of various models both in-sample and out-of-sample testing. Section 4.4 analyzes the equity jump risk premium, volatility risk premium (variance risk premium, VRP) and its decomposition.

4.1. Data and preliminary analysis

The daily returns and call options for Standard & Poor's 500 index are obtained from Datastream. The U.S. 1 year Treasury Zero-Coupon Yield is used as the risk-free rate. The sample period extends from January 1, 2003, through August 31, 2017, for a total of 3827 business days. The sample period includes two severe episodes of market turmoil which are the 2008-2009 global financial crisis and the 2011 European sovereign debt crisis. Table 4 provides summary statistics for the daily log returns of S&P500 index prices and log returns. The daily mean of index returns is about 2.70e-04, and its average historical volatility is about 1.32e-04. Index returns are left-skewed and leptokurtic as the skewness is negative -0.33 and the kurtosis is 12.2, suggesting the presence of rare and large movements.

We apply several exclusion filters to construct option data set (see Aït-Sahalia (1998)). First, we keep options with more than 6 days and less than a half calendar year to expiration and moneyness between 0.92 and 1.08, because they tend to be more liquid. Second, we only keep Wednesday options because it is the unlikely day to be a holiday and reduces the computational burden of the estimation which mentioned in Andersen, Fusari, and Todorov (2015a), Bates (2000), Christoffersen, Heston, and Jacobs (2009), Pan (2002), Johannes,, Polson, and Stroud (2009), Ornthanalai (2014), Bardgett, Gourier, and Leippold (2018), and etc. Third, in order to mitigate the impact of price discreteness on price valuation, we eliminate call option prices lower than \$0.375. We also eliminate call options which fall into the conditions $C_t > S_t$ and $C_t < S_t - e^{-r(T-t)}K$, where C_t is the call option, S_t is stock price at time t and K is the strike price, because those contracts have the arbitrary opportunities (see Bakshi, Cao, and Chen (1997)). Moreover, in order to balance the features of option-implied volatility and computation efficiency, we take the call options for every 20 strike prices. These adjustments leave a total of 22,828 S&P500 call options with a daily average of 41 S&P500 call options.

According to the moneyness, call options can be classified as six categories, (i) deep-out-of-the-money while moneyness $S/K \leq 0.94$, (ii) out-of-the-money while moneyness $0.94 < S/K \leq 0.97$, (iii) at-the-money while moneyness $0.97 < S/K \leq 1.00$ or $1.00 < S/K \leq 1.03$, (iv) in-the-money while moneyness $1.03 < S/K \leq 1.06$ and (v) deep-in-the-money while moneyness $1.06 \leq S/K$. According to different maturity, call options can be classified as six categories, (i) extremely short-term (≤ 30 days); (ii) short-term ($30-60$ days); (iii) near-term ($60-90$ days); (iv) middle-maturity ($90-120$ days); (v) long-term ($120-150$ days); (vi) extremely long-term (≥ 150 days). Thus, the moneyness and days-to-expiration classifications resulted in 36 categories for empirical studies. Table 5 describes sample statistics properties of the S&P 500 call prices by dividing the call option data into several categories. From Table 5, Panel A, there is a total numbers of 22,828 call option contracts, with at-the-

money, out-of-the-money and in-the-money options respectively taking up 40.64%, 31.35% and 28.01% of total sample. From Table 5, Panel B, call price ranges from \$2.48 for extremely short-term and deep out-of-the-money options to \$147.77 for extremely long-term and deep in-the-money options. Panel C of Table 5 compute average implied volatilities (IVs) which are implied by Black-Scholes formula. S&P500 IVs range in our sample from 4.75% to 93.01% with an average of 16.1%. The implied volatility term structure in Panel C reflects volatility smirk and slightly downward sloping on average during the sample period.

Panel A of Figure 1 exhibits the daily S&P500 returns from January 1, 2007 to August 31, 2017. Panel B shows the average weekly IV for at-the-money S&P500 options and the VIX index. ATM options are those with moneyness between 0.97 and 1.03. During the periods of market turmoil, ATM IV and VIX become higher levels than before. The bailout of Lehman Brothers in September 2008 accelerates the crash in S&P500 market with the large increase in the VIX index. For example, following the bankruptcy of Lehman Brothers in September 2008, daily returns change from 1.13% on August 22, 2008 to -9.47% on October 15, 2008 and the VIX index suddenly increase more than 80%. The option IV surface displays several characteristics such as IV level, IV term structure, and IV smirks and smiles. These provide investors with protection against different movement in returns, such as the negative skewness of the volatility smile reflects their risk aversion toward such movements.

We separate the option-implied volatility surface into several characteristics including level, slope, curvature and term structure (TS). Panel C of Figure 1 plots the term structure of IVs which is the difference between the long- and short-dated ATM IVs. Panel D of Figure 1 plots the slope between short-term OTM and ITM IVs (label Slope 1). Panel E of Figure 1 plots the slope between short-term ATM and ITM IVs (label Slope 2). From Panel F of Figure 1, the curvature of IVs measures the difference between Slope 2 and Slope 1. Short-dated options are those with rough 30 days to maturity, and long-dated options are about 180 days to maturity. ATM options have moneyness equal to 0.92. OTM options have moneyness equal to 1.08. ITM options have moneyness equal 1.00.

During the large shocks (between September 15, 2008 and March 23, 2009), we find the curvatures, Slope 1 and Slope 2, are flatter than other time periods from Panels D, E and F of Figure 1. Besides, the TSs are larger than other time periods in Panel C of Figure 1. That is, the investors have different risk attitudes to volatilities and jump risks in different time periods. Interestingly, during the large shock period, the investors mainly hedge the volatility risk and may change to hedge jump risk after this time period. We further find that Slope 2 has larger value after the large shock such as financial crisis and European debt crisis. This economic implication indicates investors change their risk attitude to the upside jump risk, that is, they expect the upside jumps happen more frequently than before. Hence,

we need a multifactor stochastic volatility model to capture the dynamic processes of returns and option surfaces and to examine the associated risk premiums which are embedded in equity index returns and option surfaces.

4.2. Estimated parameters

In this subselection, we estimate the model parameters using daily S&P500 index returns from January 1, 2003 to August 31, 2017. We estimate the parameters of stochastic volatility model with/without Lévy-type jump using the proposed econometric method discussed in the section 3 under the physical measures ($\mathbb{P}$) and discuss the decompositions of return variances and jump risks for the aggregate stock. Table 6 reports the daily estimated parameters and standard deviation of parameter estimates under $\mathbb{P}$ with respect to each model. We also discuss the choice of the model specification and analyzes how the model performs in the data under $\mathbb{P}$, depending on which Lévy-type jump is embedded in the stochastic volatility model.

4.2.1. Model estimation

Take SV-DEJ-JV as example in the sixth column of Table 6, for the parameters of the dynamic process of log return, the instantaneous expected rates of daily return $\mu = 0.037\%$ is also known as trend factor of log returns which presents that the log returns increase year-by-year and close to the sample volatility mean of 0.027% in Panel B of Table 4. The average upside exponential jump size is $\eta^+ = 0.056$ in the log asset returns, downside exponential jump size is $\eta^- = 0.061$, upside jump probability $p = 0.43$ and the jump frequency is $\lambda_y = 0.033$. This means that about $8\,(\approx 0.033 \times 252)$ days jumps once year, that implies about $30\,(\approx 1/0.033)$ days occur once jump and the left-skewed distribution of the return.

For the parameters of the dynamic process of the stochastic volatility, the long-term mean level is $\theta = 0.011\%$,mean-reverting speed $\kappa = 0.013$ tells us that the stochastic volatility will return to the long-term mean level needing about $3\,(\approx 0.013 \times 252)$ days once year if the current volatility level diverge from the long-term mean level. The volatility of the variance is $\sigma_v = 0.001$. The correlation coefficient of Wiener processes of return and volatility is ρ = -0.43 which has a significant leverage effect. The average implied-standard-deviation is 16.10% and is close to the sample volatility variance of $18.24\% = \sqrt{0.0132 \times 252}$ in Panel B of Table 4. The average of the jump amplitude of the stochastic volatility is μ_v = 4.86E-05 and the correlation coefficient between the return jump and the volatility jump is $\rho_J = 0.21$.

Overall, we observe parameters of the return variance (volatility) equation in Table 6. Figure 2 show that the latent stochastic volatility variables of all the seven models. These

models are estimated by the particle filtering (PF), smoothing filtering (SF) and EM algorithms with 300 particles for each time step from the corresponding model using parameters estimated in Table 6 and the daily S&P500 index returns between January 1, 2003 and August 31, 2017, respectively. We find that the estimates of ρ for the seven models range from -0.424 to -0.464. This means all models exhibit strong negative correlations between volatility and returns. The models share similar estimates of the volatility of return variance σ_v of the volatility processes range from 1.30E-03 to 1.86E-03. The models also share similar estimates of the long-run mean θ of the volatility processes range from 9.11E-05 to 1.26E-04.

These seven models also differ from each other. For example, the volatility process of the SV-DEJ-JV model has the smallest mean-reversion κ with 0.013, followed by the SV-DEJ and SV-NIG model with 0.013, the SV-MJ-JV, model with 0.015, the SV-MJ model with 0.015, the SV-VG model with 0.016, and finally the SV model with 0.017. Clearly, we find that the model obtains smaller mean-reversion κ than others seen from Figure 2 when we add the correlated jumps in volatility into the model. Moreover, if we add the return jumps into the model without volatility jumps, the models also have smaller κ than the SV model. In other words, the return jumps can replace some part of return variance. Note that there are significant volatility clustering effects in the financial crisis period (from August 2007 to June 2009) and the European sovereign debt crisis period (from January 2010 to December 2012) from Figure 2.

Next, we discuss the parameters of the finite-activity jump and the infinite-activity jump models. The estimated return (correlated volatility) jump intensities $\lambda_y\,(=\lambda_v=\lambda)$ for SV-MJ, SV-MJ-JV, SV-DEJ, and SV-DEJ-JV models suggest that, on average, there are about 2 ($\approx 0.008\times 252$) to 8 ($\approx 0.033\times 252$) jumps per year. From Figure 3 shows that there are a few large return (correlated volatility) jump numbers in both finite-activity and infinite-activity models. On the other hand, estimated return jump sizes for SV-VG and SV-NIG suggest that there are many frequent small jumps in returns. From Figure 3 show that there are many small return jump sizes in infinite-activity models SV-VG and SV-NIG.

4.2.2. Decompositions of return variance and jump risk

Panel A of Figure 4 show that the SV-MJ model has the largest jump magnitude about -9.798% on September 29, 2008 during the 2008 financial crisis and -4.727% on August 9, 2011 during European sovereign debt crisis. However, we can find that the SV-MJ model has difficulty capturing large positive and negative returns simultaneously in Panel A of Figure 3. This finding is likely due to the jump structure of Merton jump. Because the jumps in returns tend to have a negative mean seen in Table 6 (see Eraker (2004), Li, Wells, and Yu (2008)), a normal distribution which is used to model the jump sizes has to

shift its location position and this result may lead to non-monotone density for negative jumps and small density for positive jumps. The nonmonotonicity might be problematic in modeling small jumps and small density for positive jumps might lead difficultly to capture large negative jump and positive jump simultaneously (see Kou, Yu, and Zhong (2016)).

On the other hand, Panel D of Figure 4 show that the SV-DEJ-JV model can simultaneously capture large negative return jump magnitude about -6.957% on September 29, 2008 and large positive return jump magnitude about 8.596% on October 13, 2008 during the 2008 financial crisis. This result may come from that the heavy-tail feature of the double-exponential distribution leads to a better performance than the model with Merton jumps. Panel E and Panel F Figure 3 show that the SV-VG and the SV-NIG models can significantly capture the large and small jumps simultaneously. There is an issue for return variations how much percentage of return variations is caused by return jumps. First, we set the return y_t to follow the discrete-time version of the dynamic process

$$y_t = \left(\mu - \frac{1}{2}v_{t-1} - \psi^{\mathbb{P}}_{J_y}\right)\Delta + \sqrt{v_{t-1}\Delta}\varepsilon_{y,t} + J^{\mathbb{P}}_{y,t},$$

where Δ is the time interval. Thus, y_t follow a normal distribution given by

$$y_t \sim \mathcal{N}\left(\left(\mu - \frac{1}{2}v_t\right)\Delta, v_{t-1}\Delta + \left(J^{\mathbb{P}}_{y,t} - \psi^{\mathbb{P}}_{J_y}\Delta\right)^2\right),$$

Thus, the return mean is

$$E\left(y_t\right) = \left(\mu - \frac{1}{2}v_t\right)\Delta,$$

and the return variation is

$$Var\left(y_t\right) = v_{t-1}\Delta + \left(J^{\mathbb{P}}_{y,t} - \psi^{\mathbb{P}}_{J_y}\Delta\right)^2.$$

We can divide return variation into two parts $v_{t-1}\Delta$ and $\left(J^{\mathbb{P}}_{y,t} - \psi^{\mathbb{P}}_{J_y}\Delta\right)^2$. Then, we can calculate how much the percentage of return jump account for the total return variation PJV_t and the mean of PJV_t, $MPJV$. That is,

$$PJV_t = \frac{\left(J^{\mathbb{P}}_{y,t} - \psi^{\mathbb{P}}_{J_y}\Delta\right)^2}{v_{t-1}\Delta + \left(J^{\mathbb{P}}_{y,t} - \psi^{\mathbb{P}}_{J_y}\Delta\right)^2}, \quad t = 1, ..., T.$$

Panel D of Table 6 show that all the $MPJV$ of models are smaller than 1.34. Moreover,

Panel A of Figure 4 show that the PJV_t of the SV-DEJ-JV model up to 92.35% on September 29, 2008 and 78.73% on October 28, 2008 during the early stages of a financial crisis. After these dates, the PJV_t of the SV-DEJ-JV model approximately declined by 100 percent into zero percent. That is, most of the return variations are caused by the stochastic volatility and return jumps only affect at the beginning period of the 2008 financial crisis.

4.2.3. Performances in modelling the spot returns

In this section, we examine the performance of the seven models in capturing the physical dynamics of the S&P500 index returns. In order to check the goodness of fit of the models under the $\mathbb{P}$ measure, we calculate the standardized residuals for return ϵ^y_{t+1} based on estimated models parameters in Table 6 and follow Li, Wells, and Yu (2008) and Kou, Yu, and Zhong (2016) to use the Kolmogorov-Smirnov (KS) test of the hypothesis to examine whether the standardized residuals of a fitted returns dynamic model follow a standard normal distribution. That is,

$$\epsilon^y_{t+1} = \frac{y_{t+1} - y_t - \mu\Delta - J^y_{t+1}}{\sqrt{v_t\Delta}} \sim \mathcal{N}(0,1).$$

We use the Kolmogorov-Smirnov (KS) test to diagnosis whether the p- the value of the KS test statistics is significant or not. If the p-value of the KS test statistics is significantly more than 0.05 under the 95% credible interval, we do not reject the null hypothesis. That is, the standardized residuals follow a standard normal distribution.

Table 7 reports that the KS test statistics of the seven models. Clearly, the p-value of the KS test statistics of all seven models are significant (more than 5%). In other words, the standardized residuals of all seven models follow a standard normal distribution. We focus on the p-value of the seven models to analyze the difference between the models. We find that the p-value of the models which have the return jump are higher than the SV model with 0.0521. We also find that the p-value of the compound Poisson jump processes with Meton jump SV-MJ with 0.0867 is less than the infinity-activity models SV-VG and SV-NIG with p-value 0.1047 and 0.1069. However, when we consider the volatility jump, the fitting performances of the compound Poisson jump models are better than the infinity-activity models, the SV-DEJ-JV model especially has the best fitting performance with p-value 0.2772.

It is possible to increase the log-likelihood by adding parameters of the model when we fit the model to the data. This result may lead to the overfitting with the complex model we selected. Thus, we use the Akaike information criterion (AIC) and Bayesian information criterion (BIC) for model selection to solve this problem by introducing a penalty term for

the number of parameters in the model. Note that the penalty term in BIC is large than in AIC, because BIC considers the penalty with both the number of parameters and the sample size. From Table 6, we find that the SV-DEJ-JV model has the highest log likelihood value with 13,013.01, followed by the SV-DEJ model with 12,960.12, and the SV-MJ-JV model with 12,925.38. This ranking result is consistent with AIC and BIC.

4.3. Option pricing performance

In this subselection, we estimate the model parameters using daily S&P500 index returns from January 1, 2003 to August 31, 2017 and options data from January 1, 2007 to August 31, 2017. We use the joint estimation and the rolling time-window method to estimate the parameters under the risk-neutral measures ($\mathbb{Q}$) discussed in section 3.2. We also discuss the choice of the model specification and analyzes how the model performs in the data under the $\mathbb{Q}$ measures, depending on which Lévy-type jump is embedded in the stochastic volatility model.

4.3.1. Dynamic joint estimation

Table 8 reports the results of dynamic joint estimation discussed in subsection for each model. The sample period is rolling from January 1, 2003 to August 31, 2017 for the daily S&P500 index returns and January 1, 2007 to August 31, 2017 for the weekly cross-sectional S&P500 call options data. The average parameters are reported first, followed by its standard errors in parentheses. Panel A of Table 8 reports the average parameters of stochastic volatility dynamic process of each model, the parameters are estimated on daily S&P500 index returns over the past four years of each trading date. Panel B and C of Table 8 report the average parameters of return and volatility jump dynamic process of each model. Panel D of Table 8 reports parameters of volatility and jump risk premiums of each model, the parameters are calibrated jointly through the S&P500 call option prices. The last three rows of Table 8 summarizes the joint log-likelihood values (L(Joint)) discussed in the subsection, the Akaike information criterion values (AIC) and the Bayesian information criterion values (BIC) for each model. The bold font represents the top three log-likelihood function values of seven models, the last three AIC values of seven models, and the last three BIC values of even models.

We summarize the empirical findings from Table 8 as follows. We look at the joint log-likelihood values L(Joint) of fitting S&P500 index returns and call options data simultaneously, the SV-DEJ-JV model has the best performance with 2714.56, following by the SV-NIG model with 2712.22, and then the SV-DEJ model with 2704.85. When we use the

AIC for model selection to solve this problem by introducing a penalty term for the number of parameters in the model, we find that the SV-DEJ-JV model still has the best performance with -5413.13, following by the SV-NIG model with -5404.43, and then the SV-DEJ model with -5387.69. On the other hand, when we use the BIC for model selection to solve this problem by introducing a penalty term for the number of parameters with sample size in the model, we find that the SV-NIG model become the best performance with -5361.18, following by the SV-DEJ-JV model with -5356.91, and then the SV-DEJ model with -5340.12. Interestingly, this sorting result of the BIC is different to the Panel D of Table 6 estimated only under the $\mathbb{P}$ measure. That is, the SV-DEJ-JV and SV-NIG models are the best models when we jointly estimate the parameters with S&P500 index returns and call options data under the different criteria.

Next, we compare the applicability of different pricing models with their option pricing error. As mentioned in Bakshi, Cao, and Chen (1997), a complex model which contains more parameters will generally lead to better in sample fitting than simple model. However, it may bring the poor results in the out-of-sample testing. Therefore, it is important to analyze the model which should perform better than other models in both in-sample and out-of-sample testing.

4.3.2. In-sample pricing performance

After the model parameters are calibrated by minimizing the sum of squared errors of implied volatility, the in-sample average absolute pricing errors can be represented as follows:

$$\varepsilon^{A}_{t,in-sample} = \frac{1}{m_t}\sum_{j=1}^{m_t} |O^{\text{BS}}_{t,j} - O^{\text{Model}}_{t,j}|, \quad t = 1, ..., T, \tag{17}$$

where m_t is the number of options data at time t in the market, $\text{IV}_t\left(O^{BS}_{t,j}\right)$ is the Black-Scholes IV of the j-th market-observed call option price, $O^{\text{BS}}_{t,j} = C\left(S_{t,j}, K_{t,j}, r_{t,j}, \tau_{t,j}\right)$ at time t, $\text{IV}_t\left(O^{\text{Model}}_{t,j}\right)$ is the Black-Scholes IV of the j-th call option price, $O^{\text{Model}}_{t,j} = C\left(\Theta_t | S_{t,j}, K_{t,j}, r_{t,j}, \tau_{t,j}\right)$ computed using the specific model at time t, where the parameters $S_{t,j}, K_{t,j}, r_{t,j}, \tau_{t,j}$ are the underlying S&P500 index, strike, days-to-expiration, risk-less rate, and Θ_t is the parameter vector containing the model risk-neutral parameter and risk premiums at time t.

Panel A (B) of Table 9 reports the in-sample average RMSE of the IV (in-sample absolute pricing errors) for each model. First, we force on the type of Merton's jumps, the ranking of the models is consistent with our prior, the SV-MJ-JV model outperforms the SV-MJ model and finally the SV model. In Panel A (B) of Table 9, SV-MJ-JV model produces an average RMSE of the IV of 13.55%(3.30) versus 13.84%(3.46) by the SV-MJ model. Second, in the

type of double-exponential jumps, the ranking of the models is also consistent with our prior, the SV-DEJ-JV model outperforms the SV-DEJ model and finally the SV model. In Panel A(B) of Table 9, SV-DEJ-JV model produces an average RMSE of the IV of 12.43%(3.11) versus 12.95%(3.19) by the SV-DEJ model. Third, in the type of the infinite-activity jumps, the SV-VG model does not outperform all others. For example, in the Panel A of Table 9, the SV-VG model produces an average RMSE of the implied volatility(absolute pricing errors) of 13.51%(3.49) versus 12.98%(3.48) by the SV-NIG model. Overall, the SV-DEJ-JV model outperforms all others, following by the SV-DEJ, and finally the SV-NIG model.

Panel C of Table 9 reports Diebold-Mariano (DM) pairwise statistics for weekly RIVRMSE. The DM statistics measure the difference between the squared pricing error of the Benchmark model X and the Test model Y. Note that a positive and significant value for DM statistic means that X has a larger RIVRMSE than Y. Looking at the first row of Panel C of Table 9 reveals that all test statistics are positive and significant at 5% level for a one-sided test, suggesting that all jump models significantly outperform the SV model. Looking at the pairwise tests under column SV-DEJ-JV, the SV-DEJ-JV model outperforms other models all positive statistics and significant level at 5%. Moreover, the pairwise test statistic under column SV-NIG and row SV-DEJ-JV shows that the SV-NIG model underperforms the SV-DEJ-JV model, i.e., the test statistic is -4.41. Overall, we find strong evidence that among the jump models, the SV-DEJ-JV model has a significant difference to other models and the smallest squared in-sample pricing errors.

4.3.3. Out-of-sample pricing performance

To examine out-of-sample cross-sectional pricing performance for each model. The out-of-sample average absolute pricing errors can be represented as follows:

$$\varepsilon^{A}_{t+1,out-of-sample} = \frac{1}{m_t}\sum_{j=1}^{m_t} |O^{\text{BS}}_{t+1,j} - O^{\text{Model}}_{t+1,j}|, \quad t = 0, ..., T-1, \tag{18}$$

where $IV_{t+1}\left(O^{\text{BS}}_{t+1,j}\right)$ is the Black-Scholes IV of the j-th market-observed call options price $O^{\text{BS}}_{t+1,j} = C\left(S_{t+1,j}, K_{t+1,j}, r_{t+1,j}, \tau_{t+1,j}\right)$ at time $t+1$, $IV_{t+1}\left(O^{\text{Model}}_{t+1,j}\right)$ is the Black-Scholes IV of the j-th call options price $O^{\text{Model}}_{t+1,j} = C\left(\Theta_t | S_{t+1,j}, K_{t+1,j}, r_{t+1,j}, \tau_{t+1,j}\right)$, computed using the specific model at time $t+1$.

Panel A (B) of Table 10 reports the out-of-sample average RMSE of the IV (out-of-sample absolute pricing errors) for each model. First, we force on the type of Merton's jumps, the ranking of the models is consistent with our prior, the SV-MJ-JV model outperforms the SV-MJ model and finally the SV model. In Panel A (B) of Table 10, SV-MJ-JV model

produces an average RMSE of the IV of 16,94% (4.31) versus 17.43% (4.46) by the SV-MJ model. Second, in the type of double-exponential jumps, the ranking of the models is also consistent with our prior, the SV-DEJ-JV model outperforms the SV-DEJ model and finally the SV model. In Panel A (B) of Table 10, SV-DEJ-JV model produces an average RMSE of the IV of 16.72% (4.22) versus 16.79% (4.24) by the SV-DEJ model. Third, in the type of the infinite-activity jumps, the SV-VG model does not outperform all others. For example, in the Panel A of Table 10, the SV-VG model produces an average RMSE of the implied volatility(absolute pricing errors) of 17.40% (4.52) versus 16.81% (4.43) by the SV-NIG model. Overall, the SV-DEJ-JV model outperforms all others, following by the SV-DEJ, and finally the SV-NIG model, and this ranking result is the same to in-sample testing.

Panel C of Table 10 reports Diebold-Mariano (DM) pairwise statistics for weekly RIVRMSE. Looking at the first row of Panel C of Table 10 reveals that the SV-DEJ-JV model significantly outperforms the SV model at 5% level and the SV-DEJ model and the SV-MJ-JV model are significantly outperform the SV model at 10% level. Moreover, the pairwise test statistic under column SV-NIG and row SV-VG shows that the SV-NIG model performs the SV-VG model, i.e., the test statistic is 1.54 at significant level 10%. Overall, we find slight evidence that among the jump models, the SV-DEJ-JV model has the difference to other models and the smallest squared out-of-sample pricing errors.

4.4. Time-varying risk premia

In this subsection, we turn to analyze the dynamic properties of risk premiums. The model in equations 1 and 2 features four main instantaneous risk premiums: A price diffusive risk premium (PDRP), a price jump risk premium (PJRP), a diffusive variance risk premium (DVRP), and variance jump risk premium (VJRP). which are defined as

$$\begin{aligned} \text{PDRP}_t &= \eta_s \times v_t, \quad \text{PJRP}_t = \psi_J^{\mathbb{P}}(-i) - \psi_J^{\mathbb{Q}}(-i), \\ \text{DVRP}_t &= \eta_v \times v_t, \quad \text{VJRP}_t = \mu_v^{\mathbb{Q}}\lambda_v^{\mathbb{Q}} - \mu_v^{\mathbb{P}}\lambda_v^{\mathbb{P}}, \end{aligned} \tag{19}$$

where the PDRP_t and DVRP_t are the linear function of the latent variable, v_t, with the equity and volatility risk premium coefficients (Heston (1993)). PJRP_t and VJRP_t are the difference of compensations of price and volatility jump risk between $\mathbb{P}$ and $\mathbb{Q}$, respectively. In the Table 2, our estimation emphasizes that the separation between the jump size and jump intensity[14] where the usual practice in the empirical option pricing literature that

[14] Du and Luo (2018) evidence that the differentiation between jump size and jump intensity risk premium follows their distinct impacts on the term structure of option-implied volatility skew.

focuses on the jump size premium by constrainting, $\lambda^{\mathbb{P}} = \lambda^{\mathbb{Q}}$ (Pan (2002), Eraker (2004), Broadie, Chernov, and Johannes (2007), Aït-Sahalia, Karaman, and Mancini (2018)).

In this paper, we mainly focus on discussing the economic implications of the time-varying PJRP and VRP where PDRP had discussed in a few papers (Bollerslev and Todorov (2011); Aït-Sahalia, Karaman, and Mancini (2018)). PJRP and VRP are the compensations of risks required by the investors for being exposed to unexpected changes in the jump and the variance risks. The VRP is defined as the wedge between the expectations of the variances of asset returns under the risk-neutral and physical measures which have been interpreted as an indicator of the representative agent's time-varying risk aversion (Todorov (2010); Bollerslev, Gibson and Zhou (2011)), parameter uncertainty (Bollerslev, Tauchen and Zhou (2009)), or economic uncertainty (Drechsler and Yaron (2011); Drechsler (2013)). Under the correlated jump models, we can further decompose VRP into the DVRP and the VJRP.

Using the dynamic joint estimation under $\mathbb{P}$ and $\mathbb{Q}$, we receive the different estimated risk premia coefficient in the Panel D of Table 8. We can recognize that the estimated VRP coefficients are all mean positive values and statistical significance, but jump risk premium coefficients are all mean negative values and not all statistical significance. Panel A of Table 11 reports the PJRPs for each model. The mean and skewness values of PJRP are all positive and kurtosis is all quite large. Therefore, the risk-neutral mean of compensation of the price jump is lower than the objective mean, $\psi_J^{\mathbb{P}}(-i) > \psi_J^{\mathbb{Q}}(-i)$. This economic implication indicates that investors require positive expected return causing by price jump risk (Bollerslev and Todorov (2011)). By dynamic analysis, we obtain the time series of PJRPs in Figure 6. Table 12 take the mean values of each time intervals for PJRP_ts in the Figure 6 with red lines. We find that the average PJRP of the SV-DEJ-JV model is significantly increasing from 0.003% to 0.019% during and after the large shock time period in the financial crisis. This special pattern also appears in during and after the large shock time period in the European debt crisis. These patterns illustrate that investors reflect the panic of bearing jump risk in the post-crisis period more significant and request more expected returns.

Next, we discuss the changing of the time series of PJRP_t estimated by stochastic volatility with the different jump-types. From Panels A, B, C and D of Figure 6, we find that the PJRP_ts of the finite-activity models increase significantly after the large shock time period in the financial crisis, but the PJRP_ts of SV-DEJ and SV-DEJ-JV models are still having this dramatic change during and after the European debt crisis. This estimated result may come from the nature of double-exponential jump, i.e., monotonic decreasing property. Based on this feature, we can connect this result with the characteristic of short-term IV surfaces in Figure 1. As discussed in 4.1, the characteristics of IV surface represent different investors'

reflection to volatility and jump risks. The investors may tend to hedge the volatility risk during the large shock time periods. However, this mentality may decrease after these time periods and is gradually being replaced by the reaction of a panic of bearing jump risk. That is, the slope of the term structure of IVs will decline, but the curvature of IVs will rise.

In section 4.1, we further discuss the pattern of Slope 1 and Slope 2 representing the investors' attitude that might be attributed to the downside and upside jump risks, respectively. Due to the monotonic structure of the double-exponential jump (label DEJ) (**?**Kou2016)), the models can capture the large negative and positive jump under $\mathbb{P}$ and also fit the OTM and ATM short-term IV under $\mathbb{Q}$. In contrast to the DEJ, the normal distribution with negative mean does not have a monotone structure. It focuses on capture the large negative jump and tuning the downside jump risk premium, that is, it only emphasis on fitting the OTM short-term IV. In Panel D of Figure 1, Slope 1 significantly rise after the large shock time period in the financial crisis but slightly rise after the large shock time period in the European debt crisis. In Panel E of Figure 1, Slope 2 significantly rise after the large shock time period in both the financial crisis and European debt crisis. This feature may cause the PJRPs of the SV-DEJ and SV-DEJ-JV models to increase significantly after the large shock time periods in both the financial crisis and the European debt crisis. However, the PJRP_t of Merton's jump can significantly increase after the financial crisis but not after the European debt crisis in Panels A and B of Figure 6. In the Panels E and F of Figure 6, we find that the PJRP_ts are relatively smaller than the finite-activity jump models. This estimated result might be attributed to the properties of the infinite-activity jump models which emphasize on fitting the small jumps. Since we find that the return variations is mainly explained by the stochastic volatility, small jump risk premiums are replaced by the volatility risk premium and thus the PJRP_t is relatively smaller.

Panel B of Table 11 reports the DVRP for each model resulting from the model estimation. We find that the mean values range from 0.006% to 0.149%. This reflects that the speed of mean reversion and the mean-reversion level of the variance are both smaller under the risk-neutral measure, i.e., $\kappa^{\mathbb{P}} - \kappa^{\mathbb{Q}} > 0$ and $\theta^{\mathbb{P}} - \theta^{\mathbb{Q}} > 0$ in equation 4. That is, the investors consider that the return variations will reverse quickly to the long-term mean and do not continue to happen the large shocks. However, the minimum of the DVRP of each model is all negative[15] range from -0.831% to -0.042%. To better understand this result, we study the time series of the DVRPs. Panels of Figure 5 plots that the DVRPs fluctuate between positive and negative values and is generally large than zero, the exception occurs on September 15, 2008 to March 23, 2009 during the financial crisis and August 4, 2011 to November 11, 2011 during the European debt crisis when the DVRP takes extreme negative

[15]The negative sign of the variance risk premium is discuss in Bakshi and Kapadia (2003), Carr and Wu (2009).

values. The dynamic pattern of the DVRP in all Panels of Figure 5 are consisted with the estimates resulting from nonparametric models and plot the sign and shape of the DVRP consistent across different models. All DVRPs display the great variability and the dramatic decrease of DVRPs takes place simultaneously around Lehman Brothers' bankruptcy. These negative spikes might be attributed to the term structure of IV surface in Panel D of Figure 1. Average negative values of the DVRPs are consistent with the fact that investors in the market regard diffusion variance risk as unfavorable and therefore willing to pay a premium to hedge against a market crash increase after extreme events happening.

Take the SV-DEJ-JV model as an example, the annualized average DVRP is approximate to -0.029% and 0.003% during the large shock time period in the financial crisis and the European debt crisis, respectively. This is essentially due to the dramatic increase in the instantaneous volatility in Figure 2 and the properties of the IV surface in Figure 1. Before August 2007 (mid-2007), the DVRP stays around zero until Lehman Brothers' bankruptcy (September 2007) in Figure 5. It reaches its peak of about -0.174% meaning that investors are willing to pay 0.174% of their notional per year to be hedged against variance fluctuations during the financial crisis, followed by a recovery period, bringing the DVRP up to 0.460%. The European debt crisis prompts a second drop to -0.039%, followed by a second recovery period, bringing the DVRP up to 0.324%. In the large shock time period, we obtain different economic implications that the speed of mean reversion and the mean-reversion level of the variance are both larger under the risk-neutral measure (Broadie, Chernov, and Johannes (2007)). That is, the investors expect that the return variations will not rapidly return to the long-term mean and may continue to happen the large shocks. The signs and magnitudes of the VRP suggest that investors are willing to pay a premium for an asset that pays off when the variance is high. After these time periods (2) and (4), the DVRPs in the time intervals (3) and (5) become to all positive and larger than last time period, respectively; for example, the DVRP of the SV-DEJ-JV model change from -0.029% in the time interval (2) to 0.114% in the time interval (3) in the Panel A of Table 12. These facts indicate that investors are particularly averse to price fluctuations during periods of market turmoil.

Panel C of Table 11 report the estimated VJRPs of the SV-MJ-JV and SV-DEJ-JV models. This risk premium is estimated to be positive but small[16]. This estimated result might be attributed to the trajectory of latent variables of volatility jump risk using particle filter, smoothing filter, and EM algorithm to track. Moreover, we further investigate that the VJRP of the SV-DEJ-JV model can be decomposed into VUJRP and VDJRP where VUJRP is estimated to be negative -2.06E-06, and VDJRP is estimated to be positive 2.72E-

[16] Eraker, Johannes, and Polson (2003) and Eraker (2004) set $\mu_v^{\mathbb{P}} = \mu_v^{\mathbb{Q}}$ because it does not substantially change our estimates of risk premia based on the model in the equation 1 and 2.

06. That is, the investors are willing to hedge the variance downside jump risk and to take the variance upside jump risk.

4.5. Return predictability

4.5.1. In-sample predictions

Bollerslev, Tauchen and Zhou (2009), using the difference between risk-neutral and realized return expectations of the forward aggregate market variances as proxy for the VRP, find that the VRP has a significant in-sample predictive power of future market returns in short run (quarterly horizon (3 months) to semi-annual horizon (six-months)). This predictability tapers off for longer horizons beyond 6 months. This finding is robust and has been confirmed in subsequent papers[17]. More generally, as we work in an affine framework and the diffusion VRP in equation 19 is a linear function of the state variable, i.e., stochastic volatility v_t, we investigate the predictive power of the diffusion variance risk premium (DVRP) of the SV-DEJ-JV model which has the best fitting performance in both spot and option markets discussed in section 4.2 and section 4.3 on the S&P500 excess returns. All in-sample predictive regressions presented in this section have the following form,

$$r_{t,t+h} = \beta_0(h) + \beta_1(h) DVRP_t + u_{t,t+h}, \tag{20}$$

where $r_{t,t+h}$ is the S&P500 log excess return from the first day of next month $t+1$ to the last day of month $t+h$, depending on the horizon h. The horizon range from h=1 to h=18. We perform the predictive analysis at weekly frequency. The weekly DVRP_t is estimated using the processes discussed in section 3. For statistical inference on the slope coefficient $\beta_1(h)$ in the overlapping multi-period regression, we use the regular heteroskedasticity and autocorrelation robust Newey and West (1987) t-statistic with a lag length equal to two times the return horizon, $2h$[18], to correct for auto-correlation introduced by overlapping data.

The results of in-sample ordinary least squares (OLS) regression are summarized in Table 13, which reports the estimated parameters for all regressions, including univariate regression using a single explanatory variable DVRP and weekly observations. In Panel A of Table 13 and Figure 10, when using the DVRP as the sole explanatory variable and for

[17]See also Drechsler and Yaron (2011), Drechsler (2013), Bollerslev, Marrone, Xu and Zhou (2014), Bollerslev, Todorov, and Xu (2015), Bandi and Reno (2016),Carr and Wu (2016), Bardgett, Gourier, and Leippold (2018), Buss, Schoenleber, and Vilkov (2018), Kilic and Shaliastovich (2018), Fan, Xiao, and Zhou (2018), and Li and Zinna (2018). Moreover, these findings are distinctly different from the longer-run multiyear return predictability patterns, in which the predictability is typically associated with popular predictor variables such as dividend yields, price-to-earnings (P/E) ratio, the default spread, or consumption-wealth ratios (see Fama and French (1988), Campbell and Shiller (1988), and Ang and Bekaert (2007), among others.).

[18]This setup is consistent with the approach of Bollerslev, Todorov, and Xu (2015).

2007:01 to 2017:08 sample period, it is highly statistically significant for horizons of up to 4 months, with a maximum adjusted R^2 5.40%[19]. Panel A of Figure 10 show that the adjusted R^2 displays a tent-shaped pattern: it ranges from 2.79% at the one-month horizon to 5.40% at four-month and then decreases at longer maturities. As we see from Table 13, the OLS estimate of β_1 in equation 20 is positive, confirming the usual results: the larger the DVRP (in absolute value), the larger future returns on average, and highly statistically significant for the forecasting horizons ranging from one to five months. For the longer horizons, the DVRP has weak explanatory power and the coefficient β_1 is even smaller than 0.2 which is approximate one-third of the β_1 of the quarterly horizon.

Figure 7 presents results on the relation between the different horizon excess returns and the SV-DEJ-JV model's DVRP. The SV-DEJ-JV model's DVRP is estimated from the implied volatility surface of the S&P500 index options discussed in the section 3. We plot the pairwise combinations for horizons of one, three, six, and 12 (one-year) months (Panel A to D). The dash line represents the regression fit to all the observations with slope coefficient and R^2 reported in the plot legend. The solid line represents the regression fit to the blue observations with slope coefficient and R^2 reported in the plot legend. The blue observations are the dots that the absolute values of the DVRP are greater than or equal to 0.01%. The orange observations are the dots that the absolute values of the DVRP are smaller than 0.01%. The date is weekly from January 2007 to August 2017. In the Panel D of Figure 7, the orange dots (the absolute of DVRP is small or equal to 0.01) do not have the predictability from the annualized excess return -0.6% to 0.4%. This result shows that the large of small DVRPs are noise and may not have predictability to excess return. Therefore, we set the filter which DVRP is large than 0.01% to run our regression.

In Panel C of Table 13 and Figure 10, for 2008:09 to 2009:03 sample period (Large shock period during the 2008-2009 financial crisis), DVRP has the β_1 estimate (2.179) with the largest adjusted R^2 statistics of 34.96%. Moreover, the return predictability of DVRP can be extended to one year (12 months) in this period. In Panel D of Table 13 and Figure 10, DVRP has the β_1 estimate (0.24) with the largest adjusted R^2 statistics of 1.28% for 2009:07 to 2017:08 sample period (The period after the 2008-2009 financial crisis). Although the economic significance is smaller than 2008:09 to 2009:03 period, it still can achieve the statistical significance levels as 5% for 4 months horizon. Overall, these results report that the DVRP is a powerful predictive factor for excess return which particularly has return predictability concentrate in the large fluctuation during the Great Recession (Bad time) (see Cujean and Hasler (2017)).

[19]These results are similar to the findings in Bollerslev, Tauchen and Zhou (2009), Bollerslev, Marrone, Xu and Zhou (2014), Bardgett, Gourier, and Leippold (2018), and Buss, Schoenleber, and Vilkov (2018), who demonstrate that the variance risk premium can predict market excess returns for a horizon of up to three or four months and then goes down.

Figure 8 analyzes the relation between the different horizon excess returns and the SV-DEJ-JV model's DVRP and particularly focus on analyzing the economic meaning during the financial crisis. We plot the pairwise combinations for horizons of three, four, five, and six months (Panel A to D). The red solid line represents the regression fit to the red crosses with slope coefficient and R^2 reported in the plot legend. The yellow squares are the observations from August 1, 2007 to September 15, 2008 (Before the large shock time period in the financial crisis). The red crosses are the observations from September 15, 2008 to March 23, 2009 (During the large shock time period in the financial crisis). The purple triangles are the observations from March 23, 2009 to October 1, 2010 (After the large shock time period in the financial crisis and before the large shock time period in the European debt crisis). The remaining observations are blue observations. We can find that DVRP have the significant predictability power during the large shock period in the financial crisis (red crosses).

Johnson (2018) argues that the predictive slope of the VRP is insignificant with weighted least squares (WLS) if we test on the original sample of Bollerslev, Tauchen and Zhou (2009), 1990-2007. He claims that the return predictability of VRP is driven by several extreme events with high volatility, such as the financial crisis and the European debt crisis. To check for the possibility that using WLS may alter the results, in addition to OLS, I also consider WLS. Table 14 summarizes the WLS regression coefficient, p-values, and adjusted R^2 for the different horizons and time periods. In Panel A of Table 14, we WLS slope is not much different in magnitude, although it is slightly smaller. Overall, the regression coefficient is statistically significant with smaller p-value with adjusted R^2 1.12% than the OLS regression. These results are consistent with Johnson (2018) that the level of significance of the VRP predictive regressions is not largely affected by using WLS. Moreover,we also run a predictive regression for subsamples. Panel C of Table 14 reports that 2008:09-2009:03 sample period has the largest adjusted R^2 of 24.71% with estimates β_1 of 2.17 which is also slightly smaller than OLS regression, but it still has the high and statistically significant during this period. Overall, the predictive power of the DVRP depends on the relationship between returns and variance innovations.

In sum, similar to earlier studies, we find evidence of short-run equity return predictability when conditioning on the DVRP. Moreover, we also show that the return predictability of DVRP mainly concentrate during the high fluctuation period in the financial crisis. The results are largely unchanged when we use the WLS to test the regression results.

4.5.2. Out-of-sample predictions

We use the traditional approach to providing out-of-sample (OOS) forecast[20] of time $t+h$ excess returns consists of two stages. First, we run a predictive regression 20 using pass k months of historical data (from time $t-k-1$ to t). Then, we use the coefficient estimated at time t to forecast S&P500 excess return for horizon h, $\widehat{r}_{t,t+h}$. For out-of-sample predictive regression, we calculate a return forecast as

$$\widehat{r}_{t,t+h} = \widehat{\beta}_0(h) + \widehat{\beta}_1(h) DVRP_t, \tag{21}$$

where $\widehat{\beta}_0$ and $\widehat{\beta}_1$ are OLS estimates from regression 20.

Next, we follow Goyal and Welch (2008) and Campbell and Thompson (2008) to use OOS R^2 to evaluate the OOS predictive performance. The OOS R^2 is defined as

$$\begin{aligned} \text{OOS } R^2_h = 1 - \frac{\text{MSE}_\text{h}}{\text{MSE}_{bm}}, \quad \text{MSE}_\text{h} = \frac{1}{T}\sum_{t=1}^{T}\left(r_{t,t+h} - \widehat{r}_{t,t+h}\right)^2, \\ \text{and} \quad \text{MSE}_\text{bm} = \frac{1}{T}\sum_{t=1}^{T}\left(r_{t,t+h} - \bar{r}_{t,t+h}\right)^2, \end{aligned} \tag{22}$$

where T is the number of observations in the post-training sample period. MSE_h is the mean-squared forecast error of the predictive regression, and MSE_{bm} is the benchmark mean-squared forecast error using the average excess return $\bar{r}_{t,t+h}$ from the beginning of the sample through month t that we follow Goyal and Welch (2008) and Campbell and Thompson (2008) to use the market's historical average excess returns as an equity premium forecast. If the OOS R^2 is positive, then the predictive regression has lower average mean-squared prediction error than the historical average return. We follow Pyun (2018) to use Giacomini and White (2006)'s Wald statistic to test the significance of the predictor. The Wald statistic is given as

$$W = T\left(T^{-1}\sum_{t=1}^{T}\Delta L_{t+1}\right)\widehat{\Omega}^{-1}\left(T^{-1}\sum_{t=1}^{T}\Delta L_{t+1}\right), \tag{23}$$

where $\Delta L_{t+1} = \left(\bar{r}_{t,t+h} - r_{t,t+h}\right)^2 - \left(\widehat{r}_{t,t+h} - r_{t,t+h}\right)^2$ and $\widehat{\Omega}^{-1} = \frac{1}{T}\sum_{t=1}^{T}\left(\Delta L_{t+1} - \overline{\Delta L}\right)^2$. Asymptotically, this Wald statistic follows a Chi-square distribution with degrees of freedom equal to the difference in the number of predictors.

Each of the OOS R^2 values is computed by comparing the performance using the historical

[20] See also Dangl and Halling (2012), Henkel (2011), Johannes, Polson, and Stroud (2014), Pettenuzzo, Timmermann, and Valkanov (2014), Rapach, Ringgenberg, and Zhou (2016), Pyun (2018), Fan, Xiao, and Zhou (2018), and Johnson (2018).

average as the predictor. We use the rolling window of the past one year of data to compute the historical mean as a benchmark. Table 15 reports the OOS R^2 and Wald statistic, along with p-values, for the different horizons and time periods. As shown in Goyal and Welch (2008), many variables can significantly predict market return in-sample tests, but most of them perform poorly in the out-of-sample tests. Panel A of Table 15 and Figure 10 show that the OOS R^2 are positive at two- to six-month horizons and the maximum OOS R^2 of 3.46% achieved at three-month horizon. Despite having the positive OOS R^2, none of the predictions of the traditional approach is statistically significant, even at the 10% level. Panel B of Table 15 and Figure 10 show that OOS R^2 are all negative and not significant in 2008:09-2009:03 sample period. This means that it is hard to use the DVRP to predict the excess returns during the large shock period in the financial crisis, because there are many unknown events that the investors in options market did not expect to happen even though in-sample test in section 4.5.1 has significant economical meanings. On the other hand, Panel C of Table 15 and Figure 10 show that OOS R^2 are positive at one- to seven-month horizons and the maximum OOS R^2 of 35.00% achieved at two-month horizon in the time interval after the large shock time period: 2009:03 to 2009:12. This means that the investors in options market were starting to hedging and use the suitable approach to face the fluctuation in the spot market after the large shock period in the financial crisis.

4.5.3. Evaluating economic significance – Asset allocation

Campbell and Thompson (2008) argue that even very small positive Goyal and Welch (2008)'s[21] OOS R^2 explanatory power can signal an economically meaningful degree of return predictability in terms of increased annual portfolio returns for a mean-variance investor. Therefore, we follow Campbell and Thompson (2008), Rapach, Ringgenberg, and Zhou (2016), and Rapach, Strauss, and Zhou (2010) to measure the economic value of DVRP of the SV-DEJ-JV model return predictive ability from an asset allocation perspective. We consider a mean-variance investor who allocates his or her wealth between risky S&P500 index futures and risk-free three-month Treasury bills (T-bills). using a predictive regression forecast of excess stock returns. At the end of month t, the investor optimally allocates the following share of his or her portfolio to equities during the subsequent month. The optimal weights w_t are determined by predicting the future stock return using the predictive regressions:

$$w_t = \frac{\widehat{r}_{t,t+h}}{\zeta \cdot \widehat{\sigma}^2_{t,t+h}}, \tag{24}$$

[21] Goyal and Welch (2008) argue that the historical average excess stock return forecasts future excess stock better than regressions of excess returns on predictor variables.

where ζ is the investor's coefficient of relative risk aversion. $\widehat{r}_{t,t+h}$ and $\widehat{\sigma}^2_{t,t+h}$ are the forecast of excess return and return variance h-month ahead. We use Johnson (2017)'s term structure of VIX^2 from option data[22], VIX$^2_{t,t+h}$, as a forward-looking measure of the excess return variance, because it reflects investor's expectation of return variations in the future. The remaining proportion 1 - w_t is invested in the risk-free asset. Following Campbell and Thompson (2008) Rapach, Ringgenberg, and Zhou (2016) and Fan, Xiao, and Zhou (2018), we consider two scenarios. In the first scenario without short-sale restriction, we restrict the portfolio weight w_t to lie within the range of -0.5 and 1.5, which produces better-behaved portfolio weights given the well-known sensitivity of mean-variance optimal weights to return forecast. In the second scenario with short-sale restriction, we impose a constraint for the portfolio weight to be larger than zero and smaller than 1.5. We also follow Pyun (2018) who had a concern that the weights might rely too much on VRP-based forecasts during periods when returns and variance innovations are unrelated. Therefore, we consider an alternative strategy, the weight invested in the risky asset becomes

$$w_t = \frac{\widehat{r}_{t,t+h}}{\zeta \cdot \widehat{\sigma}^2_{t,t+h}} \sqrt{\widehat{\rho}^2_t} + \frac{\bar{r}_{t,t+h}}{\zeta \cdot \widehat{\sigma}^2_{t,t+h}} \sqrt{1 - \widehat{\rho}^2_t}, \tag{25}$$

where $\widehat{\rho}^2_t$ is the estimated correlation between index return and variance innovation using the estimated method in section 3. To distinguish this strategy formed on the conditional value of the correlation from the basic trading strategy, we call this the conditional trading strategy and the first one as the unconditional trading strategy.

The certain equivalent return (CER) for investor who allocates assets using equation 24 or equation 25 is computed as

$$CE = \bar{R}_p - \frac{\zeta}{2} \widehat{\mathrm{Var}}\left(R_p\right) \tag{26}$$

where $\bar{R}_p$ and $\widehat{\mathrm{Var}}\left(R_p\right)$ are the sample mean and variance of the portfolio returns, respectively. We also compute the CER for the investor when he or she uses the prevailing mean[23] as excess return forecast and VIX^2 term structure as variance forecast. The CER gain is then the difference between the CER for the investor when he or she uses the predictive regression forecast to guide asset allocation and the CER when he or she uses the prevailing mean benchmark forecast. We annualize the CER gain so that it can be interpreted as the annual portfolio management fee that the investor would be willing to pay to have access to the predictive regression forecast in place of the prevailing mean forecast. In this way, we

[22]The VIX term structure date can be available download from Travis L. Johnson's webpage at http://travislakejohnson.com/data.html.

[23]The historical mean is assumed to be the best predictor of future returns.

measure the direct economic value of return predictability. To analyze the economic value of return predictability at longer horizons, we follow Rapach, Ringgenberg, and Zhou (2016) to assume that the investor rebalances at the same frequency as the forecast horizon.

The results of OOS annualized CER and CER gains for the entire 2008:01-2017:08 forecast evaluation period are reported in Table 16. In Panel A of Table 16, we report the CER and CER gains of the unconditional trading strategies based on DVRP when there are with/without short-selling constraint on the portfolio weight. The predictive regressions of DVRP are able to generate positive CER gains from quarterly horizons (three-month) to the annual horizon (twelve-month) with a relative risk aversion coefficient $\zeta = 3$, 4, and 5 under the without short selling constraint. The performance of DVRP clearly stands out. DVRP almost always generate higher CER gains than buy-and-hold[24] trading strategy, suggesting that the DVRP measure has economic value for a risk-averse investor. For the unconditional trading strategy, the gains in CER are extremely smaller and negative when an investor uses the buy-and-hold trading strategy, but increase substantially when using the DVRP to construct the trading strategy. DVRP achieves the highest CER gains at three-month to nine-month with different levels of risk aversion. When ζ is equal to 3 and without selling short constraint, DVRP provides the highest CER gain of 166 basis points at the quarterly horizon. As reported in Rapach, Ringgenberg, and Zhou (2016), most of the popular predictors generate negative CER gains. The performance of DVRP is comparable to that of short interest documented in Rapach, Ringgenberg, and Zhou (2016) from three-month to twelve-month under the without short selling constraint. At one year horizon, the CER gains of DVRP are still considerably larger than that of the buy-and-hold trading strategy which is negative at all horizons and the levels of risk aversion. On the other hand, we also report the CER gains when the portfolio weights are updated with short-selling constraints. The overall result is not similar to without short-selling constraints, DVRP generates smaller CER gains of 18, -59, and -84 basis points for $\zeta = 3$, 4, and 5 at the quarterly horizon.

In Panel B of Table 16, we report the CER and CER gains of conditional trading strategies. Although the predictive regressions of DVRP are not able to generate all positive CER gains through the different horizons and risk-aversion coefficients, it generates the higher CER gain than the unconditional trading strategy when the horizon is short-term. For example, when the risk-aversion coefficient is equal to 4 and horizon is three-month, the CER gains are 159 basis points for the conditional trading strategy which is larger than 82 basis points for the unconditional trading strategy. However, the performances are slightly worse for the conditional trading strategies compared to the unconditional trading strategies

[24]The investor holds the fixed weight on the market portfolio and this trading strategy serves as a benchmark.

when the horizons are more than three-month. As discussed, this is presumably because the correlation between the return and variance innovations may be a temporal relationship. These results also indicate that predictions under unconditional trading strategy could be misleading during short-term periods when returns and variance innovations are unrelated.

Table 17 reports OOS annualized SRs and SR gains for the entire 2008:01-2017:08 forecast evaluation period, which allow us to compare portfolio performance independently of relative risk aversion. In Panel A of Table 17, the SRs for the portfolio based on the benchmark buy-and-hold trading strategy range from 0.20 to 0.22 at the various horizons when the risk-aversion coefficient is equal to 3. DVRP produces SRs that range from 0.35 to 0.50. Clearly, the SRs of DVRP are approximately two times larger than the buy-and-hold trading strategy. From Table 17, we can find that the SRs and SRs gain of DVRP are always greater than those for the buy-and-hold trading strategy through the different horizons and risk-aversion coefficients.

5. Conclusion

In this paper, we attempt to answer four questions: (i) On average, what do the proportion of the stochastic volatility and return jumps account for the total return variations in S&P500 index? In particular, which one has more influence than the other does on the total return variations? (ii) Is the fitting performance of infinite-activity jump models better than that of finite-activity jump models both in the spot and option markets? (iii) When will investors require significantly higher risk premiums? Specifically, were there significant changes in volatility and jump risk premiums during the time period of the extreme events? (iv) Does the model-based variance risk premium have predictive power on S&P500 returns?

For the first question, we find that most of the return variations are explained by the stochastic volatility. In fact, the return jump accounts for the higher percentage than the stochastic volatility at the beginning of the crises. To answer the second question, we adopt the EM algorithm with the particle filter and dynamic joint estimation to obtain the stochastic volatility model with double-exponential jumps and correlated jumps in volatility and the stochastic volatility model with normal inverse Gaussian jumps fit S&P500 index returns and options well in different criterion. For the third question, we observe that the time-varying volatility and jump risk premiums have different changing behaviours during the crises. In particular, the jump risk premiums significantly increase after each crisis periods, that is, the panic of bearing jump risk in the post-crisis period causes investors to require more expected returns. Finally, for the fourth question, we find that DVRP has predictive power both in-sample and out-of-sample, with adjusted R^2 statistics of 5.40% and 3.46%, respectively.

We further investigate the economic significance of the out-of-sample predictability on the basis of asset allocations with DVRP, and the mean-variance portfolio generates substantial economic gains of over 166 basis points and a Sharpe ratio of 0.44 per annum at three-month horizon.

References

Aït-Sahalia, Y., Lo, A., 1998, Nonparametric estimation of state-price densities implicit in financial asset prices, *Journal of Finance*, Vol. 53, 499-547.

Aït-Sahalia, Y., 2004, Disentangling diffusion from jumps, *Journal of Financial Economics*, Vol. 74, 487-528.

Aït-Sahalia, Y., Karaman, M., Mancini, L., 2018, The term structure of variance swaps and risk premia, *Swiss Finance Institute Research Paper*, 18-37.

Andersen, T., L. Benzoni, J. Lund., 2002, An empirical investigation of continuous-time equity return models, *Journal of Finance*, Vol. 57, 1239-1284.

Andersen, T. G., T. Bollerslev, F. X. Diebold., 2007, Roughing it up: Including jump components in the measurement, modelling, and forecasting of return volatility, *Review of Economics and Statistics*, Vol. 89, 701-720.

Andersen, T., Fusari, N., Todorov, V., 2015a, Parametric inference and dynamic state recovery from option panels, *Econometrica*, Vol. 83, 1081-1145.

Andersen, T., Fusari, N., Todorov, V., 2015b, The risk premia embedded in index options, *Journal of Financial Economics*, Vol. 117, 558-584.

Ang, A., Bekaert, G., 2007, Stock return predictability: Is it there?, *Review of Financial Studies*, Vol. 20, 651-707.

Bates, D. S., 1996, Jumps and stochastic volatility: exchange rate processes implicit in Deutsche Mark options, *Review of Financial Studies*, Vol. 9, 69-107.

Bates, D.S., 2000, Post 87 crash fears in the S&P 500 futures option market, *Journal of Econometrics*, Vol. 94, 181-238.

Bates, D, S., 2006, Maximum likelihood estimation of latent affine processes, *Review of Financial Studies*, Vol. 19, 909-965.

Bates, D, S., 2012, US stock market crash risk, 1926–2010, *Journal of Financial Economics*, Vol. 105, 229-259.

Bakshi, G., Cao, C., Chen, Z., 1997, Empirical performance of alternative option pricing models, *Journal of Finance*, Vol. 52, 2003-2049.

Bakshi, G., Madan, D., 2000, Spanning and derivative-security valuation, *Journal of Financial Economics*, Vol. 55, 205-238.

Bakshi, G., Kapadia, N., 2003, Delta-hedged gains and the negative market volatility risk premium, *Review of Financial Studies*, Vol. 16, 527-566.

Bakshi, G., Carr, P., Wu, L., 2008, Stochastic risk premiums, stochastic skewness in currency options, and stochastic discount factors in international economies, *Journal of Financial Economics*, Vol. 87, 132-156.

Bakshi, G., Wu, L. 2010, The behavior of risk and market prices of risk over the Nasdaq bubble period, *Management Science*, Vol. 56, 2251-2264.

Bandi, F., Reno, R., 2016, Price and volatility co-jumps, *Journal of Financial Economics*, Vol. 119, 107-146.

Bardgett, C., Gourier, E., Leippold, M., 2018, Inferring volatility dynamics and risk premia from the S&P 500 ad VIX markets, *Journal of Financial Economics*, Vol. 17, 1-26.

Barndorff-Nielsen, O.E., 1997, Normal inverse Gaussian distributions and stochastic volatility modelling, *Journal of Statistics*, Vol. 24, 1-13.

Barndorff-Nielsen, O.E., 1998, Processes of normal inverse Gaussian type, *Finance And Stochastics*, Vol. 2, 41-68.

Black, F., Scholes, M., 1973, The pricing of options and corporate liabilities, *Journal of Political Economy*, Vol. 81, 637-654.

Black, F., 1976, Studies of stock price volatility changes, *In: Proceedings of the 1976 Meeting of the Business and Economic Statistics Section, American Statistical Association, Washington DC*, 177-181.

Bollerslev, T., Tauchen, G., Zhou, H., 2009, Expected stock returns and variance risk premia, *Review of Financial Studies*, Vol. 22, 4463-4492.

Bollerslev, T., Todorov, V., 2011, Tails, fears, and risk premia, *Journal of Finance*, Vol. 66, 2165-2211.

Bollerslev, T., Gibson, M., Zhou, H., 2011, Dynamic estimation of volatility risk premia and investor risk aversion from option-implied and realized volatilities, *Journal of Econometrics*, Vol. 160, 235-245.

Bollerslev, T., Marrone, J., Xu, L., Zhou, H., 2014, Stock return predictability and variance risk premia: statistical inference and international evidence, *Journal of Financial and Quantitative Analysis*, Vol. 49, 633-661.

Bollerslev, T., Todorov, V., Xu, L., 2015, Tail risk premia and return predictability, *Journal of Financial Economics*, Vol. 118, 113-134.

Broadie, M., Chernov, M., Johannes, M., 2007, Model specification and risk premia: evidence from futures options, *Journal of Finance*, Vol. 62, 1453-1490.

Buss, A., Schoenleber, L., Vilkov, G., 2018, Expected stock returns and the correlation risk premium, *Working paper*.

Campbell, J., Shiller, R., 1988, Stock prices, earnings, and expected dividends, *Journal of Finance*, Vol. 43, 661-676.

Campbell, J., Thompson, S., 2008, Predicting excess stock returns out of sample: can anything beat the historical average?, *Review of Financial Studies*, Vol. 21, 1509-1531.

Carr, P., Madan, D., 1999, Option valuation using the fast Fourier transform, *Journal of Computational Finance*, Vol. 2, 1-18.

Carr, P., Geman, H., Madan, D., Yor, M., 2003, Stochastic volatility for Levy processes, *Mathematical Finance*, Vol. 13, 345-382.

Carr, P., Wu, L., 2004, Time-changed Levy processes and option pricing, *Journal of Financial Economics*, Vol. 71, 113–141.

Carr, P., Wu, L., 2009, Variance risk premiums, *Review of Financial Studies*, Vol. 22, 1311-1341.

Carr, P., Wu, L., 2016, Analyzing volatility risk and risk premum in option contracts: A new theory, *Journal of Financial Economics*, Vol. 120, 1-20.

Cox, J.C., J.E. Ingersoll, S.A. Ross., 1985, "A theory of the term structure of interest rates", *Econometrica*, Vol. 53, 385-408.

Christoffersen, P., Heston, S., Jacobs, K., 2009, The shape and term structure of the index option smirk: why multifactor stochastic volatility models work so well, *Management Science*, Vol. 55, 1914-1932.

Christoffersen, P., Jacobs, K., Mimouni, K., 2010, Volatility dynamics for the S&P500: Evidence from realized volatility, daily returns, and option prices, *Review of Financial Studies*, Vol. 23, 3141-3189.

Christoffersen, P., Jacobs, K., Ornthanalai, C. 2012, Dynamic jump intensities and risk premiums: Evidence from S&P500 returns and options, *Journal of Financial Economics*, Vol. 106, 447-472.

Chernov, M., Ghysels, E., 2000, A study towards a unified approach to the joint estimation of objective and risk-neutral measures for the purpose of option valuation, *Journal of Financial Economics*, Vol. 56, 407-458.

Cujean, J., Hasler, M., 2017, Why does return predictability concentrate in bad times?, *Journal of Finance*, Vol. 72, 2717-2758.

Dangl, T., Halling, M., 2012, Predictive regressions with time-varying coefficients, *Journal of Financial Economics*, Vol. 106, 157-181.

Diebold, F., Mariano, R., 1995, Comparing predictive accuracy, *Journal of Business and Economic Statistics*, Vol. 13, 134-144.

Duffie, D., Pan, J., Singleton, K., 2000, Transform analysis and asset pricing for affine jump-diffusions, *Econometrica*, Vol. 68, 1343-1376.

Du, D., Luo, D., 2017, The pricing of jump propagation: Evidence from spot and options markets, *Management Science*, Forthcoming.

Drechsler, I., Yaron, A., 2011, What's vol got to do with it?, *Review of Financial Studies*, Vol. 24, 1-45.

Drechsler, I., 2013, Uncertainty, time-varying fear, and asset prices, *Journal of Finance*, Vol. 68, 1843-1889.

Eraker, B., Johannes, M.S., Polson, N., 2003, The impact of jumps in volatility and returns, *Journal of Finance*, Vol. 58, 1269-1300.

Eraker, B., 2004, Do stock prices and volatility jump? Reconciling evidence from spot and option prices, *Journal of Finance*, Vol. 59, 1367-1404.

Esscher, F. 1932, On the probability function in the collective theory of risk, *Skandinavisk Aktuarietidskrift*, Vol. 15, 175–195.

Fama, E., French, K., 1988, Dividend yields and expected stock returns, *Journal of Financial Economics*, Vol. 22, 3-25.

Fan, Z., X. Xiao, H. Zhou, 2018, Variance risk premium, higher order risk premium, and expected stock returns, *Working Paper*

Gerber, H. U., Shiu, Elias S. W., 1994, Option pricing by Esscher transforms, *Transactions of the Society of Actuaries*, Vol. 46, 99–191.

Giacomini, R., White, H., 2006, Tests of conditional predictive ability, *Econometrica*, Vol. 74, 1545-1578.

Gordon, N. J., Salmond, D. J., Smith, A. F. M., 1993, Novel approach to nonlinear non-Gaussian Bayesian state estimation, *IEE-Proceedings F*, Vol. 140, 107-133.

Godsill, S. J., Doucet, A., West, M., 2004, Monte carlo smoothing for nonlinear time series, *Journal of the American Statistical Association*, Vol. 99, 156-168.

Goyal, A., Welch, I., 2008, A comprehensive look at the empirical performance of equity premium predication, *Review of Financial Studies*, Vol. 21, 1455-1508.

Hull, J., White, A., 1987, The pricing of options on assets with stochastic volatilities, *Journal of Finance*, Vol. 42, 281-300.

Heston, S., 1993, A closed-form solution for options with stochastic volatility with applications to bond and currency options, *Review of Financial Studies*, Vol. 6, 327-343.

Henkel, S., Martin, J., Nardari, F., 2011, Time-varying short-horizon predictability, *Journal of Financial Economics*, Vol. 99, 560-580.

Huang, J. Z., Wu, Z., 2004, Specification analysis of option pricing models based on time-changed Lévy processes, *Journal of Finance*, Vol. 59, 1405-1439.

Huang, X., and Tauchen, G., 2005, The relative contribution of jumps to total price variance, *Journal of Financial Econometrics*, Vol. 3, 456-499.

Hu, F., Zidek, J.V, 2002, The weighted likelihood, *Canadian Journal of Statistics*, Vol. 30, 347–371.

Johannes, M., Polson, N., Stroud, J., 2009, Optimal filtering of jump diffusions: Extracting latent states from asset prices, *Review of Financial Studies*, Vol. 22, 2759-2799.

Johannes, M., Korteweg, A., Polson, N., 2014, Sequential learning, predictability, and optimal portfolio returns, *Review of Finance*, Vol. 69, 611-644.

Johnson, T. L., 2017, Risk premia and the VIX term structure, *Journal of Financial and Quantitative Analysis*, Vol. 52, 2461-2490.

Johnson, T. L., 2018, A fresh look at return predictability using a more efficient estimator, *Review of Asset Pricing Studies*, Forthcoming.

Kou, S., 2002, A jump-diffusion model for option pricing, *Management Science*, Vol. 48, 1086-1101.

Kou, S., Yu, C., Zhong, H., 2016, Jumps in equity index returns before and during the recent financial crisis: a Bayesian analysis, *Management Science*, Vol. 4, 988-1010.

Kilic, M., I. Shaliastovich, 2018, Good and bad variance premia and expected returns, *Management Science*, Forthcoming.

Li, J., G. Zinna., 2018, The variance risk premium: components, term structures, and stock return predictability, *Journal of Business and Economic Statistics*, Vol. 36, 411-425.

Kimand, J., Stoffer, D. S., 2008, Fitting stochastic volatility models in the presence of irregular sampling via particle methods and the EM algorithm, *Journal of Time Series Analysis*, Vol. 29, 811-833.

Li, H., Wells, M., Yu, C., 2008, A Bayesian analysis of return dynamics with Lévy jumps, *Review of Financial Studies*, Vol. 21, 2345-2378.

Li H., Wells M., Yu C., 2011, MCMC estimation of Lévy jump models using stock and option prices, *Mathematical Finance*, Vol. 21, 383-422.

Madan, D.B., Seneta, E., 1990, The Variance Gamma (V.G.) Model for Share Market Returns, *Journal of Business*, Vol. 63, 511-24.

Madan, D., P. Carr, E. Chang, 1998, The Variance Gamma Process and Option Pricing, *European Finance Review*, Vol. 2, 79–105.

Martin, I., 2017, What is the expected return on the market?, *Quarterly Journal of Economics*, Vol. 132, 367–433.

Newey, W.K., West, K.D., 2017, A simple, positive semi-definite, heteroskedasticity and autocorrelation consistent covariance matrix, *Econometrica*, Vol. 55, 703–708.

Ornthanalai, C., 2014, Lévy jump risk: evidence from options and returns, *Journal of Financial Economics*, Vol. 112, 69-90.

Pan, J., 2002, The jump-risk premia implicit in options: evidence from an integrated time-series study, *Journal of Financial Economics*, Vol. 63, 3-50.

Pettenuzzo, D., Timmermann, A., Valkanov, R., 2014, Forecasting stock returns under economic constraints, *Journal of Financial Economics*, Vol. 114, 517-553.

Pitt, M. K., Shephard, N., 1999, Filtering via simulation: auxiliary particle filter, *Journal of the American Statistical Association*, Vol. 94, 590-599.

Pitt, M., 2002, Smooth particle filters for likelihood evaluation and maximisation, Unpublished working paper, University of Warwick.

Pyun, S., 2018, Variance risk in aggregate stock returns and time-varying return predictability, *Journal of Financial Economics*, Forthcoming.

Rapach, D. E., Strauss, J. K., Zhou, G., 2010, Out-of-sample equity premium predication: Combination forecasts and links to the real economy, *Review of Financial Studies*, Vol 23, 821-862.

Rapach, D. E., Ringgenberg, M. C., Zhou, G., 2016, Short interest and aggregate stock returns, *Journal of Financial Economics*, Vol 121, 46-65.

Santa-Clara, P., Yan, S., 2010, Crashes, volatility, and the equity premium: lessons from S&P 500 options, *Review of Economics and Statistics*, Vol 92, 435-451.

Todorov, V., 2010, Variance risk premium dynamics: The role of jumps, *Review of Financial Studies*, Vol 23, 345-383.

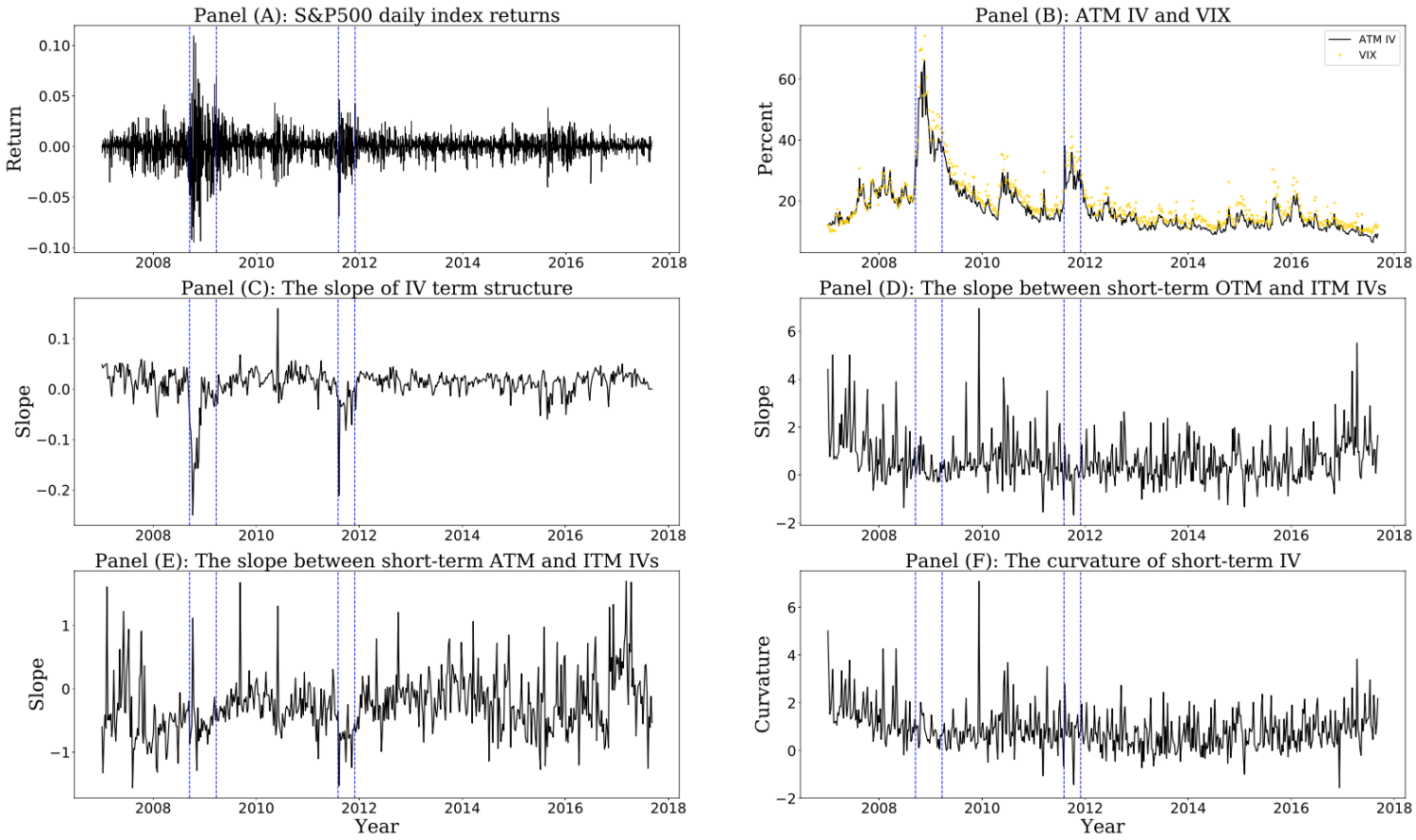

Fig. 1. Daily S&P500 index returns and implied volatility (IV) surface characteristics.

Panel (A) plots the daily S&P500 index returns from January 1, s2007 to August 31, 2017. Panel (B) plots the average weekly IVs for ATM S&P500 options and the weekly VIX index from January 1, 2007 to August 31, 2017. ATM options are those with moneyness between 0.97 and 1.03. From Panel C, the term structure of IVs is the difference between the long- and short-dated ATM IVs. Panel (D) plots the slope between short-term OTM and ITM IVs (label Slope 1). Panel (E) plots the slope between short-term ATM and ITM IVs (label Slope 2). From Panel (F), the curvature of IVs measures the difference between Slope 2 and Slope 1. Short-dated options are those with 30 days to maturity, and long-dated options have 180 days to maturity. ATM options have moneyness equal to 0.92. OTM options have moneyness equal to 1.08. ITM options have moneyness equal 1.00.

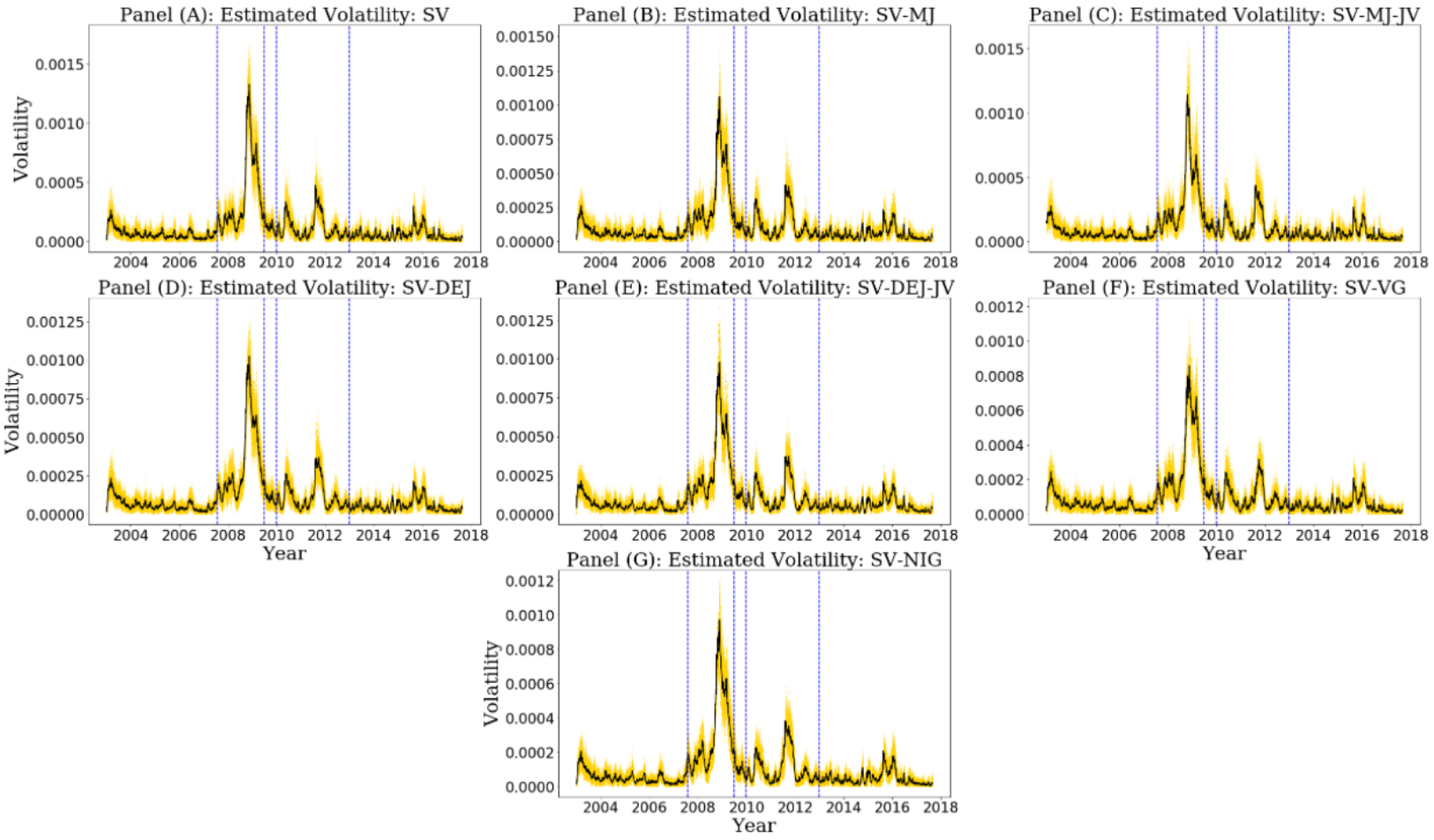

Fig. 2. Filtered latent stochastic volatility.

The panel (A) to panel (G) are the latent stochastic volatility estimated by the particle filtering, smoothing filtering and expectation-maximization (EM) algorithm from the corresponding model using parameters estimated in Table 6. The dotted vertical lines indicate the financial crisis from August 2007 to June 2009 and the European sovereign debt crisis from January 2010 to December 2012, respectively. The yellow marker "o" plots the daily particles.

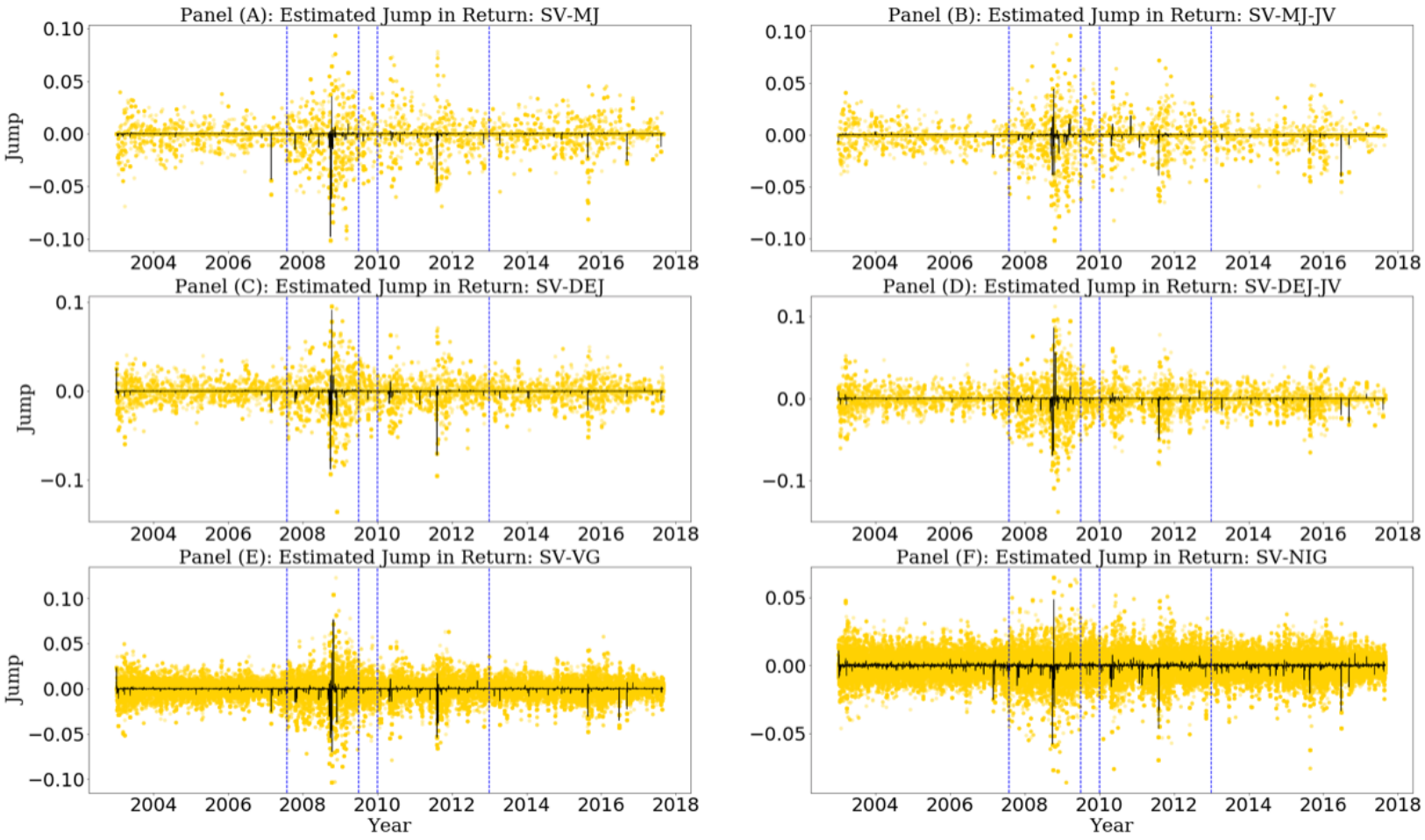

Fig. 3. Filtered latent return jump.

The panel (A) to panel (F) are the latent return jump estimated by the particle filtering, smoothing filtering and expectation-maximization (EM) algorithm from the corresponding model using parameters estimated in Table 6. The dotted vertical lines indicate the financial crisis from August 2007 to June 2009 and the European sovereign debt crisis from January 2010 to December 2012, respectively. The yellow marker "o" plots the daily particles.

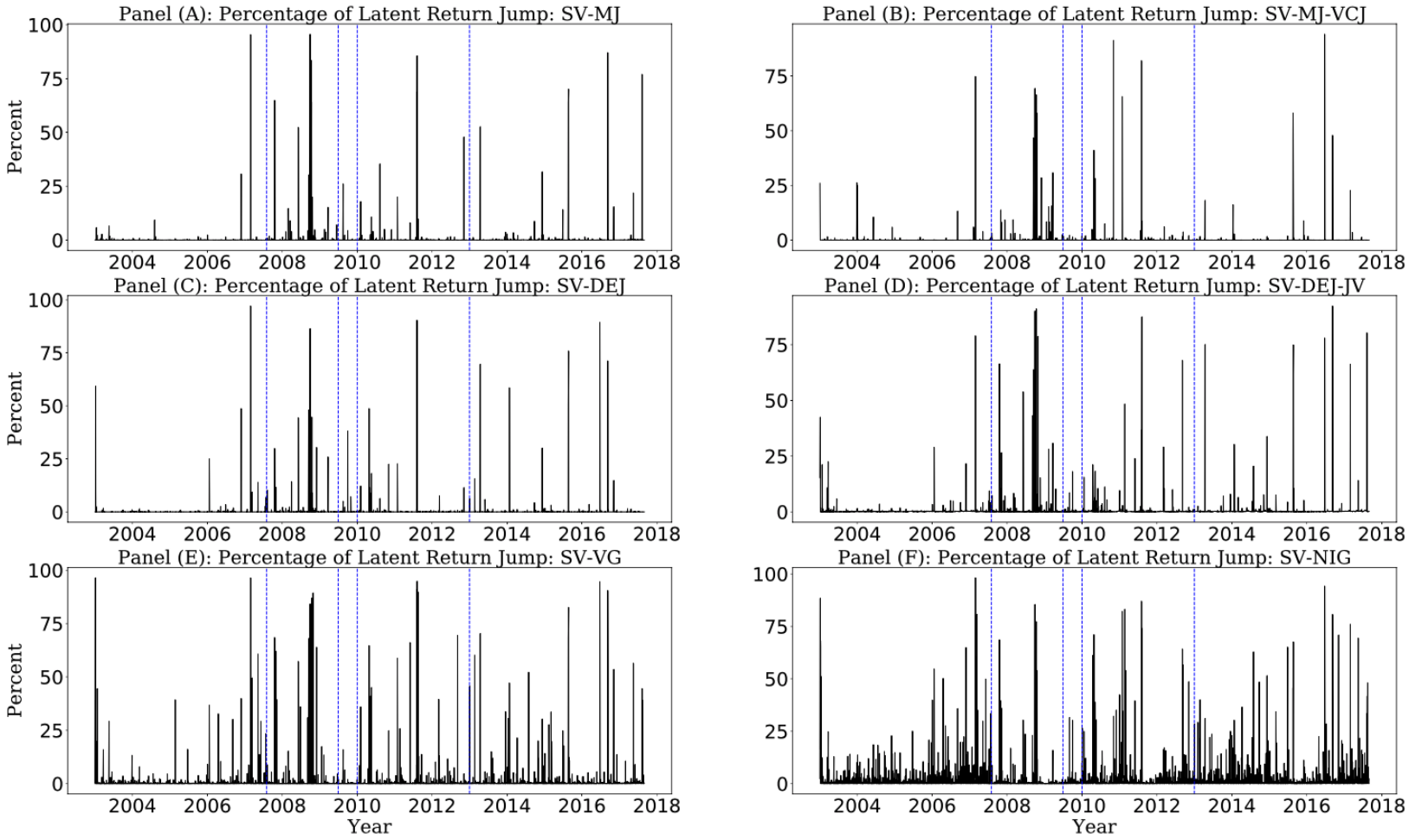

Fig. 4. Percentage of latent return jump.

The panel (A) to panel (F) are the percentage of latent jump estimated by the particle filtering, smoothing filtering and expectation-maximization (EM) algorithm from the corresponding model using parameters estimated in Table 6. The dotted vertical lines indicate the financial crisis from August 2007 to June 2009 and the European sovereign debt crisis from January 2010 to December 2012, respectively.

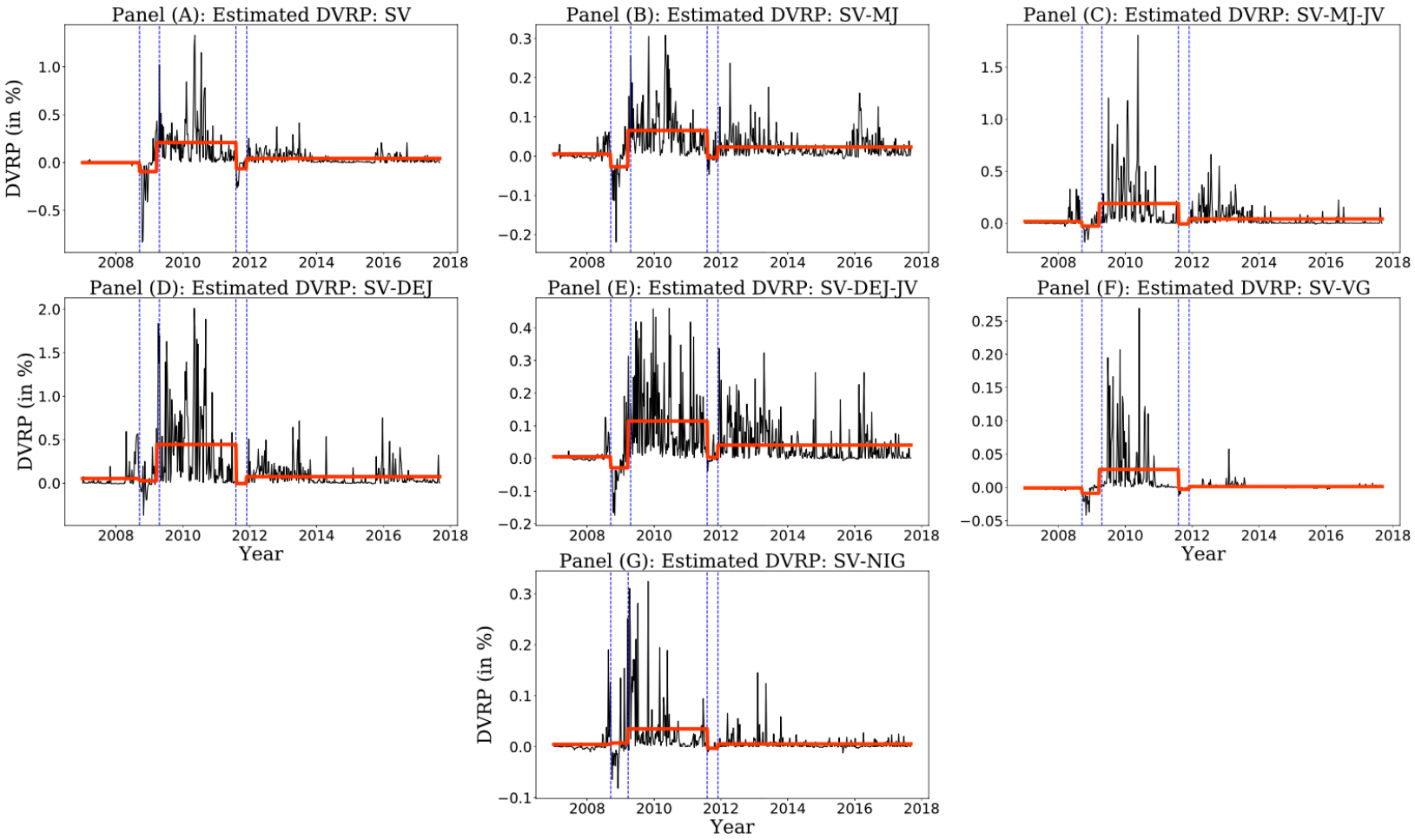

Fig. 5. Time series of the estimated diffusive variance risk premium for each model.

This figure shows the time series of the diffusive variance risk premium (DVRP) for each model from to January 2007 to August 2017. DVRP is defined in equation 19. The dotted vertical lines indicate the large shock time periods during the financial crisis from September 15, 2008 to March 23, 2009 and during the European sovereign debt crisis from October 1, 2010 to December 30, 2012, respectively.

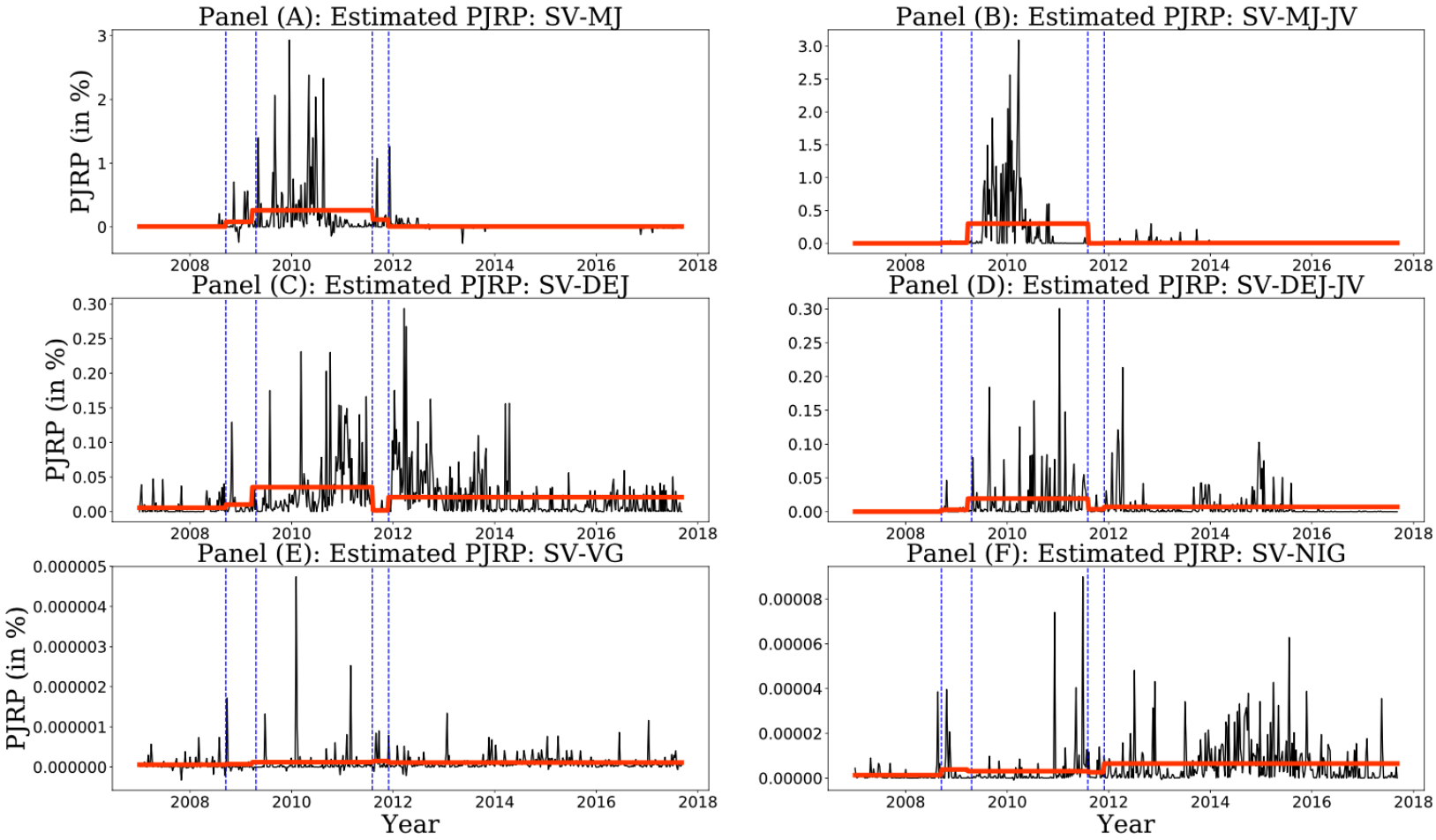

Fig. 6. Time series of the estimated price jump risk premium for each model.

This figure shows the time series of the price jump risk premium (PJRP) for each model from to January 2007 to August 2017. PJRP is defined in equation 19. The dotted vertical lines indicate the large shock time periods during the financial crisis from September 15, 2008 to March 23, 2009 and during the European sovereign debt crisis from October 1, 2010 to December 30, 2012, respectively.

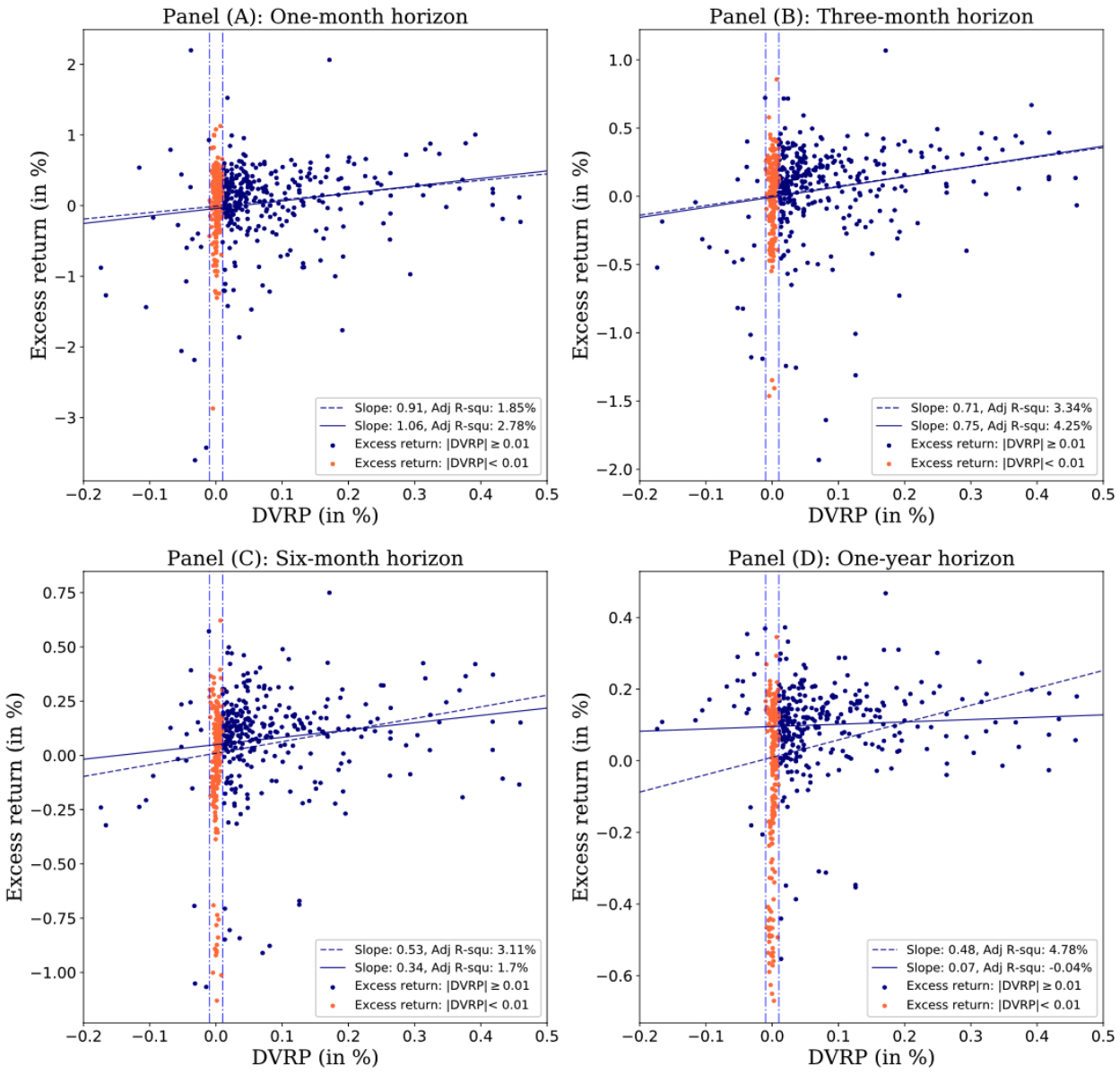

Fig. 7. The relation between the different horizon excess returns and the SV-DEJ-JV model's DVRP

Figure 7 presents results on the relation between the different horizon excess returns and the SV-DEJ-JV model's DVRP. We compute the time-series of the different horizon S&P500 index returns in excess of the risk-free rate. The SV-DEJ-JV model's DVRP is estimated from the implied volatility surface of the S&P500 index options discussed in the section 3. We plot the pairwise combinations for horizons of one, three, six, and 12 (one-year) months (Panel A to D). The dash line represents the regression fit to all the observations with slope coefficient and R-squared reported in the plot legend. The solid line represents the regression fit to the blue observations with slope coefficient and R-squared reported in the plot legend. The blue observations are the dots that the absolute values of the DVRP are greater than or equal to 0.01%. The orange observations are the dots that the absolute values of the DVRP are smaller than 0.01%. The date is weekly from January 2007 to August 2017.

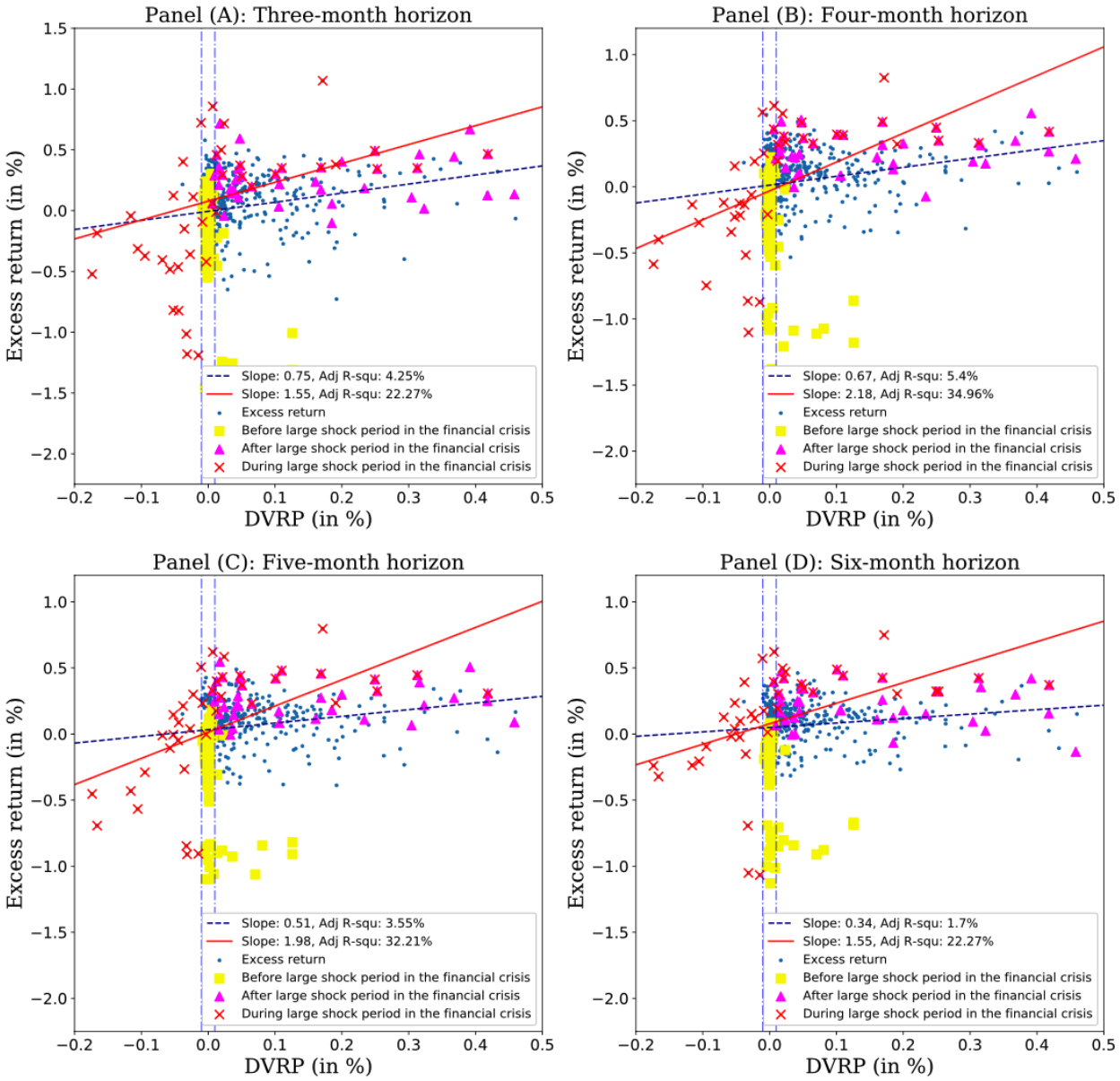

Fig. 8. The relation between the different horizon excess returns and the SV-DEJ-JV model's DVRP before, during and after the large shock time period in the financial crisis

Figure 8 presents results on the relation between the different horizon excess returns and the SV-DEJ-JV model's DVRP. We compute the time-series of the different horizon S&P500 index returns in excess of the risk-free rate. The SV-DEJ-JV model's DVRP is estimated from the implied volatility surface of the S&P500 index options discussed in the section 3. We plot the pairwise combinations for horizons of three, four, five, and six months (Panel A to D). The dash line represents the regression fit to the observations that the absolute values of the DVRP are greater than or equal to 0.01 with slope coefficient and R-squared reported in the plot legend. The red solid line represents the regression fit to the red crosses with slope coefficient and R-squared reported in the plot legend. The yellow squares are the observations from the August 1, 2007 to September 15, 2008 (Before the large shock time period in the financial crisis). The red crosses are the observations from September 15, 2008 to March 23, 2009 (During the large shock time period in the financial crisis). The purple triangles are the observations from March 23, 2009 to October 1, 2010 (After the large shock time period in the financial crisis and before the large shock time period in the European debt crisis). The remaining observations are blue observations. The date is weekly from January 2007 to August 2017.

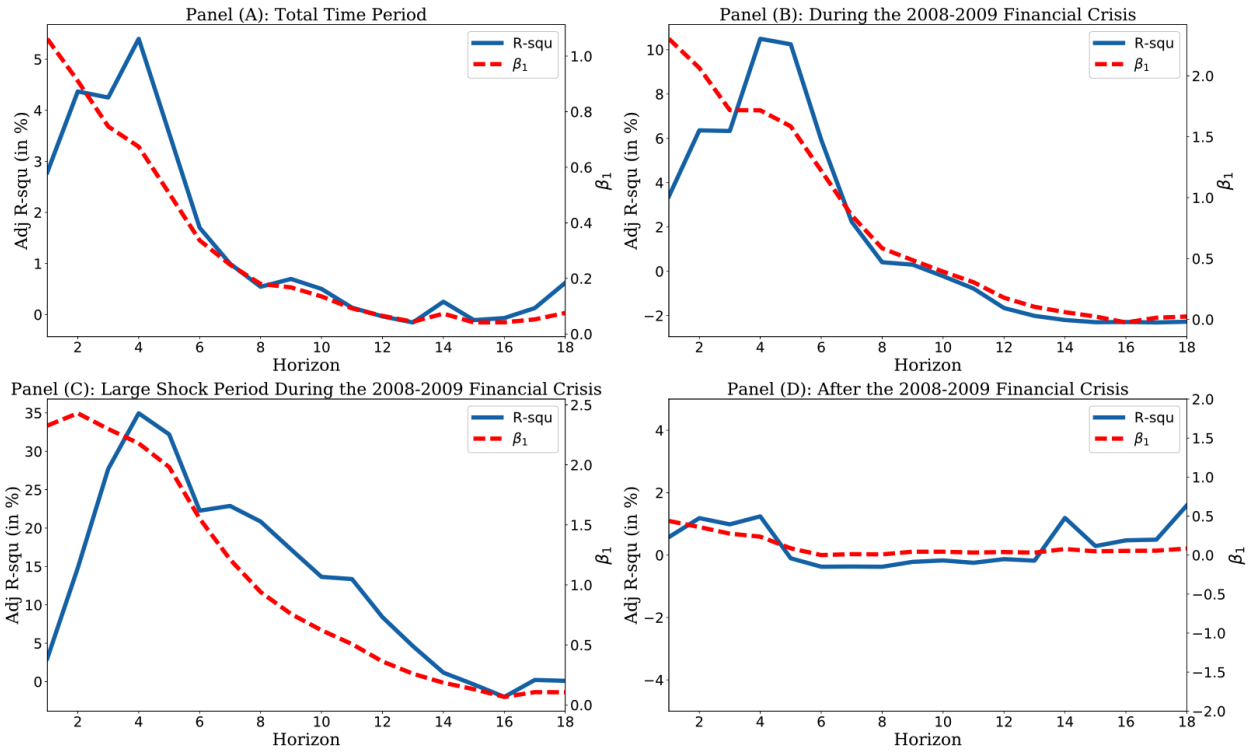

Fig. 9. In-sample R-squared and β_1 of predictive regression of the SV-DEJ-JV model's DVRP.

This figure shows that the slope coefficient and adjusted R^2s from in-sample regressions of the scaled h-period returns on the SV-DEJ-JV model's DVRP with the different time periods. All of the regressions are based on weekly observations from January 2007 to August 2017.

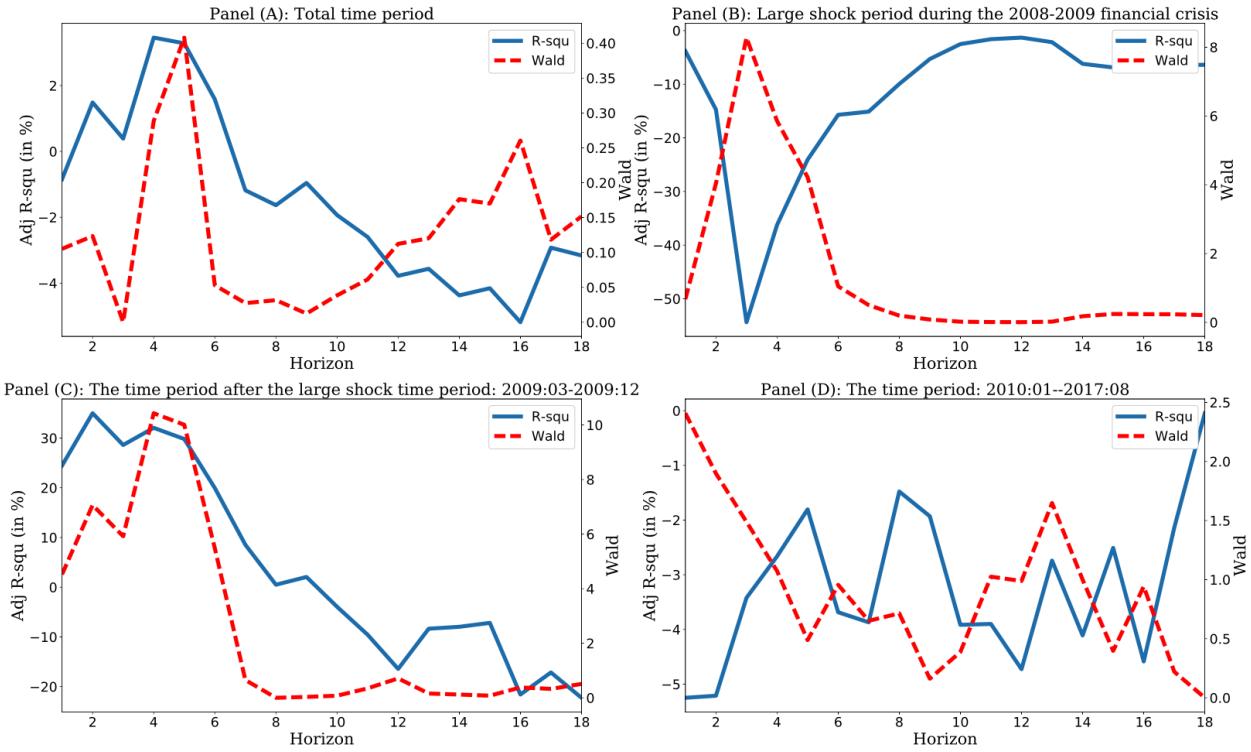

Fig. 10. Out-of-sample R-squared and β_1 of predictive regression of the SV-DEJ-JV model's DVRP.

This figure shows that the slope coefficient and adjusted R^2s from out-of-sample regressions of the scaled h-period returns on the SV-DEJ-JV model's DVRP with the different time periods. All of the regressions are based on weekly observations from January 2007 to August 2017.

Table 1: The Lévy measures and characteristic functions for selected pure jump Lévy processes.

Pure Lévy jump components	Lévy measures $\nu(x)$	Characteristic Functions $\psi(u)$
Panel A. Finite-activity jump processes		
Merton jump	$\frac{\lambda}{\sqrt{2\pi\delta^2}}\exp\left(-(x-\gamma)^2/2\delta^2\right)$	$\lambda\left(\exp\left(\gamma iu-\frac{1}{2}u^2\delta^2\right)-1\right)$
Correlated Merton jump	$\frac{\lambda}{\sqrt{2\pi\delta^2}}\exp\left(-(x-(\gamma+\rho_J V))^2/2\delta^2\right)$	$\lambda\left(\frac{\exp\left(\gamma iu-\frac{1}{2}u^2\delta^2\right)}{1-\rho_J\mu_v}-1\right)$
Double-exponential jump	$\lambda\left(\frac{p}{\eta^+}e^{-\frac{x}{\eta^+}}1_{\{x\geq 0\}}+\frac{q}{\eta^-}e^{\frac{x}{\eta^-}}1_{\{x<0\}}\right)$	$\lambda\left(\frac{p}{1-\eta^+iu}+\frac{q}{1+\eta^-iu}-1\right)$
Correlated double-exponential jump	$\lambda\begin{cases}\left[p\left(\frac{1}{\eta^+-\mu_v\rho_J}\right)\left(e^{-\frac{x}{\eta^+}}-e^{-\frac{x}{\mu_v\rho_J}}\right)+q\left(\frac{1}{\eta^-+\mu_v\rho_J}\right)\left(e^{-\frac{x}{\eta^+}}\right)\right]1_{\{x\geq 0\}} & \\ +\left[q\left(\frac{1}{\eta^-+\mu_v\rho_J}\right)\left(e^{\frac{x}{\eta^-}}\right)\right]1_{\{x<0\}}, & \text{if } \rho_J>0, \\ \left[p\left(\frac{1}{\eta^+-\mu_v\rho_J}\right)\left(e^{-\frac{x}{\eta^+}}\right)\right]1_{\{x\geq 0\}} & \\ +\left[p\left(\frac{1}{\eta^+-\mu_v\rho_J}\right)\left(e^{-\frac{x}{\mu_v\rho_J}}\right)+q\left(\frac{1}{\eta^-+\mu_v\rho_J}\right)\left(e^{\frac{x}{\eta^-}}-e^{-\frac{x}{\mu_v\rho_J}}\right)\right]1_{\{x<0\}}, & \text{if } \rho_J<0, \\ \left[p\frac{1}{\eta^+}e^{-\frac{x}{\eta^+}}\right]1_{\{x\geq 0\}}+\left[q\frac{1}{\eta^-}e^{-\frac{x}{\eta^-}}\right]1_{\{x<0\}}, & \text{if } \rho_J=0,\end{cases}$	$\lambda\left(\left(\frac{1}{1-\mu_v\rho_J}\right)\cdot\left(\frac{p}{1-\eta^+iu}+\frac{q}{1+\eta^-iu}\right)-1\right)$
Panel B. Infinite-activity jump processes		
Variance Gamma	$\frac{\mu_\pm^2}{\nu_\pm}\cdot\frac{\exp\left(-\frac{\mu_\pm}{\nu_\pm}\lvert x\rvert\right)}{\lvert x\rvert}$, $\mu_\pm=\frac{1}{2}\sqrt{\gamma^2+\frac{2\sigma^2}{\nu}}\pm\frac{\theta}{2}$, $\nu_\pm=\mu_\pm^2\nu$	$-\frac{1}{\nu}\cdot ln\left(1-iu\gamma\nu+\frac{1}{2}\sigma^2u^2\nu\right)$
Normal inverse Gaussian	$\frac{\alpha\delta}{\pi}\cdot\frac{e^{\beta\lvert x\rvert}\cdot K_1(\alpha\lvert x\rvert)}{\lvert x\rvert}$	$\delta\left(\sqrt{\alpha^2-\beta^2}-\sqrt{\alpha^2-(\beta+iu)^2}\right)$

Table 2: Summary of measure change

Table 2 shows the resulting risk-neutral measure $\mathbb{Q}$ distributions from the change of physical measure $\mathbb{P}$ through the Esscher transform for selected pure Lévy jump that we present in Table 1. h_3 is a jump risk premium for each model.

Pure Lévy jump components	$\mathbb{P}$ measure	$\mathbb{Q}$ measure	Parameter Transformation
Panel A. Finite-activity jump processes			
Merton jump	$\gamma^{\mathbb{P}}$, $\delta^{\mathbb{P}}$, $\lambda_y^{\mathbb{P}}$	$\gamma^{\mathbb{Q}}$, $\delta^{\mathbb{Q}}$, $\lambda_y^{\mathbb{Q}}$	$\gamma^{\mathbb{Q}}=\gamma^{\mathbb{P}}+h_3(\delta^{\mathbb{P}})^2$, $\delta^{\mathbb{Q}}=\delta^{\mathbb{P}}$ $\lambda_y^{\mathbb{Q}}=\lambda^{\mathbb{P}}{}_y\cdot\exp\left(h_3\gamma^{\mathbb{P}}+\frac{1}{2}h_3^2(\delta^{\mathbb{P}})^2\right)$
Correlated Merton jump	$\gamma^{\mathbb{P}}$, $\delta^{\mathbb{P}}$, $\lambda_y^{\mathbb{P}}$, $\mu_v^{\mathbb{P}}$	$\gamma^{\mathbb{Q}}$, $\delta^{\mathbb{Q}}$, $\lambda_y^{\mathbb{Q}}$, $\mu_v^{\mathbb{Q}}$	$\gamma^{\mathbb{Q}}=\gamma^{\mathbb{P}}+\rho_J\xi_{v,t}+h_3(\delta^{\mathbb{P}})^2$, $\delta^{\mathbb{Q}}=\delta^{\mathbb{P}}$ $\lambda_y^{\mathbb{Q}}=\lambda^{\mathbb{P}}{}_y\cdot\frac{\exp\left(h_3\gamma^{\mathbb{P}}+\frac{1}{2}h_3^2(\delta^{\mathbb{P}})^2\right)}{1-h_3\rho_J\mu^{\mathbb{P}}{}_v}$, $\mu_v^{\mathbb{Q}}=\frac{\mu_v^{\mathbb{P}}}{1-h_3\rho_J\mu_v^{\mathbb{P}}}$
Double-exponential jump	$\eta^{+,\mathbb{P}}$, $\eta^{-,\mathbb{P}}$, $p^{\mathbb{P}}$, $\lambda_y^{\mathbb{P}}$	$\eta^{+,\mathbb{Q}}$, $\eta^{-,\mathbb{Q}}$, $p^{\mathbb{Q}}$, $\lambda_y^{\mathbb{Q}}$	$\eta^{+\mathbb{Q}}=\left(\frac{1}{\eta^+}-h_3\right)^{-1}$, $\eta^{-\mathbb{Q}}=\left(\frac{1}{\eta^-}+h_3\right)^{-1}$ $\lambda_y^{\mathbb{Q}}=\lambda^{\mathbb{P}}{}_y\left(\frac{p^{\mathbb{P}}}{1-h_3\eta^{+,\mathbb{P}}}+\frac{q^{\mathbb{P}}}{1+h_3\eta^{-,\mathbb{P}}}\right)$ $p^{\mathbb{Q}}=\left(\frac{p^{\mathbb{P}}}{1-h_3\eta^{+,\mathbb{P}}}+\frac{q^{\mathbb{P}}}{1+h_3\eta^{-,\mathbb{P}}}\right)^{-1}\left(\frac{p^{\mathbb{P}}}{1-h_3\eta^{+,\mathbb{P}}}\right)$
Correlated double-exponential jump	$\eta^{+,\mathbb{P}}$, $\eta^{-,\mathbb{P}}$, $p^{\mathbb{P}}$, $\lambda_y^{\mathbb{P}}$, $\mu_v^{\mathbb{P}}$	$\eta^{+,\mathbb{Q}}$, $\eta^{-,\mathbb{Q}}$, $p^{\mathbb{Q}}$, $\lambda_y^{\mathbb{Q}}$, $\mu_v^{\mathbb{Q}}$	$\eta^{+\mathbb{Q}}=\left(\frac{1}{\eta^{+,\mathbb{P}}}-h_3\right)^{-1}$, $\eta^{-\mathbb{Q}}=\left(\frac{1}{\eta^{-,\mathbb{P}}}+h_3\right)^{-1}$ $\lambda_y^{\mathbb{Q}}=\lambda_y^{\mathbb{P}}\left(\frac{p^{\mathbb{P}}}{1-h_3\eta^{+,\mathbb{P}}}+\frac{q^{\mathbb{P}}}{1+h_3\eta^{-,\mathbb{P}}}\right)\left(\frac{1}{1-h_3\mu_v^{\mathbb{P}}\rho_J}\right)$ $p^{\mathbb{Q}}=\left(\frac{p^{\mathbb{P}}}{1-h_3\eta^{+,\mathbb{P}}}+\frac{q^{\mathbb{P}}}{1+h_3\eta^{-,\mathbb{P}}}\right)^{-1}\left(\frac{p^{\mathbb{P}}}{1-h_3\eta^{+,\mathbb{P}}}\right)$
Panel B: Infinite-activity jump processes			
Variance Gamma jump	$\gamma^{\mathbb{P}}$, $\sigma_J^{\mathbb{P}}$, $\alpha^{\mathbb{P}}$, $\beta^{\mathbb{P}}$	$\gamma^{\mathbb{Q}}$, $\sigma_J^{\mathbb{Q}}$, $\alpha^{\mathbb{Q}}$, $\beta^{\mathbb{Q}}$	$\gamma^{\mathbb{Q}}=\gamma^{\mathbb{P}}+h_3(\sigma_J^{\mathbb{P}})^2$, $\sigma_J^{\mathbb{Q}}=\sigma_J^{\mathbb{P}}$, $\alpha^{\mathbb{Q}}=\alpha^{\mathbb{P}}$ $\beta^{\mathbb{Q}}=\beta^{\mathbb{P}}-\frac{1}{2}\left(2\gamma^{\mathbb{P}}+h_3(\sigma_J^{\mathbb{P}})^2\right)$
Normal inverse Gaussian jump	$\alpha^{\mathbb{P}}$, $\beta^{\mathbb{P}}$, $\delta^{\mathbb{P}}$	$\alpha^{\mathbb{Q}}$, $\beta^{\mathbb{Q}}$, $\delta^{\mathbb{Q}}$	$\alpha^{\mathbb{Q}}=\alpha^{\mathbb{P}}$, $\beta^{\mathbb{Q}}=\beta^{\mathbb{P}}+h_3$, $\delta^{\mathbb{Q}}=\delta^{\mathbb{P}}$

Table 3: The specifications of g_{RJ} and $g_{CRJ}(\tau)$

Lévy jump	The specifications of g_{RJ} and $g_{CRJ}(\tau)$
Panel A. Finite-activity return jump processes.	$\pi^{\mathbb{Q}}_{RJ}(x)=\lambda^{\mathbb{Q}}_{y}\cdot f_{\xi^{\mathbb{Q}}_{y,t}}(x)$
Merton jump	$g_{MJ}=\lambda^{\mathbb{Q}}_{y}\cdot\left(\exp\left(i\phi\gamma^{\mathbb{Q}}-\frac{1}{2}\phi^{2}(\delta^{\mathbb{Q}})^{2}\right)-1\right)$
Double-exponential jump	$g_{DEJ}=\lambda^{\mathbb{Q}}_{y}\cdot\left(\left(\frac{p^{\mathbb{Q}}}{1-i\phi\eta^{+,\mathbb{Q}}}+\frac{q^{\mathbb{Q}}}{1+i\phi\eta^{-,\mathbb{Q}}}\right)-1\right)$
Panel B. Infinite-activity return jump processes.	$\pi^{\mathbb{Q}}_{RJ}(x)$
Variance Gamma	$g_{VG}=-\alpha^{\mathbb{Q}}\cdot\ln\left(1-\frac{i\phi\gamma^{\mathbb{Q}}-\frac{1}{2}\phi^{2}\left(\sigma^{\mathbb{Q}}_{J}\right)^{2}}{\beta^{\mathbb{Q}}}\right)$
Normal inverse Gaussian	$g_{NIG}=\delta^{\mathbb{Q}}\cdot\left(\sqrt{(\alpha^{\mathbb{Q}})-(\beta^{\mathbb{Q}})^{2}}\right)\text{-}\left(\sqrt{(\alpha^{\mathbb{Q}})-(\beta^{\mathbb{Q}}+i\phi)^{2}}\right)$
Panel C. Finite-activity correlated return jump processes.	$\pi^{\mathbb{Q}}_{CRJ}(x)=\lambda^{\mathbb{Q}}_{y}\cdot f_{\xi^{\mathbb{Q}}_{y,t}}(y)\cdot f_{\xi^{\mathbb{Q}}_{y,t}\mid\xi^{\mathbb{Q}}_{v,t}}(x\mid y)$
Correlated Merton jump	$g_{MJ-JV}=\lambda^{\mathbb{Q}}_{y}\cdot\left(\exp\left(i\phi\left(\gamma^{\mathbb{Q}}+h_{3}\left(\delta^{\mathbb{P}}\right)^{2}\right)-\frac{1}{2}\phi^{2}(\delta^{\mathbb{Q}})^{2}\right)\cdot\frac{1}{\mu^{\mathbb{Q}}_{v}}\cdot\Upsilon\left(\frac{1}{\mu^{\mathbb{Q}}_{v}}-i\phi\rho_{J}\right)-1\right)$
Correlated double-exponential jump	$g_{DEJ-JV}=\lambda^{\mathbb{Q}}_{y}\cdot\left(\left(\frac{p^{\mathbb{Q}}}{1-i\phi\eta^{+,\mathbb{Q}}}+\frac{q^{\mathbb{Q}}}{1+i\phi\eta^{-,\mathbb{Q}}}\right)\cdot\frac{1}{\mu^{\mathbb{Q}}_{v}}\cdot\Upsilon\left(\frac{1}{\mu^{\mathbb{Q}}_{v}}-i\phi\rho_{J}\right)-1\right)$

where

$$\Upsilon\left(C\right)=\int_{0}^{\tau}\frac{1}{C-B(s;\phi)}ds=\ln\left(\frac{(C-D)e^{-h\tau}+(-Cd+D)}{C(1-d)}\right)\cdot\left(\frac{1}{(C-D)\cdot(-h)}-\frac{1}{(-Cd+D)\cdot h}\right)+\frac{d\tau}{Cd-D}$$

Table 4: Descriptive statistics and option characteristics

Panel A and Panel B report the descriptive statistics of S&P500 index prices and returns from January 2003 – August 2017. Panel C and Panel D report the statistics of the curvature of ATM IV surface and the term structure of short-dated IV surface from January 2007 – August 2017.

Mean	Std.Dev.	Skewness	Kurtosis	Minimum	Maximum	Returns>3%	Returns<-3%
Panel A: S&P500 index prices							
1.457E+03	4.210E+02	6.809E-01	-5.863E-01	6.765E+02	2.481E+03	NA	NA
Panel B: S&P500 returns							
1.997E-04	1.260E-02	-3.439E-01	1.108E+01	-9.469E-02	1.096E-01	3.900E+01	5.300E+01
Panel C: The term structure of short-dated IV surface							
1.096E-02	1.011E-03	-3.133E-00	1.893E+02	-2.498E-01	1.597E-01	NA	NA
Panel D: The slope between short-term ATM and ITM IVs							
-2.581E-01	4.747E+01	8.744E-01	2.180E+00	-1.562E+00	1.698E+00	NA	NA
Panel E: The slope between short-term OTM and ITM IVs							
6.408E-01	9.700E-01	1.819E+00	6.452E+00	-1.670E+00	6.953E+00	NA	NA
Panel F: The curvature of short-term ATM IV							
6.409E-01	9.409E-01	1.819E-00	6.453E+00	-1.670E-00	6.953E-00	NA	NA

Table 5: S&P500 call options

Note that we use the European call options for Standard & Poor's 500 index (S&P500). The data are obtained from Datastream with the sample period from each Wednesday during January 1, 2007 to August 31, 2017. The call options with 6 to 180 days-to-expiration, 0.92 to 1.08 moneyness (S/K), call prices more than $0.375 and nonarbitrary opportunities are reserved. After filtering sample, there are a total number of 22828 available observations for call options. The sample is divided into 36 categories, i.e., 6 types of days-to-expiration (extremely short-term for $\leq$ 30 days; short-term 30-60 days; near-term 60-90 days; middle-maturity 90-120 days; long-term 120-150 days; extremely long-term $\geq$150 days) and 6 types of moneyness (S/K) (deep-out-of-the-money for; out-of-the-money for; at-the-money for; in-the-money for and deep-in-the-money for). The table lists the sample properties of S&P500 call options like the average call option price and average implied volatility for each categories.

Panel A: Number of call options							
Moneyness	Days-to-Expiration						
(S/K)	$\leq$ 30	30-60	60-90	90-120	120-150	$\geq$ 150	Subtotal
$<$ 0.94	243	715	792	632	161	84	2,627
0.94−0.97	835	1,254	1,166	877	270	127	4,529
0.97−1.00	1,208	1,217	1,135	866	269	136	4,831
1.00−1.03	1,131	1,123	1,050	797	239	106	4,446
1.03−1.06	917	1046	985	761	233	131	4073
1.06 $\leq$	439	607	609	470	144	53	2322
Subtotal	4773	5962	5737	4403	1316	637	22828
Panel B: Average of Call option prices							
	$\leq$ 30	30-60	60-90	90-120	120-150	$\geq$ 150	Subtotal
$<$ 0.94	2.48	3.48	5.62	8.33	15.38	19.73	6.44
0.94−0.97	3.57	7.48	13.00	18.32	24.05	32.80	11.98
0.97−1.00	10.93	22.18	31.73	39.70	48.43	55.45	27.15
1.00−1.03	38.30	50.97	60.68	70.17	75.17	86.08	55.62
1.03−1.06	76.03	87.33	96.21	105.15	109.16	114.56	92.39
1.06 $\leq$	107.97	118.57	127.50	136.04	138.02	147.77	124.31
Subtotal	37.13	45.51	50.85	58.05	64.80	71.16	48.82
Panel C: Average implied volatility							
	$\leq$ 30	30-60	60-90	90-120	120-150	$\geq$ 150	Subtotal
$<$ 0.94	0.200	0.141	0.130	0.127	0.145	0.144	0.140
0.94−0.97	0.156	0.135	0.137	0.135	0.141	0.155	0.140
0.97−1.00	0.142	0.147	0.150	0.148	0.161	0.159	0.148
1.00−1.03	0.168	0.166	0.165	0.162	0.171	0.183	0.166
1.03−1.06	0.206	0.185	0.182	0.175	0.183	0.188	0.187
1.06 $\leq$	0.200	0.156	0.142	0.168	0.206	0.248	0.176
Subtotal	0.176	0.159	0.157	0.153	0.163	0.169	0.161

Table 6: Estimated parameters for S&P500 index under the physical measure

	SV	SV-MJ	SV-MJ-JV	SV-DEJ	SV-DEJ-JV	SV-VG	SV-NIG
Panel A: Parameters of stochastic volatility							
μ	2.52E-04	1.7934E-04	2.23E-04	4.82E-04	3.67E-04	4.39E-04	3.08E-04
	(4.37E-05)	(1.68E-05)	(5.66E-05)	(9.39E-05)	(8.80E-04)	(3.46E-05)	(1.84E-04)
κ	1.68E-02	1.53E-02	1.51E-02	1.28E-02	1.26E-02	1.64E-02	1.28E-02
	(7.48E-04)	(1.08E-04)	(6.42E-04)	(1.91E-03)	(1.96E-03)	(7.46E-03)	(4.11E-03)
θ	1.20E-04	1.26E-04	1.14E-04	1.10E-04	1.08E-04	9.11E-05	1.09E-04
	(4.89E-06)	(8.03E-06)	(9.28E-05)	(2.45E-05)	(8.19E-05)	(1.24E-05)	(2.44E-05)
σ_v	1.86E-03	1.77E-03	1.71E-03	1.38E-03	1.44E-03	1.49E-03	1.30E-03
	(1.41E-05)	(2.07E-04)	(3.82E-04)	(2.30E-04)	(1.56E-05)	(1.14E-05)	(1.22E-05)
ρ	-4.64E-01	-4.55E-01	-4.56E-01	-4.55E-01	-4.24E-01	-4.50E-01	-4.42E-01
	(8.02E-03)	(8.75E-03)	(4.86E-03)	(4.26E-03)	(3.20E-02)	(4.73E-02)	(9.50E-02)
$\sqrt{v_t \times 252}$	17.0949	16.2618	16.5728	16.2816	16.1031	15.4387	16.1372
	(4.16E-03)	(3.69E-03)	(4.13E-03)	(3.72E-03)	(3.76E-03)	(3.22E-03)	(3.91E-03)
Panel B: Parameters of return jump							
$\lambda_y\,(=\lambda_v=\lambda)$		8.11E-03	1.54E-02	1.58E-02	3.27E-02		
		(2.69E-03)	(1.48E-03)	(8.48E-03)	(1.26E-03)		
γ		-1.65E-02	-4.91E-03			1.31E-04	
		(1.87E-03)	(3.69E-03)			(3.56E-04)	
δ		4.64E-02	4.81E-02			8.92E-03	1.78E-04
		(9.27E-02)	(7.67E-02)			(2.72E-03)	(1.02E-04)
η^+				4.10E-02	5.60E-02		
				(2.19E-02)	(6.05E-02)		
η^-				4.25E-02	6.02E-02		
				(2.71E-02)	(9.98E-03)		
p				4.72E-01	4.26E-01		
				(1.48E-01)	(3.11E-01)		
α						9.30E-03	3.08E+01
						(4.76E-04)	(1.00E+00)
β						1.45E-02	-8.72E-01
						(4.54E-02)	(2.20E-01)

Table 6: Continued.

	SV	SV-MJ	SV-MJ-JV	SV-DEJ	SV-DEJ-JV	SV-VG	SV-NIG
Panel C: Parameters of volatility jump							
μ_v			5.99e-05		4.86e-05		
			(9.67E-05)		(5.28E-05)		
ρ_v			-9.48E-04		2.11E-01		
			(1.00E-05)		(9.70E-03)		
Panel D: Criteria of model selection							
$MPJV(\%)$	0.0000	0.4760	0.3836	0.4412	0.7672	1.3485	2.1349
L_P	12842.67	12869.04	**12925.38**	**12960.12**	**13013.01**	12911.17	12924.78
AIC	-25674.67	-25722.09	-25830.75	**-25902.23**	**-26004.01**	-25804.33	**-25833.55**
BIC	-25643.43	-25672.09	-25768.26	**-25845.99**	**-25935.27**	-25748.09	**-25783.56**

Note that we use the daily Standard & Poor's 500 index (S&P500). The data are obtained from Datastream with the sample period from each trading day during January 1, 2003 to August 31, 2017. Table 6 report the parameters of the SV, SV-MJ, SV-MJ-JV, SV-DEJ, SV-DEJ-JV, SV-VG, and SV-NIG models are estimated by the particle filtering and EM algorithms as shown in section 3. The estimated parameters is reported first, followed by its standard error of each parameter in the parentheses. Panel A report parameters of stochastic volatility dynamic process of each model, Panel B report parameters of return jump dynamic process of each model, and Panel C report parameters of volatility jump dynamic process of each model. Moreover, the last four rows list the mean of the percentage of return jump account for the total return variance ($MPJV$), the log-likelihood function (L_P), the Akaike information criterion (AIC) and the Bayesian information criterion (BIC), respectively. The bold font represents the top three log-likelihood function values of seven models, the last three Akaike information criterion values of seven models, and the last three Bayesian information criterion values of seven models.

Table 7: Kolmogorov-Smirnov Test Statistics and p-Values for Each Model

Table 7 report the Kolmogorov-Smirnov test statistics and p-values for each model.

	Return Residuals						
Model	SV	SV-MJ	SV-MJ-JV	SV-DEJ	SV-DEJ-JV	SV-VG	SV-NIG
KS statistics	0.026**	0.0237**	0.0191***	0.214***	0.1879***	0.0230***	0.0229***
p-values	0.0521	0.0867	0.2592	0.1535	0.2772	0.1047	0.1069

***, **, and * are the statistical significance levels as 1%, 5%, 10%, respectively.

Table 8: Estimated parameters for S&P500 indexs and options (Joint estimation)

	SV	SV-MJ	SV-MJ-JV	SV-DEJ	SV-DEJ-JV	SV-VG	SV-NIG
Panel A: Parameters of stochastic volatility							
μ	-3.01E-04	-3.77E-04	-3.02E-04	-3.17E-04	-3.04E-04	-2.41E-04	-2.61E-04
	(3.00E-05)	(3.09E-05)	(2.99E-05)	(2.97E-05)	(3.00E-05)	(2.89E-05)	(2.64E-05)
κ	7.14E-04	3.43E-04	3.69E-04	6.24E-04	4.20E-04	6.93E-05	1.29E-04
	(2.78E-05)	(1.09E-05)	(1.83E-05)	(2.33E-05)	(1.67E-05)	(1.94E-06)	(5.56E-05)
θ	2.41E-04	2.23E-04	2.90E-04	3.21E-04	2.74E-04	1.99E-04	2.30E-04
	(7.61E-06)	(6.48E-06)	(1.17E-05)	(1.16E-05)	(8.56E-06)	(9.18E-06)	(1.02E-05)
σ_v	5.13E-03	6.12E-03	5.17E-03	5.16E-03	5.18E-03	5.85E-03	6.81E-03
	(1.36E-04)	(2.07E-04)	(1.39E-04)	(1.40E-04)	(1.40E-04)	(1.73E-04)	(2.28E-04)
ρ	-3.91E-01	-3.48E-01	-3.89E-01	-3.89E-01	-3.90E-01	-3.96E-01	-3.91E-01
	(8.83E-04)	(2.94E-03)	(9.56E-04)	(8.39E-04)	(8.24E-04)	(3.39E-04)	(6.28E-04)
Panel B: Parameters of return jump							
$\lambda_y\,(=\lambda_v=\lambda)$		4.36E-03	5.32E-04	3.14E-03	1.96E-03		
		(1.52E-04)	(3.37E-05)	(4.32E-05)	(1.26E-04)		
γ		-2.09E-02	-2.02E-02			2.68E-04	
		(8.75E-04)	(9.18E-04)			(2.15E-06)	
δ		3.89E-02	3.97E-02			4.09E-03	8.40E-05
		(1.06E-03)	(9.10E-04)			(9.04E-05)	(2.27E-06)
η^+				4.61E-02	4.49E-02		
				(3.03E-04)	(2.82E-04)		
η^-				4.75E-02	4.57E-02		
				(3.79E-04)	(3.20E-04)		
p				4.52E-01	4.63E-01		
				(2.42E-03)	(1.15E-03)		
α						5.12E-03	3.07E+01
						(4.44E-05)	(1.54E-02)
β						(3.49E-02)	(-8.98E-01)
						(4.71E-04)	(2.74E-01)

Table 8: Continued.

	SV	SV-MJ	SV-MJ-JV	SV-DEJ	SV-DEJ-JV	SV-VG	SV-NIG
Panel C: Parameters of volatility jump							
μ_v			1.53E-05		2.30E-07		
			(8.31E-07)		(1.93E-10)		
ρ_v			-3.99E-02		-2.06E-03		
			(1.23E-02)		(3.72E-04)		
Panel D: Parameters of risk premium							
h_2	3.64E-01	1.82E-01	3.61E-01	7.09E-01	3.53E-01	2.52E-02	7.92E-02
	(1.65E-02)	(7.89E-03)	(2.54E-02)	(3.37E-02)	(1.92E-02)	(2.69E-03)	(8.51E-03)
h_3		-5.46E-05	-5.57E-02	-3.74E-2	-1.47E-03	-2.47E-08	-1.99E-06
		(9.69E-06)	(7.65E-03)	(2.77E-02)	(1.39E-04)	(7.18E-09)	(1.44E-07)
Panel E: Criteria of model selection							
L_J	2457.18	2592.69	2679.37	**2704.85**	**2714.56**	2607.11	**2712.22**
AIC	-4902.35	-5165.38	-5334.74	**-5387.69**	**-5413.13**	-5192.22	**-5404.43**
BIC	-4876.40	-5122.14	-5282.85	**-5340.12**	**-5356.91**	-5144.66	**-5361.18**

Note that we use the daily Standard & Poor's 500 index (S&P500). The data are obtained from Datastream with the sample period from each trading day during January 1, 2003 to August 31, 2017. Table 8 report the parameters of the SV, SV-MJ, SV-MJ-JV, SV-DEJ, SV-DEJ-JV, SV-VG, and SV-NIG models are estimated by the particle filtering, EM algorithms and rolling window method as shown in section 3. The parameters of a given model are estimated by maximizing the log-likelihood function for each model. The estimated parameters is reported first, followed by its standard error of each parameter in the parentheses. Panel A report parameters of stochastic volatility dynamic process of each model, Panel B of report parameters of return jump dynamic process of each model, and Panel C report parameters of volatility jump dynamic process of each model, and Panel D report parameters of risk premium of each model. Moreover, the last three rows list the joint log-likelihood function (L(Joint)), the Akaike information criterion (AIC) and the Bayesian information criterion (BIC). The bold font represents the top three log-likelihood function values of seven models, the last three Akaike information criterion values of seven models, and the last three Bayesian information criterion values of seven models.

Table 9: Weekly in-sample option pricing performance

In Table 9, we compute the price of each call options for S&P500 index using the **same** day's implied parameters from Table 8 and implied volatility (IV). The data are obtained from Datastream with the sample period from each Wednesday during January 3, 2007 to August 31, 2017. The call options with 6 to 180 days-to-expiration, 0.92 to 1.08 moneyness (S/K), call prices more than \$0.375 and nonarbitrary opportunities are reserved. After filtering sample, there are a total number of 22828 available observations for call options. Those call options are used to compute weekly time-series of relative IV root-mean-squared error (RIVRMSE). Panel A reports the time series mean and standard error of sample mean of the weekly RIVRMSE. Panel B list the absolute pricing error which are in-sample average of the absolute difference between the market price and the model price. Panel C reports Diebold-Mariano (DM) pairwise statistics for weekly RIVRMSE. The DM statistics measure the difference between the squared pricing error of the Benchmark model X and the Test model Y. Note that a positive and significant value for DM statistic means that X has a larger RIVRMSE than Y (alternative hypothesis) under the null hypothesis that the two models have equal squared pricing errors. ***, **, and * are the statistical significance levels at 1%, 5%, and 10% for a one-sided test, respectively. If p-value is lower than 10% significance level, we can not reject the null hypothesis that the accuracy of Y is better than X.

	SV	SV-MJ	SV-MJ-JV	SV-DEJ	SV-DEJ-JV	SV-VG	SV-NIG
Panel A: Time-series mean of the weekly in-sample RIVRMSE							
Mean	14.35%	13.84%	13.55%	12.95%	12.43%	13.51%	12.98%
	(0.0035%)	(0.0025%)	(0.0017%)	(0.0018%)	(0.0018%)	(0.0020%)	(0.0019%)
Panel B: Time-series mean of the weekly in-sample absolute pricing error							
Mean	3.45	3.46	3.30	3.19	3.11	3.49	3.48
Panel C: Diebold-Mariano (DM) pair-wise statistics for weekly in-sample RIVRMSE							
Benchmark	Test model Y						
X	SV	SV-MJ	SV-MJ-JV	SV-DEJ	SV-DEJ-JV	SV-VG	SV-NIG
SV		1.7620**	2.4624***	2.8895***	3.3364***	2.0875**	2.8047***
(p-value)		(3.93E-02)	(7.05E-03)	(2.01-E03)	(4.53E-04)	(1.87E-02)	(2.61E-03)
SV-MJ			1.6711**	2.5619***	3.3013***	1.3186*	2.5723***
			(4.76E-02)	(5.34E-03)	(5.12E-04)	(9.39E-02)	(5.18E-03)
SV-MJ-JV				2.5522***	5.7685***	-0.6157	2.3583*
				(0.0055)	(6.64E-09)	(7.31E-01)	(9.35E-02)
SV-DEJ					4.3235***	-2.9599	-0.2571
					(9.01E-06)	(9.98E-01)	(6.01E-01)
SV-DEJ-JV						-6.2694	-4.4104
						(1.00E-00)	(1.00E-00)
SV-VG							3.0138***
							(1.35E-03)

Table 10: Weekly out-of-sample option pricing performance

In Table 10, we compute the price of each call options for S&P500 index using the **previous** day's implied parameters from Table 8 and implied volatility (IV). The data are obtained from Datastream with the sample period from each Wednesday during January 3, 2007 to August 31, 2017. The call options with 6 to 180 days-to-expiration, 0.92 to 1.08 moneyness (S/K), call prices more than \$0.375 and nonarbitrary opportunities are reserved. After filtering sample, there are a total number of 22828 available observations for call options. Those call options are used to compute weekly time-series of relative IV root-mean-squared error (RIVRMSE). Panel A reports the time series mean and standard error of sample mean of the weekly RIVRMSE. Panel B list the absolute pricing error which are out-of-sample average of the absolute difference between the market price and the model price. Panel C reports Diebold-Mariano (DM) pairwise statistics for weekly RIVRMSE. The DM statistics measure the difference between the squared pricing error of the Benchmark model X and the Test model Y. Note that a positive and significant value for DM statistic means that X has a larger RIVRMSE than Y (alternative hypothesis) under the null hypothesis that the two models have equal squared pricing errors. ***, **, and * are the statistical significance levels at 1%, 5%, and 10% for a one-sided test, respectively. If p-value is lower than 10% significance level, we can not reject the null hypothesis that the accuracy of Y is better than X.

	SV	SV-MJ	SV-MJ-JV	SV-DEJ	SV-DEJ-JV	SV-VG	SV-NIG
Panel A: Time-series mean of the weekly out-of-sample RIVRMSE							
Mean	17.58%	17.43%	16.94%	16.79%	16.72%	17.40%	16.81%
	(0.0034)	(0.0034)	(0.0032)	(0.0030)	(0.0033)	(0.0032)	(0.0034)
Panel B: Time-series mean of the weekly out-of-sample absolute pricing error							
Mean	4.45	4.46	4.31	4.24	4.22	4.52	4.43
Panel C: Diebold-Mariano (DM) pair-wise statistics for weekly out-of-sample RIVRMSE							
Benchmark	Test model Y						
X	SV	SV-MJ	SV-MJ-JV	SV-DEJ	SV-DEJ-JV	SV-VG	SV-NIG
SV		-0.1517	1.6390*	1.4478*	1.9003**	0.3258	1.2051
(p-value)		(5.60E-01)	(5.09E-02)	(7.41E-02)	(2.90E-02)	(3.72E-01)	(1.14E-01)
SV-MJ			1.4019*	1.6020*	1.6120*	0.4076	1.1150
			(8.08E-02)	(5.49E-02)	(5.38E-02)	(3.42E-01)	(1.33E-01)
SV-MJ-JV				0.1451	0.6424	-1.8631	-0.3555
				(4.42E-01)	(2.60E-01)	(9.69E-01)	(6.39E-01)
SV-DEJ					0.0897	-1.2095	-0.3659
					(4.64E-01)	(8.87E-01)	(6.42E-01)
SV-DEJ-JV						-2.4121	-0.9963
						(9.92E-01)	(8.40E-01)
SV-VG							1.5415*
							(6.19E-02)

Table 11: Summary statistics of the risk premium.

This table presents the statistics of the weekly risk premia resulting from the model estimation. Each risk premium is computed according to the equation 19. Panel A, B, and C present the annualized price jump risk premium (PJRP), annualized diffusion volatility risk premium (DVRP), and annualized volatility (upside and downside) jump risk premium (VJRP (VUJRP/VDJRP)) for each model discussed in section 2, respectively. "Mean" reports the average and are displaced in percent. "Std Dev" displays the standard deviation and are displaced in percent. "Max" and "Min" show the maximum and the minimum and are displaced in percent, respectively. Finally, "Skew" and "Kurt" show the skewness and the kurtosis, respectively.

Panel A: Annualized price jump risk premium (PJRP)							
	SV	SV-MJ	SV-MJ-JV	SV-DEJ	SV-DEJ-JV	SV-VG	SV-NIG
Mean(%)		6.96E-02	7.02E-02	2.06E-02	8.38E-03	1.03E-07	4.68E-06
St.Dev(%)		2.82E-01	2.92E-01	3.73E-02	2.60E-02	2.91E-07	9.34E-06
Max(%)		2.93E+00	3.09E+00	2.94E-01	3.01E-01	4.74E-06	8.99E-05
Min(%)		-2.58E-01	-5.99E-06	-4.66E-05	-1.04E-05	-3.25E-07	-8.58E-07
Skew		6.24E+00	5.99E+00	3.45E+00	5.74E+00	≈ 0	≈ 0
Kurt		4.57E+01	4.26E+01	1.50E+01	4.42E+01	≈ 0	≈ 0
Panel B: Annualized diffusion volatility risk premium (DVRP)							
	SV	SV-MJ	SV-MJ-JV	SV-DEJ	SV-DEJ-JV	SV-VG	SV-NIG
Mean(%)	6.34E-02	2.72E-02	6.75E-02	1.49E-01	4.72E-02	6.07E-03	1.28E-02
St.Dev(%)	1.64E-01	4.88E-02	1.72E-01	3.07E-01	8.53E-02	2.61E-02	4.48E-02
Max(%)	1.33E+00	3.08E-01	1.81E+00	2.01E+00	4.60E-01	2.69E-01	5.70E-01
Min(%)	-8.31E-01	-2.19E-01	-1.81E-01	-3.68E-01	-1.74E-01	-4.17E-02	-8.14E-02
Skew	2.59E+00	2.12E+00	4.61E+00	3.27E+00	2.27E+00	5.72E+00	6.42E+00
Kurt	2.08E+01	9.28E+00	2.96E+01	1.23E+00	6.24E+00	3.88E+01	5.64E+01
Panel C: Annualized volatility (upside/downside) jump risk premium (VJRP(VUJRP/VDJRP))							
	SV	SV-MJ	SV-MJ-JV	SV-DEJ	SV-DEJ-JV	SV-VG	SV-NIG
Mean(%)			3.64E-07	6.52E-07 (-2.06E-06/2.72E-06)			
St.Dev(%)			3.13E-06	2.02E-06 (6.24E-06/8.16E-06)			
Max(%)			3.82E-05	1.66E-05 (3.73E-09/8.24E-05)			
Min(%)			-2.07E-05	-6.89E-08 (-7.18E-05/-4.12E-09)			
Skew			≈ 0	≈ 0 (≈ 0/≈ 0)			
Kurt			≈ 0	≈ 0 (≈ 0/≈ 0)			

Table 12: The estimated average risk premia in the different time periods.

The table reports the estimated average risk premia in each time period. Note that we define two time intervals September 15, 2008 to March 23, 2009 and August 4, 2011 to November 30, 2011 as the large shock time periods in the 2008-2009 financial crisis (From August 1, 2007 to June 30, 2009) and European debt crisis (From October 1, 2010 to December 30, 2012) using the ± 0.03 returns to split these time intervals, respectively. Thus, we obtain five time intervals: (1) Before the large shock time period in the financial crisis (From August 1, 2007 to September 15, 2008), (2) During the large shock time period in the financial crisis (From September 15, 2008 to March 23, 2009), (3) After the large shock time period in the financial crisis and before the large shock time period in the European debt crisis (From March 23, 2009 to October 1, 2010), (4) During the large shock time period in the European debt crisis (From October 1, 2010 to December 30, 2012), (5) After the large shock time period in the European debt crisis (From December 30, 2012 to August 31, 2017).

Panel A: Annualized price jump risk premium (PJRP)(%)							
Time period	SV	SV-MJ	SV-MJ-JV	SV-DEJ	SV-DEJ-JV	SV-VG	SV-NIG
(1)		6.23E-03	9.96E-07	5.62E-03	5.99E-05	5.71E-08	1.33E-06
		(2.51E-02)	(3.41E-05)	(1.15E-02)	(2.17E-04)	(1.52E-07)	(4.37E-06)
(2)		7.98E-02	8.59E-03	1.02E-02	2.84E-03	7.03E-08	3.85E-06
		(2.11E-01)	(1.21E-02)	(2.48E-02)	(9.04E-03)	(3.33E-07)	(8.85E-06)
(3)		2.61E-01	3.00E-01	3.53E-02	1.94E-02	1.20E-07	3.10E-06
		(5.25E-01)	(5.63E-01)	(4.89E-02)	(4.23E-02)	(5.08E-07)	(1.11E-05)
(4)		1.14E-01	2.30E-05	1.92E-03	3.63E-03	1.49E-07	2.62E-06
		(2.66E-01)	(9.13E-05)	(4.10E-03)	(6.96E-03)	(2.94E-07)	(4.48E-06)
(5)		6.64E-03	5.63E-03	2.09E-02	7.07E-03	1.10E-07	6.49E-06
		(7.91E-02)	(2.86E-02)	(3.65E-02)	(2.08E-02)	(1.73E-07)	(9.47E-06)
Panel B: Annualized diffusion volatility risk premium (DVRP)(%)							
Time period	SV	SV-MJ	SV-MJ-JV	SV-DEJ	SV-DEJ-JV	SV-VG	SV-NIG
(1)	-4.93E-04	5.67E-03	1.71E-02	5.36E-02	5.42E-03	-7.86E-04	4.62E-03
	(6.81E-03)	(1.61E-02)	(6.46E-02)	(1.35E-01)	(2.24E-07)	(1.20E-03)	(2.52E-02)
(2)	-9.42E-02	-2.71E-02	-2.76E-02	2.70E-02	-2.87E-02	-8.89E-03	2.27E-02
	(2.88E-01)	(5.60E-02)	(6.17E-02)	(1.93E-01)	(7.84E-02)	(1.23E-02)	(6.79E-02)
(3)	2.09E-01	6.56E-02	1.89E-01	4.45E-01	1.14E-01	2.70E-02	3.51E-02
	(2.50E-01)	(6.67E-02)	(2.92E-01)	(5.08E-01)	(1.23E-01)	(4.92E-02)	(6.31E-02)
(4)	-6.43E-02	5.95E-03	-6.45E-03	3.80E-03	3.40E-03	-2.87E-03	-3.04E-03
	(9.82E-02)	(2.51E-02)	(4.07E-03)	(4.84E-03)	(2.50E-02)	(3.51E-03)	(4.04E-03)
(5)	4.31E-02	2.40E-02	4.48E-02	7.48E-02	4.10E-02	1.30E-03	6.05E-03
	(5.66E-02)	(3.03E-02)	(8.64E-02)	(1.18E-01)	(5.97E-02)	(4.01E-03)	(1.39E-02)

Table 13: In-sample return predictability with ordinary least squares (OLS) regressions at different horizons.
The table 13 reports the estimated regression coefficient β_1 and adjusted R^2 of the predictability OLS regressions from one to eighteen-month excess return on the S&P500 index. The regression takes the form of $r_{t,t+h} = \beta_0(h) + \beta_1(h) \cdot \text{DVRP}_t + u_{t,t+h}$, where $r_{t,t+h}$ is the h-month ahead S&P500 excess return from t to $t+h$, and DVRP_t is the predictor variable at time t. We use the Newey-West standard errors to correct for auto-correlation introduced by overlapping data. The p-value of Newey-West test for significance of estimated regression coefficients accounting for the overlapping in the regressions are reported in the parenthesis. Panel A reports the return predictability regression for the total time period ranging from January 2007 to August 2017. Panel B reports the return predictability regression for the time period during the financial crisis ranging from August 2007 to June 2009. Panel C reports the return predictability regression for the large shock time period during the financial crisis ranging from September 2008 to March 2009. Panel D reports the return predictability regression for the time period after the financial crisis ranging from July 2009 to August 2017. The adjusted R^2, adj R^2, is reported in percent.

Panel A: Total time period: 2007:01–2017:08.										
Horizon	1	2	3	4	5	6	9	12	15	18
β_1	1.062**	0.911***	0.747***	0.674***	0.506*	0.337	0.168	0.065	0.041	0.075
($p-$value)	(0.012)	(0.002)	(0.001)	(0.005)	(0.063)	(0.141)	(0.203)	(0.351)	(0.464)	(0.130)
Adj R^2 (%)	2.785	4.369	4.251	5.401	3.552	1.701	0.697	-0.037	-1.088	0.622
Panel B: During the 2008–2009 financial crisis: 2007:08–2009:06.										
Horizon	1	2	3	4	5	6	9	12	15	18
β_1	2.304	2.065***	1.718***	1.717***	1.586***	1.222***	0.487	0.179	0.024	0.024
($p-$value)	(0.388)	(0.002)	(0.004)	(0.000)	(0.001)	(0.003)	(0.110)	(0.515)	(0.876)	(0.864)
Adj R^2 (%)	3.381	6.360	6.332	10.494	10.246	5.937	0.298	-1.660	-2.299	-2.277
Panel C: Large shock period during the 2008–2009 financial crisis: 2008:09–2009:03										
Horizon	1	2	3	4	5	6	9	12	15	18
β_1	2.327*	2.430***	2.299***	2.179***	1.982***	1.552***	0.758***	0.362**	0.131	0.106
($p-$value)	(0.044)	(0.000)	(0.000)	(0.000)	(0.004)	(0.002)	(0.027)	(0.048)	(0.326)	(0.074)
Adj R^2 (%)	3.025	14.800	27.715	34.959	32.205	22.270	17.223	8.400	-0.365	0.104
Panel D: After the 2008–2009 financial crisis: 2009:07–2017:08										
Horizon	1	2	3	4	5	6	9	12	15	18
β_1	0.437	0.359*	0.275*	0.236**	0.086	0.000	0.043	0.039	0.049	0.084
($p-$value)	(0.135)	(0.089)	(0.051)	(0.030)	(0.496)	(0.998)	(0.648)	(0.409)	(0.365)	(0.199)
Adj R^2 (%)	0.603	1.213	1.029	1.282	-0.123	-0.422	-0.234	-0.142	0.319	0.126

***, **, and * are the statistical significance levels as 1%, 5%, 10%, respectively.

Table 14: In-sample return predictability with weighted least squares (WLS) regressions at different horizons.

The table 14 reports the estimated regression coefficient β_1 and adjusted R^2 of the predictability WLS regressions from one to eighteen-month excess return on the S&P500 index. The regression takes the form of $r_{t,t+h} \,/\, \widehat{\sigma}_{t,t+h} = \beta_0(h) + \beta_1(h) \cdot (\text{DVRP}_t \,/\, \widehat{\sigma}_{t,t+h}) + u_{t,t+h}$, where $r_{t,t+h}$ is the h-month ahead S&P500 excess return from t to $t+h$, DVRP_t is the predictor variable at time t, and $\widehat{\sigma}_{t,t+h}$ is the forecast of return variance h-month ahead. We use the VIX term structure for 1, 3, 6, 9, and 12 months as a forward-looking measure of the excess return variance. We use the Newey-West standard errors to correct for auto-correlation introduced by overlapping data. The p-value of Newey-West test for significance of estimated regression coefficients accounting for the overlapping in the regressions are reported in the parenthesis. The standard errors are corrected by Newey-West with $2h$ lags. Panel A reports the return predictability regression for the total time period ranging from January 2007 to August 2017. Panel B reports the return predictability regression for the time period during the financial crisis ranging from August 2007 to June 2009. Panel C reports the return predictability regression for the large shock time period during the financial crisis ranging from September 2008 to March 2009. Panel D reports the return predictability regression for the time period after the financial crisis ranging from July 2009 to August 2017. The adjusted R^2, adj R^2, is reported in percent.

Panel A: Total time period: 2007:01–2017:08.					
Horizon	1	3	6	9	12
β_1	0.820	0.619**	0.268	0.123	0.052
($p-$value)	0.241	0.036	0.426	0.383	0.338
Adj R^2 (%)	0.352	1.123	0.155	0.179	-0.021
Panel B: During the 2008–2009 financial crisis: 2007:08–2009:06.					
Horizon	1	3	6	9	12
β_1	1.718**	1.497**	0.634	0.091	-0.066
($p-$value)	0.094	0.072	0.455	0.894	0.903
Adj R^2 (%)	1.173	1.924	-0.993	-2.267	-2.266
Panel C: Large shock period during the 2008–2009 financial crisis: 2008:09–2009:03					
Horizon	1	3	6	9	12
β_1	2.048*	2.169***	1.454***	0.709**	0.331**
($p-$value)	0.067	0.000	0.007	0.028	0.020
Adj R^2 (%)	2.553	24.710	18.906	17.901	11.859
Panel D: After the 2008–2009 financial crisis: 2009:07–2017:08					
Horizon	1	3	6	9	12
β_1	0.026	0.117	-0.102	-0.013	0.010
($p-$value)	0.939	0.422	0.344	0.878	0.807
Adj R^2 (%)	-0.364	-0.167	0.023	-0.372	-0.382

***, **, and * are the statistical significance levels as 1%, 5%, 10%, respectively.

Table 15: Out-of-sample return predictive regressions at different horizons.

The table 15 reports the out-of-sample (OOS) predictive performance from one to eighteen-month excess return on the S&P500 index from January 2008 to August 2017, using the DVRP, estimated in rolling window method as described in section 3, as a predictor. Following the traditional approach uses the past one year of data to run the first-stage regression of weekly S&P500 index excess returns on the lagged DVRP. The regression takes the form of $\widehat{r}_{t,t+h} = \widehat{\beta}_0(h) + \widehat{\beta}_1(h) \cdot \text{DVRP}_t$, where $\widehat{r}_{t,t+h}$ is the h-month ahead S&P500 forecast excess return from t to $t+h$, and DVRP_t is the predictor variable at time t. The OOS R^2 and Wald statistics along with p-values are provided for each of the subsample classifications. Panel A reports the OOS return predictability regression for the total time period ranging from January 2008 to August 2017. Panel B reports the OOS return predictability regression for the large shock time period during the financial crisis ranging from September 2008 to March 2009. Panel C reports the OOS return predictability regression for the time period after large shock time period during the financial crisis ranging from March 2009 to December 2009. Panel D reports the return predictability regression for the time period ranging from January 2010 to August 2017. The out-of-sample R^2, OOS R^2, is reported in percent.

Panel A: Total time period: 2008:01–2017:08.										
Horizon	1	2	3	4	5	6	9	12	15	18
OOS R^2 (%)	-0.845	1.486	0.388	3.456	3.283	1.581	-0.957	-3.778	-4.156	-3.160
Wald	0.105	0.124	0.000	0.289	0.408	0.053	0.012	0.112	0.170	0.152
($p-$value)	(0.746)	(0.725)	(1.000)	(0.591)	(0.523)	(0.900)	(0.911)	(0.738)	(0.680)	(0.697)
Panel B: Large shock time period during the 2008–2009 financial crisis: 2008:09–2009:03.										
Horizon	1	2	3	4	5	6	9	12	15	18
OOS R^2 (%)	-3.832	-14.736	-54.365	-36.249	-24.071	-15.709	-5.306	-1.314	-6.875	-6.378
Wald	0.676	4.040	8.278	5.855	4.221	1.048	0.083	0.006	0.244	0.2114
($p-$value)	(0.411)	(0.044)	(0.004)	(0.015)	(0.040)	(0.306)	(0.774)	(0.939)	(0.621)	(0.646)
Panel C: The time period after the large shock time period: 2009:03-2009:12.										
Horizon	1	2	3	4	5	6	9	12	15	18
OOS R^2 (%)	24.479**	35.003***	28.612**	32.064***	29.816***	19.949**	2.059	-16.441	-7.177	-22.247
Wald	4.524	7.065	5.921	10.431	10.008	5.481	0.033	0.713	0.079	0.508
($p-$value)	(0.033)	(0.008)	(0.015)	(0.001)	(0.002)	(0.019)	(0.855)	(0.399)	(0.779)	(0.476)
Panel D: The time period: 2010:01–2017:08.										
Horizon	1	2	3	4	5	6	9	12	15	18
OOS R^2 (%)	-5.249	-5.212	-3.422	-2.664	-1.805	-3.689	-1.930	-4.727	-2.509	-0.467
Wald	2.408	1.898	1.489	1.073	0.488	0.956	0.388	1.648	0.397	0.000
($p-$value)	(0.121)	(0.168)	(0.222)	(0.300)	(0.485)	(0.328)	(0.533)	(0.199)	(0.529)	(0.989)

***, **, and * are the statistical significance levels as 1%, 5%, 10%, respectively.

Table 16: Out-of-sample CER and CER gains at different horizons.

The table reports the annualized certainty equivalent return (CER) and its gain (in percent per annum) for mean-variance with relative risk aversion coefficient of 3, 4 and 5 who allocates between the equities (S&P500 index futures) and risk-free bills (three-month Tbills) using a preditive regression excess return forecast based on the predictor variable, DVRP, in the second column relative to the prevailing mean benchmark forecast. The equity weight is constrained to lie between -0.5 and 1.5 (Without short selling constraint). The equity weight is constrained to lie between 0.0 and 1.5 (With short selling constraint). The buy-and-hold (BH) trading strategy corresponds to the investor passively holding the market portfolio using a fixed weight. We weekly rebalance the portfolio. The weight w_t of the market portfolio is determined by the OOS forecast contrusted using a fixed weight, historical average, and forecast excess return. The rest 1 - w_t is invested in the risk-free asset. The "unconditinal" weights are formed in the equation 24. The "conditional" weights depend on the size of the estimated correlations or leverage effect (ρ_t) are formed in the equation 25.

		Without short selling constraint										With short selling constraint									
		CER					CER gains					CER					CER gains				
Horizon		1	3	6	9	12	1	3	6	9	12	1	3	6	9	12	1	3	6	9	12
Panel A: Unconditional weighting																					
ζ=3	DVRP	-0.66	1.73	1.57	3.07	4.16	-0.93	1.66	1.02	1.03	0.81	0.14	1.48	1.57	2.68	3.60	-0.72	0.18	-0.08	-0.11	0.05
	BH	-0.81	-1.03	-1.36	-1.47	-1.38	-1.08	-1.10	-1.90	-3.51	-4.73	-0.81	-1.03	-1.36	-1.47	-1.38	-1.67	-2.33	-3.01	-4.26	-4.93
ζ=4	DVRP	-3.48	-0.71	0.40	2.25	2.30	-2.03	0.82	1.22	1.31	0.91	-2.15	-0.50	0.62	1.99	2.80	-1.72	-0.59	-0.14	-0.00	0.04
	BH	-2.38	-2.65	-3.04	-3.22	-3.19	-0.93	-1.12	-2.22	-4.16	-5.27	-2.38	-2.65	-3.04	-3.22	-3.19	-1.95	-2.73	-3.80	-5.22	-5.95
ζ=5	DVRP	-5.06	-1.65	0.04	1.68	2.17	-2.87	0.64	1.01	1.30	0.85	-3.53	-1.25	0.37	1.66	2.29	-2.66	-0.84	-0.23	0.00	0.03
	BH	-3.95	-4.26	-4.73	-4.97	-5.00	-1.75	-1.98	-3.76	-5.36	-6.31	-3.95	-4.26	-4.73	-4.97	-5.00	-3.08	-3.85	-5.32	-6.63	-7.25
Panel B: Conditional weighting																					
ζ=3	DVRP	-1.15	0.59	-0.60	0.84	2.41	0.27	1.68	-0.05	-0.06	0.10	-0.10	0.77	0.76	1.67	2.71	-0.18	0.33	0.21	-0.14	0.02
	BH	-0.81	-1.03	-1.36	-1.47	-1.38	0.27	0.06	-0.82	-2.38	-3.69	-0.81	-1.03	-1.36	-1.47	-1.38	-0.89	-1.48	-1.92	-3.28	-4.07
ζ=4	DVRP	-3.74	-1.74	-2.37	-0.43	1.21	-0.53	1.59	0.57	0.30	0.39	-2.17	-1.16	-0.56	0.78	0.02	-0.33	0.12	0.01	0.00	0.05
	BH	-2.38	-2.65	-3.04	-3.22	-3.19	0.84	0.68	-0.62	-2.49	-4.01	-2.38	-2.65	-3.04	-3.22	-3.19	-0.53	-1.36	-2.47	-3.99	-4.91
ζ=5	DVRP	-5.67	-3.60	-2.99	-1.16	0.56	-0.77	1.15	0.76	0.57	0.54	-3.73	-2.60	-1.05	0.26	1.41	-0.55	-0.27	0.20	0.03	0.04
	BH	-3.95	-4.26	-4.73	-4.97	-5.00	0.95	0.49	-0.98	-3.23	-5.01	-3.95	-4.26	-4.73	-4.97	-5.00	-0.78	-1.92	-3.48	-5.19	-6.36

Table 17: Out-of-sample SR and SR gains at different horizons.

The table reports the annualized Sharpe ratio (SR) and its gain for mean-variance with relative risk aversion coefficient of 3, 4 and 5 who allocates between the equities (S&P500 index futures) and risk-free bills (three-month Tbills) using a preditive regression excess return forecast based on the predictor variable, DVRP, in the second column relative to the prevailing mean benchmark forecast. The equity weight is constrained to lie between -0.5 and 1.5 (Without short selling constraint). The equity weight is constrained to lie between 0.0 and 1.5 (With short selling constraint). The buy-and-hold (BH) trading strategy corresponds to the investor passively holding the market portfolio using a fixed weight. We weekly rebalance the portfolio. The weight w_t of the market portfolio is determined by the OOS forecast contrusted using a fixed weight, historical average, and forecast excess return. The rest 1 - w_t is invested in the risk-free asset. The "unconditinal" weights are formed in the equation 24. The "conditional" weights depend on the size of the estimated correlations or leverage effect (ρ_t) are formed in the equation 25.

		Without short selling constraint										With short selling constraint									
		SR					SR gains					SR					SR gains				
Horizon		1	3	6	9	12	1	3	6	9	12	1	3	6	9	12	1	3	6	9	12
Panel A: Unconditional weighting																					
ζ=3	DVRP	0.35	0.44	0.41	0.46	0.50	-0.03	0.07	0.05	0.05	0.04	0.34	0.40	0.38	0.42	0.46	-0.03	0.03	0.01	0.00	0.00
	BH	0.22	0.21	0.20	0.20	0.21	-0.16	-0.15	-0.16	-0.21	-0.25	0.22	0.21	0.20	0.20	0.21	-0.14	-0.16	-0.17	-0.22	-0.24
ζ=4	DVRP	0.32	0.40	0.42	0.48	0.50	-0.06	0.05	0.06	0.06	0.05	0.30	0.37	0.37	0.42	0.46	-0.05	0.00	0.01	0.00	0.00
	BH	0.22	0.21	0.20	0.20	0.21	-0.13	-0.14	-0.15	-0.21	-0.24	0.22	0.21	0.20	0.20	0.21	-0.15	-0.15	-0.16	-0.21	-0.24
ζ=5	DVRP	0.29	0.39	0.42	0.48	0.50	-0.08	0.04	0.06	0.07	0.05	0.27	0.35	0.36	0.42	0.46	-0.08	-0.01	0.00	0.00	0.00
	BH	0.22	0.21	0.20	0.20	0.21	-0.15	-0.13	-0.15	-0.20	-0.23	0.22	0.21	0.20	0.20	0.21	-0.14	-0.15	-0.16	-0.21	-0.24
Panel B: Conditional weighting																					
ζ=3	DVRP	0.37	0.42	0.37	0.42	0.47	-0.01	0.05	0.00	0.00	0.01	0.36	0.39	0.38	0.41	0.48	-0.01	0.01	0.02	0.00	0.00
	BH	0.22	0.21	0.20	0.20	0.21	-0.16	-0.16	-0.17	-0.21	-0.25	0.22	0.21	0.20	0.20	0.21	-0.15	-0.17	-0.17	-0.21	-0.23
ζ=4	DVRP	0.36	0.42	0.37	0.43	0.48	-0.02	0.05	0.01	0.01	0.02	0.35	0.38	0.38	0.42	0.46	-0.02	0.01	0.01	0.00	0.00
	BH	0.22	0.21	0.20	0.20	0.21	-0.16	-0.15	-0.16	-0.21	-0.26	0.22	0.21	0.20	0.20	0.21	-0.15	-0.17	-0.17	-0.22	-0.24
ζ=5	DVRP	0.35	0.40	0.38	0.43	0.49	-0.03	0.04	0.03	0.02	0.02	0.33	0.37	0.38	0.42	0.46	-0.03	-0.01	0.02	0.00	0.00
	BH	0.22	0.21	0.20	0.20	0.21	-0.16	-0.15	-0.15	-0.21	-0.25	0.22	0.21	0.20	0.20	0.21	-0.14	-0.16	-0.17	-0.21	-0.25